Quantum target detection

Spooky vision at a distance

Athena Karsa

PhD

Computer Science
University of York

September 2021

Abstract

Quantum target detection forms a particular subset of quantum sensing protocols whereby one's task is to determine whether or not a target is present within some region of interest. The goal is to outperform the corresponding optimal classical protocol, establishing a quantum advantage. Such an advantage arises from phenomena native to quantum mechanics allowing for measurement sensitivities otherwise impossible when one is restricted to purely classical means.

This thesis studies the potential of quantum target detection starting with the quantum illumination protocol and outlining the landscape of potential future research. Later chapters provide theoretical contributions addressing the many challenges associated with quantum illumination, particularly at the microwave, in turn.

Through the study of generic Gaussian sources, we show that maximal entanglement is not strictly necessary to achieve a quantum advantage, significantly reducing the experimental burden of source generation. Microwave operation brings a unique set of experimental challenges regarding source generation, detection and idler storage. These challenges also apply to coherent states for which we provide analyses of true classical benchmarks for the microwave. We study the potential of immediate idler measurement, only storing classical outcomes for later recombination with signal outcomes in post-processing. The effective signal-to-noise ratio is derived, assuming the simulation of a phase-conjugating receiver, which may be readily adapted to include noise from arbitrary measurements. We proceed to study the effect of a non-deterministic noiseless linear amplifier at the detection stage showing a significant improvement in error exponent compared to un-amplified protocols, retaining a quantum advantage. Channel position finding is considered in an attempt to extend quantum illumination to target metrology. We show a quantum advantage across a wide class of states constrained to at most one single photon per mode and study its potential in quantum illumination-based quantum target ranging.

Contents

List of Figures

List of Acronyms

Acryonym	Definition
ADC	Amplitude Damping Channel
AQHT	Asymmetric Quantum Hypothesis Testing
CM	Covariance Matrix
CPF	Channel Position Finding
EPR	Einstein-Podolski-Rosen
LOCC	Local Operations and Classical Communication
MRR	Micro-Ring Resonator
OPA	Optical Parametric Amplifier
PC	Phase Conjugating
PDF	Probability Distribution Function
POVM	Positive-Operator Valued Measure
QBB	Quantum Bhattacharyya Bound
QCB	Quantum Chernoff Bound
QCD	Quantum Channel Discrimination
QHT	Quantum Hypothesis Testing
QI	Quantum Illumination
QRE	Quantum Relative Entropy
QREV	Quantum Relative Entropy Variance
QTR	Quantum Target Ranging
ROC	Receiver Operating Characteristic
SFG	Sum-Frequency Generation
FF-SFG	Sum-Frequency Generation with Feed-Forward
SNR	Signal-to-Noise Ratio
SPDC	Spontaneous Parametric Down Conversion
TMSV	Two-Mode Squeezed Vacuum

To my sister, Maria,
Through despair and hope,
Through faith and love,
Till we meet again
In this circle of life.

Acknowledgements

I would like to acknowledge the funding provided by the Engineering and Physical Sciences Research Council (1949572) and Leonardo UK.

I am immensely grateful and have much respect for my supervisor, Prof. Stefano Pirandola, for their advice and support throughout my PhD. His guidance and insight have enabled me to grow into a confident researcher and without him this thesis would not have been possible.

I would also like to thank David Greig at Leonardo UK for all of the valuable insights and fruitful discussions throughout the last four years.

During my time at the University of York I have had the pleasure of making new life-long friends. Jordan Cross and Chaitanya Kaul, thank you for always making me smile. Jason Pereira, you have been a wonderful office mate; I am forever grateful for the support you have offered me, stimulating discussions and adherence to our values of “live, laugh, love".

The first person to speak to me when I began my PhD initiated our conversation with the line, “I hope you like spiders". Four years later, I am about to submit my thesis and have the pleasure of calling that man my husband. Timothy Atkinson, you have been an ongoing source of love, support and encouragement for which I cannot thank you enough.

Finally, I would like to thank my mother for everything that she is and has done for me. You are my strength, my motivator and my best friend. I would not be where I am today if it were not for your eternal love and support.

Declaration

I declare that this thesis is a presentation of original work and I am the sole author. This work has not previously been presented for an award at this, or any other, University. All sources are acknowledged as References.

Some parts of this thesis have been published in journals and conference proceedings, or made available online on the arXiv; where items were published jointly with collaborators, the author of this thesis is responsible for the material presented here. The author of this thesis acknowledges the input of their collaborators, and has credited them appropriately throughout. For each published item the primary author is the first listed author. These publications are:

[1] A. Karsa, G. Spedalieri, Q. Zhuang and S. Pirandola, *Quantum illumination with a generic Gaussian source*, Phys. Rev. Res. **2**, 023414 (2020).

[2] A. Karsa and S. Pirandola, *Noisy receivers for quantum illumination*, IEEE Trans. Aerosp. Electron. Syst. Magazine 35(**11**), 22–29 (2021).

[3] A. Karsa and S. Pirandola, *Energetic Considerations in Quantum Target Ranging*, IEEE Rad. Conf. (RadarConf21), 1–4, (2021).

[4] A. Karsa and S. Pirandola, *Classical benchmarking for microwave quantum illumination*, IET Quant. Comm. 2(**4**), 246–257 (2021).

[5] A. Karsa, J. Carolan, and S. Pirandola, *Quantum channel position finding using single photons*, Phys. Rev. A (**105**), 023705 (2022).

[6] A. Karsa, M. Ghalaii and S. Pirandola, *Noiseless linear amplification in quantum target detection using Gaussian states*, under review, (2022).

1 Introduction

1.1 Motivation

Quantum technologies involve the direct use of quantum-mechanical phenomena to achieve results from quantum states that are not possible with classical matter. The field provides a large, complex landscape for research and engineering with a wide range of practical applications such as quantum computing, quantum cryptography, quantum sensing and quantum metrology.

Research into the wide variety of technological applications of quantum systems relies on the study of the interactions of these systems both with others and external factors and, as such, can be utilised for building ultimate sensors on the nanoscale. Interactions between several distinct quantum states are of particular importance as the behaviour can lead to the realisation of a so-called entangled state whose quantum mechanical correlations, with no classical counterpart, are the key ingredient for promised speed-up in quantum information processing and unprecedented resolution in measurement sensitivity. These quantum correlations can be exploited for metrological purposes to provide unparalleled resolution and sensitivities per sensor volume. Increased capability for the observation of many-body quantum systems over recent decades has allowed for sensing beyond previous limitations and within this quantum regime are promised sensitivities scaling with sensor size beyond the shot noise limit ($\propto 1/\sqrt{N}$) with Heisenberg scaling ($\propto 1/N$).

The possibility of realising practical sensing applications of quantum technologies appears to be much more tangible within the near future compared with other implementations, which require simultaneous control with high precision over many distinct quantum states, currently out of reach. Recent years have seen exciting results from the exploitation of non-classical states of radiation in theoretical and experimental quantum technologies [7–10]. One example of this, also the topic of this thesis, is quantum target detection in which the exploitation of quantum mechanical phenomena affords a theoretical quantum advantage in detection capa-

bilities. Such a task has fundamental links to a plethora of other quantum sensing protocols (see [11] for a recent review of these topics), including quantum ranging, quantum spectroscopy and, of course, quantum illumination (QI). The latter of which, otherwise called quantum radar, is an entanglement-based quantum target detection scheme promising significant improvements in target detection over not only currently used classical radar systems, but any other classical, coherent state protocols. Forming the first method for microwave quantum target detection, it will also be the primary scheme studied within this work.

1.1.1 Quantum target detection, quantum illumination and quantum radar: What's the difference?

Before continuing, it is worth defining what we mean by quantum target detection, quantum illumination and quantum radar as they are used throughout this thesis. Often these terms are used interchangeably leading to confusion regarding what they actually refer to. Note that the concepts discussed here, and the remainder of this chapter, will be further explored in more technological depth later in this thesis, particularly in Chaps. 2 and 3.

Quantum target detection is any protocol which makes use of some aspect of quantum mechanics to perform the task of target detection. That is, given some region of interest, determining whether or not a target is present there. The "quantumness" can reside in any part of the protocol, be it the source used for probing the target region, or the receiver used to perform decision-making (see also Sec. 3.2).

Quantum illumination (QI) forms a particular subset of quantum target detection protocols based on entanglement. Entanglement is a unique feature of quantum mechanics, which Einstein popularly referred to as "spooky action at a distance", whereby two distinct objects can instantaneously possess information about each other even when separated at a great distance. In QI, the probing source is entangled with the receiver, such that by the time decision-making occurs, the receiver "knows", through entanglement, additional information about what has happened to the source during its employment.

Quantum radar refers to the specific application of some quantum target detection protocols within the microwave domain. Such an application is of particular interest since the potential advantage in detection afforded by QI is maximal when there is a lot of noise present, a regime which occurs naturally in the microwave due to the cosmic microwave background. Note that while, so far, the majority of quantum radar research has been in the context of QI, it is not strictly the case that quantum radar implies the use of QI.

1.1.2 Principles of classical radar theory

Radar is a sensing technology originally developed during the first half of the 20th century, mostly just after the end of the First World War, even though reflection of radio waves by solid objects was first observed by Heinrich Hertz in 1886 [12]. The first pulse-based radar system was developed by the US Naval Research Laboratory in 1934, able to detect and estimate the range of a target. Radar has become a major field of research and development for all major military powers, but the basic principles underlying current, classical systems have not changed since their inception and beginnings of widespread use more than 50 years ago.

The generic operation of a classical monostatic, with co-locating transmitter/receiver, radar system is shown in Fig. 1.1. The transmitter emits an electromagnetic pulse of power, P_{tx}, towards the target located a distance R_{T} away. The antenna does not emit radiation isotropically; it is instead usually emitted as a narrow beam with an additional element of directionality given by the transmitter gain, G_{tx}. The gain is generally a function of spherical coordinates θ and ϕ and is a product of two terms that determine actual transmitted power: 1) the efficiency of the radar in generating a transmission signal from its input, and 2) the directivity of the antenna in terms of the actual outgoing beam. Directivity is calculated such that a perfectly isotropic antenna will have directivity of 1 in all directions and, even for those that are not isotropic (as in the case of pencil and fan beams), the mean directivity is still always 1 but varies with direction. This multiplicative factor constituting the antenna gain is used to obtain the total transmitted power in the target's direction, $P_{\text{tx}}G_{\text{tx}}$ (assuming the peak gain is in the direction of the target). The emitted electromagnetic pulse, after reflection off the target, arrives back at the receiver after a time, Δt, which can be used to compute the target range,

$$R = \frac{c\Delta t}{2}, \tag{1.1}$$

where c is the speed of light in a vacuum.

Generally speaking, however, most of the emitted energy is lost during the process. This is due to attenuation factors associated with the medium through which the pulse propagates, and also the reflectivity of the target itself, dependent on both its material and geometry. As a result, the total power density incident on the target is given by

$$W_{\text{T}} = \frac{P_{\text{tx}}G_{\text{tx}}F^2}{4\pi R_{\text{T}}^2}, \tag{1.2}$$

where $F \in [0, 1]$ is a form factor describing the transmissivity of the space between the

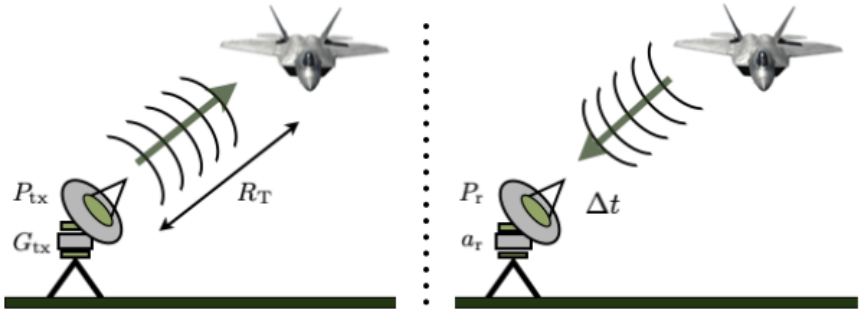

FIG. 1.1: Schematics of a generic, monostatic classical radar system. First, a radar transmitter, characterised by its transmitted power, P_{tx}, and gain, G_{tx}, sends electromagnetic pulse towards a target region at a distance, R_{T}. If the target is present, a proportion of this wave with power, P_{r}, is reflected back towards the radar receiver, arriving there after a time, Δt.

radar and the target, and the additional factor of $1/4\pi R_{\mathrm{T}}^2$ describes the loss due to the pulse propagating as a spherical wave.

The reflectivity of the target, described by a single term called the radar cross-section, σ, describes the proportion of incident power that is subsequently scattered. This then propagates back towards the receiver such that the total power density arriving back at the receiver is given by

$$W_{\mathrm{r}} = \frac{P_{\mathrm{tx}} G_{\mathrm{tx}} \sigma F^4}{(4\pi)^2 R_{\mathrm{T}}^4} = \frac{P_{\mathrm{r}}}{a_{\mathrm{r}}}, \tag{1.3}$$

where P_{r} is the power arriving at the receiver and a_{r} is the receiver's collecting area. Thus we arrive at the radar equation [13],

$$P_{\mathrm{r}} = \frac{P_{\mathrm{tx}} G_{\mathrm{tx}} a_{\mathrm{r}} \sigma F^4}{(4\pi)^2 R_{\mathrm{T}}^4}, \tag{1.4}$$

by which current state of the art classical radar systems and their performances are modelled.

The signal-to-noise ratio (SNR)

Sensitivity to thermal noise poses limitations on the strength of target signals detectable by the radar receiver [14, 15]. Arising from electronic noise intrinsic to the radar system, also called Johnson–Nyquist noise, its total associated power is given by

$$P_{\mathrm{n}} = k_B T B_{\mathrm{n}} F_{\mathrm{n}}, \tag{1.5}$$

where k_B is Boltzmann's constant, T is the system's operating temperature, B_n is the receiver's bandwidth and F_n is a dimensionless constant expressing the variation of the true noise characteristics from that of an ideal black body.

Eq. (1.5) allows us to define the signal-to-noise ratio (SNR) as

$$\mathrm{SNR} = \frac{P_\mathrm{r}}{P_\mathrm{n}} = \frac{P_\mathrm{tx} G_\mathrm{tx} a_\mathrm{r} \sigma F^4}{(4\pi)^2 R_\mathrm{T}^4 k_B T B_\mathrm{n} F_\mathrm{n}}. \tag{1.6}$$

The collecting area of the receiver, a_r, can be expressed in terms of a receiver gain, $G_\mathrm{r} = 4\pi a_\mathrm{r}/\lambda^2$, allowing us to rewrite Eq. (1.6) as

$$\mathrm{SNR} = \frac{P_\mathrm{tx} G_\mathrm{tx} G_\mathrm{r} \lambda^2 \sigma F^4}{(4\pi)^3 R^4 k_B T B_\mathrm{n} F_\mathrm{n}}. \tag{1.7}$$

Since the SNR always has a finite value, from Eq. (1.7) there exists a minimum detectable signal, $\mathrm{SNR}_\mathrm{min}$, which must exceed the system's noise floor. This in turn corresponds to a maximum detection range,

$$R_\mathrm{max} \simeq \left(\frac{P_\mathrm{tx} G_\mathrm{tx} G_\mathrm{r} \lambda^2 \sigma F^4}{(4\pi)^3 k_B T B_\mathrm{n} F_\mathrm{n} \mathrm{SNR}_\mathrm{min}} \right)^{1/4}, \tag{1.8}$$

where $\mathrm{SNR}_\mathrm{min}$ is typically of the order of 10-20 dB [15].

Radar countermeasures: clutter and jamming

Of course, countermeasures exist to defend against radar detection which may be either passive or active. Clutter occurs when signals are received from unwanted, naturally occurring sources such as non-target surfaces and atmospheric reflections causing interference in the received signal that can potentially obscure a target. This can be further enhanced by a passive jamming technique where the radar's own signal is reflected back in a diffuse form to magnify the effect of interference that would already be present.

Active jamming is a form of electronic countermeasure where signals are actively transmitted in order to disrupt radar performance. In its simplest form, radiation within the radar's operating bandwidth is transmitted to artificially increase the level of noise against which the target must be detected. More complicated techniques exist where the transmitted radar waveform is digitally sampled, modified and re-transmitted in order to deceptively create false targets, disrupting the radar's tracking capabilities as opposed to its detection capacity.

Classical hypothesis testing

Hypothesis testing [16] is a standard problem in statistics and information theory [17] in order to decide between two alternative explanations for observed data patterns. The desire to be able to make decisions, and quantify one's capability of making said decisions correctly, based on a signal of interest using noisy measurements is of great interest with applications ranging from radar and sonar to communications and biomedicine. As a result, statistical tools exist to enable systematic solutions and optimal design. For QI, performance at this task is quantified in terms of the probability of the protocol's final decision being incorrect, while at present a fundamental determinant of the quality of many classical radar signal processing operations is the SNR and, as a result, the radar cross-section. If the quantum protocol is to be adopted on an industrial scale, these figures of merit ought to be translated across regimes (quantum to classical, and vice versa) so that properly considered comparisons can be drawn between performances also relative to practical aspects of their implementations as well.

Radar detection entails, with the view of best describing a detected signal, making a decision between two possible explanatory hypotheses: 1) H_0: target is absent, the null hypothesis, and 2) H_1: the target is present, the alternative hypothesis [12]. This simple example of a binary decision task has been the subject of many studies and its analysis begins with the definition of probability density functions (pdfs) describing the measurement to be tested under each of the two available hypotheses. Supposing the sample to be tested is denoted x, then we need two pdfs:

$$\begin{aligned} p_x(x|H_0) &= \text{pdf of } x \text{ given that the target was absent,} \\ p_x(x|H_1) &= \text{pdf of } x \text{ given that the target was present,} \end{aligned} \tag{1.9}$$

which may be generalised to the M-dimensional joint pdfs $p_{\boldsymbol{x}}(\boldsymbol{x}|H_0)$ and $p_{\boldsymbol{x}}(\boldsymbol{x}|H_1)$ for a detection problem based on M i.i.d samples of data x_n forming the sample vector $\boldsymbol{x} \equiv [x_1 \dots x_M]^T$, with $n = 1, \dots, M$.

The underlying problem is reliant on the proper modelling of these two functions and their estimates are in turn reliant on the system and parameters governing the scenario in question. Optimal design depends on the ability to reliably tune these pdfs to obtain favourable outcomes in terms of desired radar detection performance capabilities. Based on the above pdfs, we may define the following probabilities of interest:

- Probability of detection, P_{det},
  The probability of a target being correctly declared present, $P(H_1|H_1)$;

- Probability of false alarm (Type I error), P_{fa},
  The probability of a target being incorrectly declared present, $P(H_1|H_0)$;
- Probability of mis-detection (Type II error), P_{miss},
  The probability of a target being incorrectly declared absent, $P(H_0|H_1)$.

Optimisation of these probabilities can be carried out in a range of ways based on the rules one wishes to follow for decision making, which may also be situation dependent. In radar, a common choice is the Neyman-Pearson criterion in which the probability of detection, P_{det}, is maximised under the constraint that the Type II false alarm probability does not exceed some predetermined, tolerable value. The overall diagnostic capability of binary classifiers, such as radars, can be evaluated by the construction of a receiver operating characteristic (ROC) curve. This graphically plots the true detection rate P_{det} against the false alarm rate which is generally fixed as part of the system specifications [12], and shows the trade-off between sensitivity (P_{det}) and specificity (1-P_{fa}). A commonly used measure of performance is given by the area under the curve, which may be interpreted as the probability that the model ranks a random positive example more highly than a random negative example.

The desire for improved radar systems is necessary for performance advantages in a wide range of applications from the military to space exploration. As a result, it is a natural progression for research in the exploitation of quantum states for sensing and detection to be extended to this field.

1.1.3 Quantum radar

Quantum radar is a form of quantum sensing that has garnered a great deal of attention over recent years [18–21]. Initially proposed in the form of QI, it promises to outperform classical counterparts, particularly in areas where they fall short, owing to the fact that the purely quantum mechanical phenomenon of entanglement is initially present in the system. In particular, it promises to do so even under circumstances where classical radar capabilities are known to be limited, that is, in cases of:

(i) Low reflectivity, as in the use of stealth technology where the reflectivity is carefully managed across angles;

(ii) Long range, owing to the presence of a minimum possible signal-to-noise ratio due to the system's intrinsic electronic noise (see Eq. (1.5));

(iii) Lossy, noisy environment, consisting of thermal background, clutter and electronic coun-

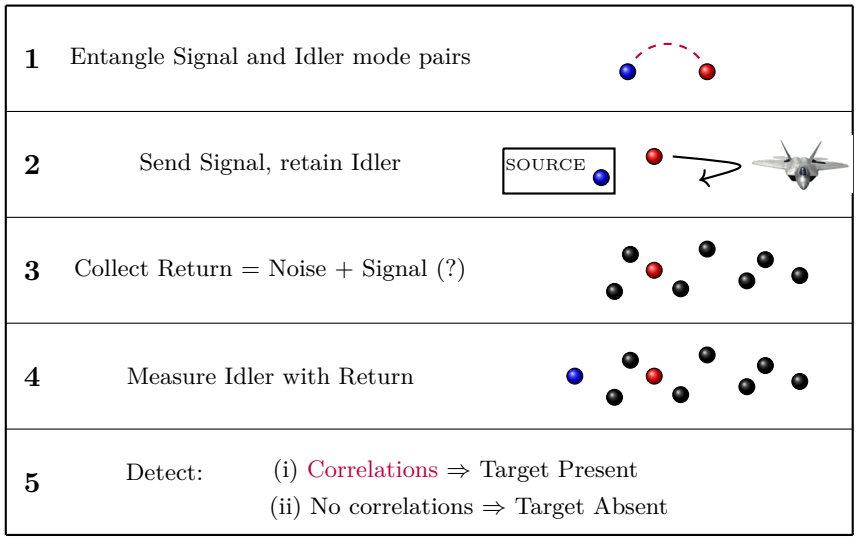

FIG. 1.2: The basic elements of the quantum illumination protocol.

termeasure contributions.

The final point, the case of a lossy, noisy environment is particularly interesting with respect to the QI advantage. Typically, in any quantum protocol, the presence of environmental interactions that result in decoherence, is detrimental to the task at hand. Remarkably, for QI, the merits of the overall results persist despite the loss of entanglement during the process. Even though the final measurement is made on mode pairs that are no longer maximally correlated, the fact that those correlations existed at the beginning is enough to ensure that the correlations survive at a high enough level throughout in order to achieve the necessary advantage to out-compete the classical protocol.

The basic protocol of QI is outlined in Fig. 1.2. It begins by preparing entangled pairs of photonic modes with one member of each pair labelled an idler photon and the other a signal photon. Signal photons are sent towards a region which may or may not contain a target while the idler photons are retained at the source for later measurement. The returning signal consists of many noise photons and, possibly, some signal photons that are all used in a joint measurement process along with the retained idlers. The problem is reduced to one of state discrimination, i.e., being able to distinguish the originally entangled signal photon from the multitude of noise photons, despite the fact that the original entanglement is lost. Correlations still exist between the mode pairs that may be exploited, such that given enough repeated measurements, the overall probability of getting an error in the discrimination process is several decibels lower than an equivalent process in a classical setting.

1.1.4 The classical benchmark for quantum radar

Throughout the literature, and this thesis, we will frequently refer to the "classical benchmark". To clarify what is meant by this, we are not referring to using the classical radar described in Sec. 1.1.2 as a benchmark, but instead what is considered the most ideal, classical quantum state within quantum optics: the coherent state. The properties of coherent states will be described in detail in Chap. 2, particularly Sec. 2.2.3. In essence, they are quantum states which saturate the Heisenberg inequality. In the sense that uncertainty is viewed as a quantum phenomenon, saturation of this and minimising uncertainty can be seen as maximising classicality within the quantum world. Further, since coherent states are Gaussian, their use in quantum optics experiments can be straightforwardly studied and modelled in frameworks which mirror those making use of true quantum mechanical phenomena. This provides a means for formally defining and isolating a quantum advantage.

1.2 Thesis outline

This thesis will be an attempt to critically and theoretically explore the emerging field of quantum detection across energy scales, particularly for the application of quantum radar. As an emerging field of research, this work is required in order to both determine potential improvements in detection performance, including range and robustness against noise, afforded by quantum technologies in comparison to classical techniques. An overriding theme will be to attempt formulation of a mapping of terminology between the two detection theories to establish a proper means for thorough comparison to assess not only the theoretical advantages that the quantum technology may have, but also the practicalities associated with its in-field application.

The rest of the thesis is structured as an incremental development starting from the context in which we work where mathematical tools and preliminary notions are introduced. The remaining chapters are given based on publications presenting the contributions made by the research project upon which this thesis is based. These contributions pertain to the theory of QI and quantum target detection and the practicalities associated with its physical implementation, particularly in the microwave domain. This thesis is broken down into the following chapters:

- **Chapter 2: Mathematical preliminaries**. Outlines the necessary mathematical tools under the formalism of continuous variables required for the understanding of the

remainder of this thesis and contributions.

- **Chapter 3: Quantum target detection**. Describes the history of quantum target detection, starting with its roots in QI and discussing its potential and challenges.
- **Chapter 4: Quantum illumination with a generic Gaussian source**. At the start of this research project, all literature on Gaussian QI considered maximal entanglement (see Sec. 2.2.3, two-mode squeezed states) which could be practically limiting. In an attempt to loosen transmitter requirements, we reformulate Gaussian QI for a generically-correlated Gaussian source and analyse its performance in the settings of symmetric and asymmetric quantum hypothesis testing (QHT). The quantum Chernoff bound (QCB) and receiver operating characteristics (ROCs) are derived and compared to the classical benchmark of coherent states subject to different measurement techniques showing that maximal entanglement is not strictly necessary in order to achieve a quantum advantage. Further, this chapter draws parallels between QI and classical radar theory showing the relation between parameters for quantum radar and real-world target detection, illustrating that, at least for now, QI applications are likely limited to short-range, e.g., biomedical or scanning.
- **Chapter 5: Noisy receivers for quantum illumination**. With the advent of prototypical experiments demonstrating QI, particularly in the microwave, and owing to the fact that optimal receivers for QI reception are technologically out of reach, there is a question as to the ultimate capabilities of QI subject to noisy receivers. There is also the problem that quantum memories are lacking in the microwave domain which could be mitigated if the classical output of an immediate measurement of the idler mode could be used to still achieve a quantum advantage through the simulation of a phase-conjugating (PC) receiver with measurement results. This chapter considers Gaussian QI under the action of a PC receiver deriving the effective SNR which may be readily adapted to include added noise from the associated measurement. The effect of heterodyne measurements is studied in particular, in light of methods used in microwave experiments, with their performances evaluated and compared through the classical Chernoff bound to the relevant classical benchmarks.
- **Chapter 6: Noiseless linear amplification for quantum target detection**. Optimal receiver design saturating the potential QI QCB remains elusive, with physically attainable Gaussian-based procedures such as the PC receiver proving sub-optimal. Gaussian designs based on amplification necessarily introduce noise ultimately render-

ing the final decision-making capabilities for quantum target detection flawed (see also Chap. 5 and Chap. 7 for a study of this on coherent state illumination). This chapter studies the introduction of non-Gaussian protocols for QI-based quantum target detection by considering the action of a noiseless linear amplifier (NLA) at the detection stage. By transforming the problem of QI with an NLA at the receiver to an equivalent protocol with modified effective parameters, we compute the QCB and compare it to the classical benchmark of coherent states under the same NLA action. Our results show that, subject to certain parameter constraints where our analysis is valid, an NLA can significantly improve the performance of QI compared to the equivalent protocol without an NLA. Finally, we initiate a procedure for potentially implementing a measurement-based NLA through appropriate post-selection of heterodyne measurement outcomes.

- **Chapter 7: Classical benchmarking for microwave quantum illumination**. While the practical limitations of QI in the microwave domain are well known, the same cannot be said for microwave coherent state illumination. When considering microwave QI, the theoretically optimal, optical classical benchmark of coherent states are believed to be appropriate when in fact it simply does not exist there; the classical benchmark in the microwave domain does not coincide with the classical benchmark at optical frequencies. This chapter outlines three possible protocols for illumination at microwave frequencies based on coherent states: one, currently used in experiments, based on amplification of an ultra-cold coherent state source, another which, if it would exist coincides with the optical, and a further alternative is proposed based on cryogenic attenuation of a room temperature maser source. This chapter provides, for each protocol, new bounds on the error probability and closed formulae for the ROC for both optimal, based on the quantum relative entropy (QRE), and homodyne detection schemes.
- **Chapter 8: Quantum channel position-finding using single photons**. Channel position finding (CPF) is a problem which can potentially allow for the extension of procedures used for detection to one's for measurement. This is necessary to allow for QI-based protocols to be utilised to perform metrological tasks such as target ranging. CPF entails finding amongst an ensemble of reference channels the location of a single target channel. In this chapter, the CPF problem is explored using discrete variable sources constrained to at most one single photon on average per mode. Various types of source are explored: single-photon (Fock) states, GHZ states where multipartite

entanglement is distributed amongst the entire ensemble, bipartite (signal-idler) entanglement and biphoton states. Biphoton states, experimentally available via integrate quantum photonics, are considered for use in two protocols: the first in a signal-idler set-up and, second, a new idler-free protocol. In all cases, fidelity-based bounds on error probability are derived and compared with the classical benchmark of coherent states under the same energy constraint. We show that a quantum advantage can exist across varying regimes and, for a Fock state source, a practical receiver based on photon counting is outlined for which the quantum advantage persists.

- **Chapter 9: Multiple quantum hypothesis testing for target metrology**. In this chapter, the CPF problem is applied to the task of quantum target ranging. We outline a potential protocol based on QI where a range interval of interest is split into discrete range bins, corresponding to specific signal-idler recombination times. The upper bound to the error probability is derived and compared to an equivalent scheme using coherent states which would form the classical benchmark for such a task. We find that under fair energetic considerations, a quantum advantage in target ranging cannot necessarily be proven with current mathematical tools.
- **Chapter 10: Conclusions and future work**. Finally, our results are summarised and we draw conclusions and discuss the direction that future study could take.

2 Mathematical preliminaries

2.1 Introduction

The role of this chapter is to introduce some of the core concepts and tools which will be used throughout the remainder of this work. Section 2.2 providing an overview of quantum information in the continuous variable setting, introducing the Gaussian state formalism. Then, Section 2.3 builds on the preceding section to detail quantum hypothesis testing (QHT) which provides the means of analytically evaluating the potential performances of any quantum detection scheme.

Should the reader have further interest in exploring the topics discussed throughout this chapter, reviews that are both extensive and of great value include Refs. [8–10, 22, 23]. There is also a more recent book on continuous variable quantum systems, Ref. [24], and Ref. [25] provides an overview of quantum optics.

Note that throughout this thesis the symbol $\mathbf{1}$ represents the two-dimensional identity matrix with higher dimensions specified by a subscript.

2.2 Quantum information with continuous variables

2.2.1 Bosonic field operators and quadratures

A quantum mechanical system is also a continuous variable system when its quantum state resides in an infinite-dimensional Hilbert space spanned by basis vectors whose observables form continuous eigenspectra. They can be decomposed in terms of bosonic creation and annihilation operators $\{\hat{a}^\dagger, \hat{a}\}$, with the simplest being that of a single-mode radiation field. This is described by the free Hamiltonian which, for a mode with the label j, reads

$$\hat{H}_j = \hbar\omega_j(\hat{a}_j^\dagger \hat{a}_j + \frac{1}{2}), \tag{2.1}$$

where $\hbar\omega_j$ is the single-photon quantisation energy and $\hat{n}_j := \hat{a}_j^\dagger \hat{a}_j$ is the photon number operator and the additional $1/2$ arises from the zero-point energy fluctuations associated with the vacuum, where $n_j = 0$. Although different formalisms exist for choice of vacuum or shot-noise, here and throughout this thesis we will treat the mathematics of continuous variables in the natural units ($\hbar = 1$) such that the vacuum or shot-noise is equal to 1.

Within this setting, the single mode behaves as a quantum harmonic oscillator residing in a separable, infinite-dimensional Hilbert space, $\mathcal{H}_j$, spanned by the Fock basis $\{|n\rangle_j\}_{n=0}^{\infty}$, also referred to as the number state representation. Our notation here, $\{|n\rangle_j\}_{n=0}^{\infty}$, refers to the set union of all number state vectors for the mode j. These form an orthonormal basis and are the eigenstates of the system's number operator, $\hat{n}_j$, which acts such that $\hat{n}_j |n\rangle_j = n_j |n\rangle_j$. For a bosonic quantum field, the number state $|n\rangle_j$ represents the presence of n_j particles (excitations of the field) in mode j. They are generated by their associated bosonic annihilation and creation operators, defined by

$$\hat{a}_j |0\rangle_j = 0, \qquad \hat{a}_j |n\rangle_j = \sqrt{n}\, |n-1\rangle_j \quad (\text{for } n \geq 1), \tag{2.2}$$

also defining the vacuum state, and

$$\hat{a}_j^\dagger |n\rangle_j = \sqrt{n+1}\, |n+1\rangle_j \quad (\text{for } n \geq 0), \tag{2.3}$$

respectively. These definitions illustrate exactly how the operators act on the system: an annihilation operator removes one particle while a creation operator adds one. Further, they obey the usual bosonic commutation relation, namely

$$\left[\hat{a}_j, \hat{a}_j^\dagger\right] = \hat{a}_j \hat{a}_j^\dagger - \hat{a}_j^\dagger \hat{a}_j = 1. \tag{2.4}$$

Note that on their own these operators do not represent any physical observables of the system since they are not Hermitian.

This formalism can readily be extended to describe an N-mode bosonic system described by density operator $\hat{\rho}$ defined on the, again, separable and infinite-dimensional, Hilbert space $\mathcal{H}^{\otimes N} = \bigotimes_{k=1}^{N} \mathcal{H}_k$. By separable, we mean that the Hilbert space is a tensor product of the individual, infinite-dimensional, Fock spaces of constituent, non-interacting modes with corresponding field operators given by the set $\{\hat{a}_k, \hat{a}_k^\dagger\}_{k=1}^{N}$. Within this multi-mode setting we can arrange the field operators into a single vectorial form $\hat{\mathbf{b}} := (\hat{a}_1, \hat{a}_1^\dagger, \ldots, \hat{a}_N, \hat{a}_N^\dagger)^T$ satisfying the same bosonic commutation relations

$$\left[\hat{b}_i, \hat{b}_j\right] = \Omega_{ij} \qquad (i, j = 1, \ldots, 2N), \tag{2.5}$$

where Ω_{ij} is an element within the $2N \times 2N$ matrix, known as the symplectic form, given by the direct sum of identical 2×2 blocks:

$$\mathbf{\Omega} := \bigoplus_{k=1}^{N} \boldsymbol{\omega} = \mathrm{diag}(\boldsymbol{\omega}, \ldots, \boldsymbol{\omega}), \qquad \boldsymbol{\omega} := \begin{pmatrix} 0 & 1 \\ -1 & 0 \end{pmatrix}. \tag{2.6}$$

The field operators for an N-mode quantum harmonic oscillator can be rewritten in terms of phase space quadrature operators $\{\hat{q}_k, \hat{p}_k)\}_{k=1}^{N}$ as

$$\hat{q}_k = \frac{1}{\sqrt{2\omega_k}}(\hat{a}_k + \hat{a}_k^\dagger), \qquad \text{and} \qquad \hat{p}_k = -i\sqrt{\frac{\omega_k}{2}}(\hat{a}_k - \hat{a}_k^\dagger), \tag{2.7}$$

obeying the commutation relations[1]

$$[\hat{q}_j, \hat{q}_k] = [\hat{p}_j, \hat{p}_k] = 0, \tag{2.8}$$

and

$$[\hat{q}_j, \hat{p}_k] = i\delta_{jk}. \tag{2.9}$$

In analogy with the vectorial field operator $\hat{\mathbf{b}}$, we can construct a similar form for the quadrature operators as $\hat{\mathbf{x}} \in \mathbb{R}^{2N}$ such that

$$\hat{\mathbf{x}} = (\hat{q}_1, \hat{p}_1, \ldots, \hat{q}_N, \hat{p}_N)^T, \tag{2.10}$$

obeying the commutation relation

$$[\hat{x}_i, \hat{x}_j] = i\Omega_{ij}. \tag{2.11}$$

The single-mode quadrature eigenstates, given by

$$\hat{q}\,|q\rangle = q\,|q\rangle\,, \qquad \text{and} \qquad \hat{p}\,|p\rangle = p\,|p\rangle\,, \tag{2.12}$$

have continuous eigenvalues $q, p \in \mathbb{R}$. The eigenstates are also related through orthogonality:

$$\langle q|q'\rangle = \delta(q - q') \qquad \text{and} \qquad \langle p|p'\rangle = \delta(p - p'), \tag{2.13}$$

and completeness:

$$\int_{-\infty}^{\infty} |q\rangle\langle q|\,\mathrm{d}q = \mathbf{1} = \int_{-\infty}^{\infty} |p\rangle\langle p|\,\mathrm{d}p. \tag{2.14}$$

[1]Note that from this point and for the remainder of this thesis we will assume the use of dimensionless pairs of quadrature operators, obtained through the rescaling $\hat{q}_k \to \sqrt{\omega_k}\hat{q}_k$ and $\hat{p_k} \to \hat{p_k}/\sqrt{\omega_k}$.

Thus, the two real and continuous sets of eigenvectors and corresponding eigenvalues given by the two quadratures provide two continuous bases which are interrelated via the Fourier transform:

$$|q\rangle = \frac{1}{\sqrt{\pi}} \int_{-\infty}^{\infty} e^{-2ipq} |p\rangle \, \mathrm{d}p \qquad \text{and} \qquad |p\rangle = \frac{1}{\sqrt{\pi}} \int_{-\infty}^{\infty} e^{+2ipq} |q\rangle \, \mathrm{d}q. \tag{2.15}$$

In general, for an N-mode state residing in tensor product space $\mathcal{H}^{\otimes N}$ we have that

$$\hat{\mathbf{x}}^T |\mathbf{x}\rangle = \mathbf{x}^T |\mathbf{x}\rangle \tag{2.16}$$

where $\mathbf{x} \in \mathbb{R}^{2N}$ and $|\mathbf{x}\rangle := (|x_1\rangle, |x_2\rangle, \ldots, |x_{2N}\rangle)^T$. The quadrature eigenvalues $\mathbf{x}$ are continuous eigenvalues describing observables pertaining to each mode constituting the entire multimode bosonic system. To exploit their use in this regime we introduce the phase space representation of quantum states.

2.2.2 Phase space representation

The quantum state of an N-mode bosonic system contains all of its physical information and is represented by the density operator, $\hat{\rho}$. This is a trace-one positive operator acting on the Hilbert space in which it resides and, as will be introduced here, has an equivalent representation in terms of quasiprobability distributions over a real phase space. One example is that of a Gaussian state whose phase space distribution function, termed the Wigner function, is of Gaussian form.

The Weyl operator, which provides us with a mapping between the Hilbert and phase spaces, is given by

$$D(\boldsymbol{\xi}) := \exp\Big(i\hat{\mathbf{x}}^T \boldsymbol{\Omega} \boldsymbol{\xi}\Big), \tag{2.17}$$

with $\boldsymbol{\xi} \in \mathbb{R}^{2N}$. This allows us to define the relationship between density operator $\hat{\rho}$ and its Wigner characteristic function

$$\chi(\boldsymbol{\xi}) := \mathrm{Tr}[\hat{\rho} D(\boldsymbol{\xi})]. \tag{2.18}$$

Thus the density operator $\hat{\rho}$ of any Fock space quantum state can always be expressed in terms of the Fourier transform of its characteristic function, $\chi(\boldsymbol{\xi})$, giving the Wigner function

$$W(\mathbf{x}) = \int_{\mathbb{R}^{2N}} \frac{\mathrm{d}^{2N}\boldsymbol{\xi}}{(2\pi)^{2N}} \exp\left(-i\mathbf{x}^T \boldsymbol{\Omega} \boldsymbol{\xi}\right) \chi(\boldsymbol{\xi}), \tag{2.19}$$

defined on the real, symplectic phase space $\mathcal{K} := (\mathbf{R}^{2N}, \boldsymbol{\Omega})$ spanned by the real, continuous variables $\mathbf{x} \in \mathbb{R}^{2N}$.

In real terms, the quasi-probabilistic character of the real-valued Wigner function means that though it has a calculable mean and variance it is generally non-positive. Proper normalisation (for a single-mode state),

$$\int\int W(q,p)\mathrm{d}q\mathrm{d}p = 1, \tag{2.20}$$

arises from the fact that any physical $\hat{\rho}$ has unit trace. This allows for the correct determination of marginal distributions via

$$\int W(q,p)\mathrm{d}q = \langle p|\,\hat{\rho}\,|p\rangle \qquad \text{and} \qquad \int W(q,p)\mathrm{d}p = \langle q|\,\hat{\rho}\,|q\rangle\,. \tag{2.21}$$

Analogous to classical averaging techniques, the expectation (mean) value of an operator $\hat{A}$ can be calculated by

$$\langle\hat{A}\rangle = \mathrm{Tr}\Big(\hat{\rho}\hat{A}\Big) = \int W(q,p)A(q,p)\mathrm{d}q\mathrm{d}p. \tag{2.22}$$

The first two statistical moments of the quantum state $\hat{\rho}$ are the most important quantities used for Wigner representations as, in this regime, they alone (for certain classes of states) are capable of fully characterising the state. The first moment is the displacement vector or mean value, given by

$$\bar{\mathbf{x}} := \langle\hat{\mathbf{x}}\rangle = \mathrm{Tr}(\hat{\rho}\hat{\mathbf{x}}). \tag{2.23}$$

The second moment is the covariance of canonical variables and is given by the covariance matrix (CM) $\mathbf{V}$ whose elements are given by

$$V_{ij} := \frac{1}{2}\,\mathrm{Tr}(\{\hat{x}_i - x_i, \hat{x}_j - x_j\}, \hat{\rho}), \tag{2.24}$$

where $\{,\}$ denotes the anticommutator and $\mathrm{Tr}\Big(\hat{\rho}\hat{O}\Big) = \bar{O} \equiv \langle\hat{O}\rangle$ is the expectation value of the operator $\hat{O}$ with $\hat{\rho}$ being the density matrix of the quantum state. Diagonal elements, V_{ii}, are simply the variances of the individual quadrature operators.

The positive-definite CM $\mathbf{V} > 0$ is real and symmetric, describing a physical state if and only if it obeys the uncertainty relation [28],

$$\mathbf{V} + i\boldsymbol{\Omega} \geq 0. \tag{2.25}$$

2.2.3 Gaussian states and examples

Quantum continuous variable systems are quantum systems obeying canonical commutation relations, requiring the adoption of infinite-dimensional Hilbert spaces regardless of the number of degrees of freedom considered. This results in complex and often mathematically intractable dynamics.

Gaussian states are a particular class of quantum states whose phase space representation can be fully described in terms of only their first and second moments, in other words, they possess density operators $\hat{\rho} := \hat{\rho}(\bar{\mathbf{x}}, \mathbf{V})$. Essentially, for what is, in fact, an infinite-dimensional system, their full character and behaviour may be modelled by only considering, for an N-mode Gaussian state, a $2N$-dimensional mean vector and a $2N \times 2N$ CM. This is powerful since it renders the study of such continuous variable quantum states tractable. At first glance, it may seem that constraining ourselves to the Gaussian realm may be rather restrictive but, as will be seen throughout the course of this work, these constraints are ordinarily met through existing experimental techniques in quantum optics. Further, Gaussian measurements which are positive-operator valued measures (POVMs) preserving Gaussian character, can be carried out with relatively high efficiency and the formalism allows for the inclusion of quantum noise to be considered quite seamlessly.

A state is considered Gaussian if its Wigner phase space representation, in terms of the characteristic χ or distribution W functions, is of Gaussian form [8, 10]. Furthermore, a Gaussian state is pure if and only if the determinant of its CM is unity, i.e., $\det\mathbf{V} = 1$. In addition, a pure state is Gaussian if and only if its Wigner function is non-negative [26, 27].

The following will provide the reader with an overview of important examples of Gaussian states which will appear frequently throughout this thesis:

1. Vacuum and thermal states

   The most fundamental single-mode Gaussian state is the vacuum state, $|0\rangle$. It is the eigenstate of the number operator with eigenvalue zero, with mean $\bar{\mathbf{x}} = (0, 0)^T$ and CM, given by

   $$\mathbf{V}_{|0\rangle} = \begin{pmatrix} 1 & 0 \\ 0 & 1 \end{pmatrix}, \tag{2.26}$$

   i.e., simply the identity matrix. Its quadratures have the minimum possible variance reachable in a symmetric manner, referred to as the vacuum or shot-noise limit. Note that all pure Gaussian states are obtained by applying unitary operations generated by second-order (in field operators) Hamiltonians on the vacuum state.

   Thermal states are a fundamental class of Gaussian states upon which all other Gaussian states may be decomposed; they are defined as the states which maximise the von Neumann entropy,

   $$S := -\operatorname{Tr}(\hat{\rho}\log\hat{\rho}), \tag{2.27}$$

   for fixed mean photon number $\bar{n} \geq 0$. In the Fock state representation they have the

form,

$$\hat{\rho}^{\text{th}}(\bar{n}) = \sum_{n=0}^{+\infty} \frac{\bar{n}^n}{(\bar{n}+1)^{n+1}} |n\rangle\langle n| \,. \tag{2.28}$$

As with the vacuum state, their first moment is zero and their CM takes the form

$$\mathbf{V}_{\text{th}} = (2\bar{n}+1) \begin{pmatrix} 1 & 0 \\ 0 & 1 \end{pmatrix}. \tag{2.29}$$

2. Coherent states

Coherent states (single- or multi-mode) are a type of Gaussian state obtained by displacing vacuum states of the right modal order. Explicitly, an M-mode coherent state is given by

$$|\boldsymbol{\alpha}\rangle\langle\boldsymbol{\alpha}| = \bigotimes_{i=1}^{M} |\alpha_i\rangle\langle\alpha_i|_i \,, \tag{2.30}$$

where the vector $\boldsymbol{\alpha} := (\alpha_1, \ldots, \alpha_M)$ is a row vector consisting of all the amplitudes $\alpha_i = (q_i + ip_i)/\sqrt{2} \in \mathbb{C}$ obtained by acting on each of the vacuum states, $|0\rangle_i$, with the displacement operator, defined by

$$D(\alpha) := \exp\Big(\alpha\hat{a}^\dagger - \alpha^\star\hat{\alpha}\Big), \tag{2.31}$$

such that $|\alpha_i\rangle_i = D(\alpha_i)\,|0\rangle_i$.

Since they arise from vacuum displacement, coherent states are also states of minimum uncertainty with CM $\mathbf{V} = \mathbf{1}$. Their mean value, however, has been displaced with a finite value $\bar{\mathbf{x}}$ completely determined by $\boldsymbol{\alpha}$ such that coherent state $|\alpha_i\rangle$ has first moments $x = \sqrt{2}\text{Re}(\alpha_i)$ and $p = \sqrt{2}\text{Im}(\alpha_i)$. They can be decomposed in the number-state representation as

$$|\alpha\rangle = \exp\left(-\frac{1}{2}|\alpha|^2\right) \sum_{n=0}^{\infty} \frac{\alpha^n}{\sqrt{n!}} |n\rangle \,. \tag{2.32}$$

In the context of quantum optics, states are classical if they can be expressed as some normalised, probabilistic superposition of coherent states, that is, coherent states can provide a basis for the decomposition of any classical state mixture [29]. Thus, such states are representative of those used in today's optics-based technologies, including classical radar protocols.

Considering the phase space representation of Gaussian states (Sec. 2.2.2), in particular,

the Wigner function and associated marginal distributions (Eq. (2.21)), the generic density operator of M bosonic modes may be written as

$$\hat{\rho} = \int \mathrm{d}^{2M}\boldsymbol{\alpha}\mathcal{P}(\alpha)\,|\boldsymbol{\alpha}\rangle\langle\boldsymbol{\alpha}|\,, \tag{2.33}$$

where $\mathcal{P}(\alpha)$ is a normalised quasi-probability distribution. This is also known as the Glauber-Sudarshan P-representation [29] of a quantum state. There are some cases in which one can think of $\mathcal{P}(\alpha)$ as a probability density for the distribution of $\boldsymbol{\alpha}$ over the complex plane, as in the case where the state is pure and the density operator is a simple projection operator. However for different values of amplitude, the projection operators are not orthogonal and this interpretation is not possible - for two coherent states $|\alpha\rangle$ and $|\beta\rangle \neq |\alpha\rangle$, the inner product $\langle\beta|\alpha\rangle \neq 0$. Nonetheless, they still form a complete set in that they resolve the identity,

$$\frac{1}{\pi}\int_{\mathbb{C}} |\alpha\rangle\langle\alpha|\,\mathrm{d}^2\alpha = \mathbf{1}. \tag{2.34}$$

Owing to these two properties, coherent states actually form an overcomplete set and, as such, allow for the diagonal decomposition of any density matrix $\hat{\rho}$.

Normalisation of the density operator demands that $\mathcal{P}(\alpha)$ be normalised also. The way in which it differs from a true probability distribution is that there are some regions on the complex plane in which $\mathcal{P}(\alpha)$ takes on negative values. Classical states are those which have $\mathcal{P}(\alpha) > 0$ and can be prepared solely through some sequence of local operations and classical communication (LOCCs) and, in fact, positivity of $\mathcal{P}(\alpha)$ is a sufficient condition for separability (though does not necessarily imply classicality). In contrast, its negativity, while not necessarily translating to entanglement, is a signature of non-classicality. Indeed, entangled states are only a subset of non-classical states [30]. We can also note, as a consequence of this, that the borderline point between classical and non-classical states is given by the case where $\mathcal{P}(\alpha) = 0$ and are thus represented by a delta function, as is the case for a coherent state.

3. Two-mode squeezing and Einstein-Podolski-Rosen states

Another important type of Gaussian state, and one which will be studied at length in this work, is the two-mode squeezed vacuum (TMSV). The effect of squeezing on a single bosonic mode is to alter the noise variances of its two associated quadratures in an asymmetric manner. Characterised by a squeezing parameter, one quadrature's noise variance is squeezed below the quantum shot noise while the other is antisqueezed above it. Applied to two-mode vacuum states, this squeezing takes place on pairs of quadratures belonging to different modes such that they become correlated, with maximum

correlation resulting in entanglement and the formation of an Einstein-Podolski-Rosen (EPR) state.

In the Heisenberg picture, quadratures are transformed by the two-mode squeezing transformation, $\mathbf{S}_r$, characterised by the squeezing parameter r,

$$\mathbf{S}_r = \begin{pmatrix} \cosh r\mathbf{1} & \sinh r\mathbf{Z} \\ \sinh r\mathbf{Z} & \cosh r\mathbf{1} \end{pmatrix}, \tag{2.35}$$

where $\mathbf{1}$ is the two-dimensional identity matrix and $\mathbf{Z} := \mathrm{diag}(1, -1)$ is the Pauli-Z operator. Applied to a two-mode vacuum, we obtain the TMSV or EPR state $\hat{\rho}_{\mathrm{EPR}}(r) = |r\rangle\langle r|_{\mathrm{EPR}}$, with

$$|r\rangle_{\mathrm{EPR}} = \sqrt{1-\lambda^2} \sum_{n=0}^{\infty} (-\lambda)^n |n\rangle_a \langle n|_b \,, \tag{2.36}$$

and $\lambda = \tanh r \in [0, 1]$. This state has zero mean ($\bar{\mathbf{x}} = 0$) and its CM is given by

$$\mathbf{V} = \begin{pmatrix} \nu\mathbf{1} & \sqrt{\nu^2-1}\mathbf{Z} \\ \sqrt{\nu^2-1}\mathbf{Z} & \nu\mathbf{1} \end{pmatrix}, \tag{2.37}$$

where $\nu = \cosh 2r$ quantifies the noise variance in the system. We will now introduce a new parametrisation of this CM which will be largely employed throughout the remainder of this thesis. By defining the mean number of thermal photons present in each mode, n_m, in terms of the squeezing parameter, r, as

$$n_m = \sinh^2 r, \tag{2.38}$$

the CM becomes

$$\mathbf{V} = \begin{pmatrix} (2n_m+1)\mathbf{1} & 2\sqrt{n_m(n_m+1)}\mathbf{Z} \\ 2\sqrt{n_m(n_m+1)}\mathbf{Z} & (2n_m+1)\mathbf{1} \end{pmatrix}. \tag{2.39}$$

For the two-mode squeezed state, it can be seen that variances between quadratures of the two modes behave as $V(\hat{q}_1 - \hat{q}_2) = V(\hat{p}_1 + \hat{p}_2) = e^{-2r}$. For $r = 0$, the state corresponds to a two-mode vacuum and these variances are equal to 1, corresponding to the quantum shot-noise. Meanwhile, any two-mode squeezing $r > 0$ results in $V(\hat{q}_1 - \hat{q}_2) = V(\hat{p}_1 + \hat{p}_2) < 1$, meaning that the correlations between the quadratures of the two systems fall below the quantum shot-noise implying the presence of bipartite entanglement. Taking the limit of $r \to \infty$ yields the ideal (though unphysical) EPR

state with perfect correlations: $\hat{q}_1 = \hat{q}_2$ and $\hat{p}_1 = -\hat{p}_2$. The EPR state is the most commonly used Gaussian entangled state and has maximally-entangled quadratures, given its average photon number.

Note: Eq. (2.21) shows that the marginal Wigner function along a given direction of phase space gives the probability distribution of quantum measurements of that associated quadrature operator such that, at least for Gaussian states, the Wigner function provides one with a local model of quadrature measurements. Restricting oneself to quadrature measurements, these systems may be modelled by some classical Gaussian distribution and signatures of non-locality will never be shown. Thus, the exploitation of quantum entanglement exhibited in such Gaussian states as the TMSV would require one to look beyond the phase space formalism.

2.2.4 Gaussian measurements

We proceed to introduce the class of non-deterministic maps which encompass well-known detection schemes within quantum optics such as homodyne and heterodyne, after first discussing (non-Gaussian) photon counting.

Photon counting detectors correspond to resolution of the identity $\mathbf{1} = \sum_{n=0}^{\infty} |n\rangle\langle n|$ where $|n\rangle$ is the Fock (photon number) state of the mode under observation. This measurement projects a quantum state $\hat{\rho}$ onto an eigenstate of the Hamiltonian (Eq. (2.1)), $|n\rangle$, rendering the possibility of distinguishing any two excitations of the field somewhat difficult, particularly at low energies. Practically, the use of photodetectors is typically rendered to an on/off format whether either no counts are recorded, returning '0', or any (one or more) are recorded, returning '1'. As such, a given photodetector will be limited in the the intensity of light it can detect, since between individual detection events there is typically a "dead time" during which it resets. Further, with respect to our particular interest in the detection of microwaves, individual photons have energies several orders of magnitude smaller than optical photons. Often, microwave single photon detection typically involves up-conversion of microwave frequencies to the optical domain which can be photodetected with relatively high efficiency (see also Section 3.3.3). Unfortunately, the converter itself typically has low efficiency.

Homodyne detection is simply the projective measurement of a canonical operator $\hat{x}_\phi = \cos\phi\hat{q} + \sin\phi\hat{p}$ with outcome probabilities $p(x_\phi) = \langle x_\phi|\,\hat{\rho}\,|x_\phi\rangle$. It results from mixing the initial state $\hat{\rho}$ with a local oscillator, typically a strong coherent state $|\alpha\rangle$ with $\alpha = |\alpha|e^{i\phi}$ and

$|\alpha| \gg 1$, at a 50:50 beam splitter and subtracting detected intensities at its output. The term "homodyne" refers to the mixing occurring at the same frequency. One can choose which quadrature to measure by tuning ϕ to be 0 or $\pi/2$ for measuring $\hat{q}$ or $\hat{p}$, respectively.

Heterodyne detection corresponds to the resolution of the identity in terms of projectors on coherent states: $\mathbf{1} = \frac{1}{\pi}\int_{\mathbb{C}} |\alpha\rangle\langle\alpha| \, \mathrm{d}^2\alpha$. Its measurement outcomes, labelled by α, are obtained with probability $\langle\alpha| \, \hat{\rho} \, |\alpha\rangle$ for single-mode $\hat{\rho}$. Practically it is similar to homodyne detection but the mixing laser frequency is not the same as the input state. Such a measurement is carried out through a scheme involving two homodyne set-ups where the signal is split into two via a 50:50 beam splitter. While allowing one to measure both quadratures simultaneously, this comes at the cost of introducing noise whose minimum is the vacuum or shot-noise, since they do not commute.

2.2.5 Symplectic decomposition of Gaussian states

One of the most powerful tools used in the study of Gaussian states is based on their symplectic decomposition in accordance with Williamson's theorem. Williamson's theorem states that every positive-definite real matrix of even dimension can be put into diagonal form by a symplectic transformation [31]. In the context of continuous variable quantum optics, the theorem can be applied to CMs such that given an arbitrary M-mode CM $\mathbf{V}$ there exists a symplectic matrix $\mathbf{S}$ which satisfies

$$\mathbf{V} = \mathbf{S}\mathbf{V}^{\oplus}\mathbf{S}^{T}, \quad \mathbf{V}^{\oplus} := \bigoplus_{j=1}^{M} \nu_j \mathbf{1}. \tag{2.40}$$

Here, the diagonal matrix $\mathbf{V}^{\oplus}$ is called the Williamson form of the CM $\mathbf{V}$. The set $\{\nu_j\}_{j=1}^{M}$ is the symplectic spectrum, consisting of each of the M positive-valued symplectic eigenvalues ν_j, can be computed by diagonalising the matrix $|i\mathbf{\Omega}\mathbf{V}|$.

The uncertainty relation, Eq. (2.25), remains invariant under symplectic transformations since $\mathbf{\Omega} = \mathbf{S}\mathbf{\Omega}\mathbf{S}^{T}$. Therefore it can be expressed in terms of the symplectic eigenvalues which are the M independent symplectic invariants of a $2M \times 2M$ CM. The condition $\mathbf{V} > 0$ implies that $\mathbf{V}^{\oplus} \geq \mathbf{1}$, posing direct restrictions on the values which the symplectic eigenvalues may take. It is required that the CM be positive definite and the symplectic eigenvalues $\nu_j \geq 1$ for $j \in [1, \ldots, M]$.

Two-mode Gaussian states may be specified by relatively simple formulae allowing for easy determination of their symplectic spectra. Consider the CM of a two-mode Gaussian state

in block form,

$$\mathbf{V} = \begin{pmatrix} \mathbf{A} & \mathbf{C} \\ \mathbf{C^T} & \mathbf{B} \end{pmatrix}, \tag{2.41}$$

where $\mathbf{A} = \mathbf{A^T}$, $\mathbf{B} = \mathbf{B^T}$ and $\mathbf{C}$ are 2×2 real matrices. The state's symplectic spectrum $\{\nu_-, \nu_+\}$ may be computed via

$$\nu_\pm = \sqrt{\frac{\Delta \pm \sqrt{\Delta^2 - 4\text{det}\mathbf{V}}}{2}}, \tag{2.42}$$

with $\Delta := \text{det}\mathbf{A} + \text{det}\mathbf{B} + 2\text{det}\mathbf{C}$ [32], such that the uncertainty relations become [28, 33]

$$\mathbf{V} > 0, \quad \text{det}\mathbf{V} \geq \mathbf{1}, \quad \text{and} \quad \Delta \leq 1 + \text{det}\mathbf{V}. \tag{2.43}$$

The above can be extended for a special class of two-mode Gaussian states with CM of the form

$$\mathbf{V} = \begin{pmatrix} a\mathbf{1} & \mathbf{C} \\ \mathbf{C} & b\mathbf{1} \end{pmatrix}, \quad \mathbf{C} = \begin{pmatrix} c_1 & 0 \\ 0 & c_2 \end{pmatrix}, \tag{2.44}$$

where a, b, c_1 and $c_2 \in \mathbb{R}$ still satisfying the uncertainty relations. When we have that $c_1 = -c_2 := c \geq 0$, the symplectic eigenvalues are [34, 35]

$$\nu_\pm = \frac{\sqrt{y} \pm (b - a)}{2}, \quad \text{where} \quad y := (a + b)^2 - 4c^2, \tag{2.45}$$

and the symplectic matrix $\mathbf{S}$ which puts $\mathbf{V}$ into its diagonal form, satisfying $\mathbf{V} = \mathbf{S}\mathbf{V}^{\otimes}\mathbf{S^T}$ is

$$\mathbf{S} = \begin{pmatrix} \omega_+\mathbf{1} & \omega_-\mathbf{Z} \\ \omega_-\mathbf{Z} & \omega_+\mathbf{1} \end{pmatrix}, \quad \omega_\pm := \sqrt{\frac{a + b \pm \sqrt{y}}{2\sqrt{y}}}. \tag{2.46}$$

The above method forms a very convenient way to compute the symplectic spectra and diagonalising symplectic matrix for a two-mode Gaussian state with CM $\mathbf{V}$. Recently, a method has been derived for the determination of the symplectic matrix $\mathbf{S}$ for an arbitrary N-mode CM $\mathbf{V}_N$ in terms of relatively straightforward to compute submatrix determinants [36]. Such a tool could allow for the analysis of more exotic Gaussian states.

2.3 Quantum hypothesis testing

Quantum illumination (QI), at its most basic level, is essentially a task of quantum hypothesis testing [37] which plays a crucial role in quantum information theory [38]. In other words,

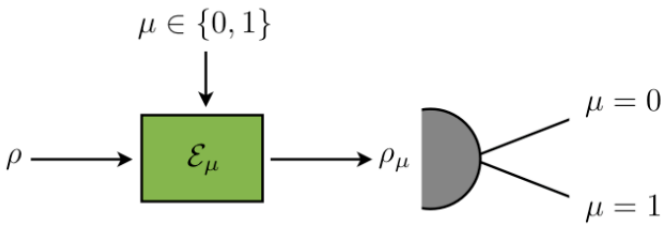

FIG. 2.1: The basic problem of hypothesis testing. An initial state $\hat{\rho}$ passes through a quantum channel which is encoded by an unknown parameter, in this case a classical bit, $\mu \in \{0, 1\}$. It is the measurement of the final state $\hat{\rho}_\mu$, parametrised by μ, with output $\mu = 0$ or $\mu = 1$ which provides the parameter estimation and in turn a determination of the underlying hypothesis.

one constructs, for two alternate hypotheses, final forms of a quantum state after entering a quantum channel encoded by the respective hypotheses and is tasked with being able to distinguish between the two. The ability to do this accurately, with a low probability of error, directly relates to an ability to determine the correct result out of the two alternate hypotheses.

Consider an experiment with dichotomous outcomes which we will call the null hypothesis, H_0, and the alternative hypothesis, H_1, corresponding to negative and positive outcomes, respectively. Let the prior probability of hypothesis H_μ be $p = p_\mu$ with $\mu \in \{0, 1\}$ such that

$$\begin{aligned} H_0 : &\quad \hat{\rho} = \hat{\rho}_0, \quad p = p_0, \\ H_1 : &\quad \hat{\rho} = \hat{\rho}_1, \quad p = p_1. \end{aligned} \tag{2.47}$$

Then, the probabilities of getting a false positive or a false negative in our determination is given by

$$P(\mu = 1|\hat{\rho} = \hat{\rho}_0) = P(H_1|H_0), \tag{2.48}$$

and

$$P(\mu = 0|\hat{\rho} = \hat{\rho}_1) = P(H_0|H_1), \tag{2.49}$$

respectively and the total probability in obtaining an error, of any kind, in our discrimination process is

$$P_{\text{err}} = p_1 P(H_0|H_1) + p_0 P(H_1|H_0) = \frac{1}{2}(P(H_0|H_1) + P(H_1|H_0)), \tag{2.50}$$

where the last equality holds in the case of equally-likely hypotheses.

Certain parameters essentially encode the quantum channel through which a quantum state passes, and this overall evolution in turn encodes the final form which the quantum state

will take, thus making this procedure possible. This, fundamentally, is the premise behind quantum technologies such as quantum sensing and quantum metrology. Parameters alter the geometry of the Hilbert space in which the quantum state resides so that as they evolve, through whatever processes, the "velocity" with which they change can vary dramatically. Considering this in the reverse, certain encodings of input quantum states, e.g. those with maximally entangled quadratures, could have similar sensitivity to given parameters, thus experiencing a more rapidly varying geometry. Such responses owing to sensitivities to state-changing parameters can be characterised in terms of the quantum Fisher information to yield ultimate sensitivity capacities.

A fundamental aspect of quantum mechanics says that it is generally impossible to perfectly distinguish between two non-orthogonal states [39]. Instead, we can consider the distinguishability of quantum states as how well they can be identified against one another. With this consideration, various measures have been constructed in order to quantify the discrepancy between these states realising distinguishability techniques such as minimum error discrimination. Such tools allow for the, albeit imperfect due to allowance of an error probability, discrimination of non-orthogonal states.

The simplest example of hypothesis testing is that of a binary decision reduced to the statistical discrimination of two hypotheses (null and alternative), each occurring with some a priori probability. Note that in the remainder of this thesis it will be assumed that the two hypotheses are equally-likely, i.e., we are faced with uninformative priors. In QI with Gaussian states, these hypotheses are formulated in terms of possible covariance matrices describing joint states of two bosonic modes whose form is dependent on the actual truth of a situation on which the decision is being made. Two forms of error may occur: a Type I error ("false alarm") where the null hypothesis is falsely rejected and, conversely, a Type II error ("false negative") where the alternative hypothesis is wrongly rejected. Associated with each of these is a "cost" of making the error, which may or may not be the same for each. For example, if we consider the possible result of a diagnostic test then it is clear that the risk associated with receiving a false negative could far outweigh that associated with a false positive. In such scenarios, one may consider asymmetric testing in order to take into account these discrepancies. On the other hand, a symmetric approach may be used if one's aim is to obtain a global minimisation over all errors, irrespective of their origin.

2.3.1 Symmetric hypothesis testing

In the case of symmetric testing both Type I and Type II errors are combined such that the total error is minimised. This achieves an overall bound describing the decay of the discrimination error probability as a function of the number of independent samples considered. It is essentially computed as the average of the two types of error, weighted by their respective hypotheses' prior probabilities. Consider M independent, identically distributed copies of the state $\hat{\rho}_\mu$ (denoted by the tensor product state $\hat{\rho}_\mu^{\otimes M}$), encoded by classical bit $\mu \in \{0, 1\}$ corresponding to two equiprobable quantum channels between which we must distinguish. The optimal measurement for the discrimination is the dichotomic POVM [37]

$$E_0 = \Pi(\gamma_+), \quad E_1 = 1 - \Pi(\gamma_+), \tag{2.51}$$

where $\Pi(\gamma_+)$ is the projector on the positive part γ_+ of the non-positive operator, also called the Helstrom matrix, $\gamma := \hat{\rho}_0 - \hat{\rho}_1$. Using such a measurement, the two states $\hat{\rho}_0$ and $\hat{\rho}_1$ may be discriminated with a *minimum* error probability given by the Helstrom bound [37],

$$P_{\text{err}}^{\text{H}} = \frac{1 - D_{\text{Tr}}(\hat{\rho}_0, \hat{\rho}_1)}{2}, \tag{2.52}$$

where $D_{\text{Tr}}(\hat{\rho}_0, \hat{\rho}_1) := \text{Tr}|\hat{\rho}_0 - \hat{\rho}_1|/2$ is the trace distance between $\hat{\rho}_0$ and $\hat{\rho}_1$.

The quantum Chernoff bound

The trace distance is often difficult to compute analytically, thus the Helstrom bound, Eq. (2.52), is often replaced with approximations. One such approximation is the quantum Chernoff bound (QCB) [40],

$$P_{\text{err}}^{\text{QCB}} := \frac{1}{2}\left(\inf_{0 \le s \le 1} C_s\right), \quad C_s := \text{Tr}\left(\hat{\rho}_0^s \hat{\rho}_1^{1-s}\right), \tag{2.53}$$

which provides an upper bound such that $P_{\text{err}}^{\text{min}} \le P_{\text{err}}^{\text{QCB}}$. Minimisation of the s-overlap C_s occurs over all values of $0 \le s \le 1$ bearing in mind the discontinuities that may occur at the interval boundaries, that is, for $s = 0, 1$ where we have $C_0 = C_1 = 1$. Note that, though not considered in this thesis, we can easily extend the QCB to cover cases where the two hypotheses are not equiprobable [40]:

$$P_{\text{QCB}} := \inf_{0 \le s \le 1} \pi_0^s \pi_1^{1-s} \,\text{Tr}\left[(\hat{\rho}_{R,I}^0)^s (\hat{\rho}_{R,I}^1)^{1-s}\right]. \tag{2.54}$$

Forgoing the minimisation process and setting $s = 1/2$ we can define a much simpler, though weaker, upper bound[2] for the error probability given by the quantum Bhattacharyya bound (QBB) [10, 41],

$$P_{\text{err}}^{\text{QBB}} := \frac{1}{2} \operatorname{Tr}\left(\sqrt{\hat{\rho}_0}\sqrt{\hat{\rho}_1}\right). \tag{2.55}$$

Note that the above formulae consider single-use protocols. Extension for arbitrary uses $M \geq 1$ is straightforward via

$$P_{\text{err}}^{\text{QCB}} := \frac{1}{2}\left(\inf_{0\leq s\leq 1} C_s\right)^M, \tag{2.56}$$

recovering the QBB for M uses by setting $s = 1/2$.

For Gaussian states, there exists a relatively simple formula for the computation of the QCB in terms of their statistical moments of the states alone [10, 41]. Consider two arbitrary N-mode Gaussian states, $\hat{\rho}_0(\bar{\mathbf{x}}_0, \mathbf{V}_0)$ and $\hat{\rho}_1(\bar{\mathbf{x}}_1, \mathbf{V}_1)$, with mean $\bar{\mathbf{x}}_i$ and CM $\mathbf{V}_i$ where $i = 0, 1$, respectively. Then we can write the Gaussian formula for the s-overlap, Eq. (2.53)

$$C_s = 2^N \sqrt{\frac{\det \boldsymbol{\Pi}_s}{\det \boldsymbol{\Sigma}_s}} \exp\left(-\frac{\delta^T \boldsymbol{\Sigma}_s^{-1} \delta}{2}\right), \tag{2.57}$$

where $\delta = \bar{\mathbf{x}}_0 - \bar{\mathbf{x}}_1$ is the difference in mean values. The functions $\boldsymbol{\Pi}_s$ and $\boldsymbol{\Sigma}_s$ are defined as

$$\boldsymbol{\Pi}_s := G_s(\mathbf{V}_0^{\oplus}) G_{1-s}(\mathbf{V}_1^{\oplus}), \tag{2.58}$$

$$\boldsymbol{\Sigma}_s := \mathbf{S}_0 \left[\Lambda_s\left(\mathbf{V}_0^{\oplus}\right)\right] \mathbf{S}_0^T + \mathbf{S}_1 \left[\Lambda_{1-s}\left(\mathbf{V}_1^{\oplus}\right)\right] \mathbf{S}_1^T, \tag{2.59}$$

where we have introduced the two real functions

$$G_s(x) = \frac{2^s}{(x+1)^s - (x-1)^s}, \tag{2.60}$$

$$\Lambda_s(x) = \frac{(x+1)^s + (x-1)^s}{(x+1)^s - (x-1)^s}, \tag{2.61}$$

which are computed over the Williamson form $\mathbf{V}_i^{\oplus}$ of CM $\mathbf{V}_i$ according to the rule

$$f\left(\mathbf{V}_i^{\oplus}\right) = f\left(\bigoplus_{k=1}^{N} \nu_k \mathbf{1}\right) = \bigoplus_{k=1}^{N} f(\nu_k)\mathbf{1}. \tag{2.62}$$

[2] Despite this bound being typically weaker, it turns out that the minimum for the problem of QI-based quantum target detection coincides with $s = 1/2$. Thus there is no loss of knowledge with making this simplification.

2.3.2 Asymmetric hypothesis testing

In asymmetric testing, we wish to minimise one type of error as much as possible while allowing for some flexibility on the other, whose cost is not necessarily as great. Formulating the problem of QHT as an M-copy discrimination problem,

$$\begin{aligned} H_0 &: \hat{\rho} = \hat{\rho}_0^{\otimes M} = \hat{\rho}_0 \otimes \ldots \otimes \hat{\rho}_0, \\ H_1 &: \hat{\rho} = \hat{\rho}_1^{\otimes M} = \hat{\rho}_1 \otimes \ldots \otimes \hat{\rho}_1, \end{aligned} \tag{2.63}$$

on which we may perform collective measurements. As in the symmetric case, the optimal choice of measurement is the dichotomic POVM given by Eq. (2.51). Associated with such a measurement are two forms of error: the probability of a false alarm

$$\alpha_M := P(H_1|H_0) = \mathrm{Tr}\left(E_1 \hat{\rho}_0^{\otimes M}\right), \tag{2.64}$$

and the probability of a false negative

$$\beta_M := P(H_0|H_1) = \mathrm{Tr}\left(E_0 \hat{\rho}_1^{\otimes M}\right). \tag{2.65}$$

The probabilities are dependent on the number of independent samples used in the test such that in the limit of a very large sample, $M \gg 1$, both error probabilities tend to zero, i.e.,

$$\alpha_M \simeq \frac{1}{2} e^{-\alpha_R M}, \quad \beta_M \simeq \frac{1}{2} e^{-\beta_R M}, \tag{2.66}$$

where we define the 'error exponents' or 'rate limits' as

$$\alpha_R = -\lim_{M \to +\infty} \frac{1}{M} \ln \alpha_M, \tag{2.67}$$

$$\beta_R = -\lim_{M \to +\infty} \frac{1}{M} \ln \beta_M. \tag{2.68}$$

Note that the above formulae for error exponents give the asymptotic behaviour only.

The quantum relative entropy

In the asymmetric setting, such as that of a medical diagnosis, the Type II error is the one we wish to ideally avoid. It is not possible to make both error probabilities arbitrarily small simultaneously so, instead, by placing a relatively loose constraint $\alpha < \epsilon$ on the Type I error allows freedom to minimise β. The quantum Stein's lemma [42, 43] states that the quantum

relative entropy (QRE) between two quantum states is the optimal decay rate for the Type II error probability, given some fixed constraint on the Type I error probability, given by

$$D\left(\hat{\rho}_0||\hat{\rho}_1\right) = \begin{cases} \mathrm{Tr}[\hat{\rho}_0(\log\hat{\rho}_0 - \log\hat{\rho}_1)], & \text{if } \mathrm{supp}(\hat{\rho}_0) \subseteq \mathrm{supp}(\hat{\rho}_1); \\ +\infty, & \text{otherwise.} \end{cases} \tag{2.69}$$

The quantum Stein's lemma further states that if the Type II error tends to 0 with an exponent larger than the QRE, $D\left(\hat{\rho}_0||\hat{\rho}_1\right)$, then the Type I error converges to 1 [43].

A formula exists [44] for computing the QRE between two arbitrary Gaussian states in terms of their statistical moments alone, without the need for determination of their symplectic spectra. Consider two arbitrary N-mode Gaussian states, $\hat{\rho}_0(\bar{\mathbf{x}}_0, \mathbf{V}_0)$ and $\hat{\rho}_1(\bar{\mathbf{x}}_1, \mathbf{V}_1)$, with mean $\bar{\mathbf{x}}_i$ and CM $\mathbf{V}_i$ where $i = 0, 1$. Then the QRE between them is given by

$$D\left(\hat{\rho}_0||\hat{\rho}_1\right) = -\Sigma\left(\mathbf{V}_0, \mathbf{V}_0\right) + \Sigma\left(\mathbf{V}_0, \mathbf{V}_1\right), \tag{2.70}$$

where

$$\Sigma\left(\mathbf{V}_0, \mathbf{V}_1\right) = \frac{\ln\det\left(\mathbf{V}_1 + \frac{i\boldsymbol{\Omega}}{2}\right) + \mathrm{Tr}\left(\mathbf{V}_0\mathbf{G}_2\right) + \delta^T\mathbf{G}_1\delta}{2\ln 2}, \tag{2.71}$$

with $\delta = \bar{\mathbf{x}}_0 - \bar{\mathbf{x}}_1$ and $\mathbf{G}_1 = 2i\boldsymbol{\Omega}\coth^{-1}\left(2\mathbf{V}_1 i\boldsymbol{\Omega}\right)$ being the Gibb's matrix [45].

Refinement of quantum Stein's lemma has been provided by considering the second-order (in M) asymptotics [46, 47] to account for the discontinuity observed in the Type I error probability, jumping sharply from 0 to 1, when the Type II error probability increases past the value set by $D\left(\hat{\rho}_0||\hat{\rho}_1\right)$. Tracking the Type II error exponent to second-order depth, that is to order $\sqrt{M}$, allows one to define the quantum relative entropy variance (QREV)

$$V\left(\hat{\rho}_0||\hat{\rho}_1\right) = \mathrm{Tr}\Big[\hat{\rho}_0(\log\hat{\rho}_0 - \log\hat{\rho}_1)^2\Big] - \left(D\left(\hat{\rho}_0||\hat{\rho}_1\right)\right)^2, \tag{2.72}$$

and in turn establish that the optimal Type II error probability, for sample size M, takes the exponential form

$$\exp\left[MD\left(\hat{\rho}_0||\hat{\rho}_1\right) + \sqrt{MV\left(\hat{\rho}_0||\hat{\rho}_1\right)}\Phi^{-1}(\epsilon) + \mathcal{O}(\log M)\right]. \tag{2.73}$$

Here, the first two terms coincide with quantum Stein's lemma and the second-order correction, respectively. The Type I error is constrained to be no larger than some constant $\epsilon \in (0, 1)$ through the use of the cumulative distribution function $\Phi(y) \equiv \frac{1}{\sqrt{2\pi}}\int_{-\infty}^{y}\mathrm{d}x\exp\left(-x^2/2\right)$ for a standard normal random variable.

A relatively simple formula exists for the computation of QREV between two Gaussian states [44], $\hat{\rho}_0$ and $\hat{\rho}_1$, given by

$$V\left(\hat{\rho}_0||\hat{\rho}_1\right) = \frac{\mathrm{Tr}\left[(\boldsymbol{\Gamma}\mathbf{V}_0)^2\right]}{2} + \frac{\mathrm{Tr}\left[(\boldsymbol{\Gamma}\boldsymbol{\Omega})^2\right]}{8} + \delta^T\mathbf{G}_1\mathbf{V}_0\mathbf{G}_1\delta, \tag{2.74}$$

where $\mathbf{\Gamma} = \mathbf{G}_0 - \mathbf{G}_1$ and all other terms are as previously defined.

Note: An alternative approach to asymmetric hypothesis testing exists which considers the quantum Hoeffding bound [48] which may be explored using Gaussian formulae developed in Ref. [49]. This is not considered in this work where we make use of the QRE and QREV described above.

3 Quantum target detection

3.1 Introduction

Quantum target detection is just one example of a quantum technology in which quantum mechanical phenomena are exploited to achieve performances unattainable solely through classical means. After preliminary results showing that entanglement can enhance the distinguishability of entanglement-breaking channels by Sacchi [50] in 2005, 2008 saw Lloyd [18] introduce the protocol of quantum illumination (QI). This approach to quantum target detection is the one most recognisable in the field today; an entanglement-based approach to improving optical radar's capability of detecting a weakly-reflecting object embedded in a bright thermal background. The source is generated in entangled pairs, only one member of which is used to probe the target region while the other is retained at the source awaiting recombination with the signal upon its eventual return. An optimal joint measurement of the pair is tasked with capturing information held by their entangled nature to yield improved sensitivity to the target detection problem.

These initial QI results ignited a plethora of theoretical and experimental investigations with goals to realise a practical quantum radar. Over the years it has been made clear that the realisation of a working quantum radar, at least one based on entanglement, is littered with many theoretical and technological issues whose resolution still remain somewhat unclear. Nonetheless, in the relatively short time that has passed since its inception, QI and our understanding of it have come a long way. While the attainment of the ultimate goal of a long-range quantum radar remains elusive, intermediate results do show that perhaps more modest applications of such a technology could certainly be a real possibility in the near future.

The aim of this chapter is to review the history of quantum target detection, primarily focusing on QI on which this thesis is largely based, and provide an overview of the main concepts, results and progress in the field. This chapter will present QI in a predominately

qualitative fashion, with the underlying mathematics covered in detail throughout the remainder of this thesis during the study of particular aspects of QI. Sec. 3.2 describes approaches to quantum radar, outlining types of quantum sensors which may constitute a real-world quantum radar of the future beyond QI-based protocols. Then, in Sec. 3.3, we cover the history of QI which forms the foundation of quantum target detection schemes, describing the promised potential of such a technology. The challenges and limitations, along with attempts at their resolution, are discussed in Sec. 3.4 and, finally, an overview of QI experiments is provided in Sec. 3.5.

3.2 Approaches to quantum radar

While it tends to be assumed that quantum radar is, definitively, a radar scheme relying on entanglement, that is, a scheme based on QI, it is not necessarily the case. While QI has formed the basis of much literature around quantum radar and quantum target detection, the general definition of these technologies ought to be viewed as: any target detection scheme that employs any non-classical part for the purposes of enhanced capabilities. The quantum mechanical aspect may be in the form of a non-classical transmitter, a non-classical receiver, or both. Succinctly, these fall into three main types of quantum sensors [13, 51]:

- **Type 1:** Non-classical quantum states of light are transmitted which are not entangled with the receiver. This includes single-photon (Fock state) quantum radars and classical LIDARS.
- **Type 2:** Classical (coherent) states are transmitted but quantum receivers are used to increase sensitivities. This type covers any quantum-enhanced LIDARS [13, 51].
- **Type 3:** Quantum states of light are transmitted which are initially entangled with the receiver.

QI falls into the category of Type 3 quantum sensors where entangled sources are used for applications in quantum radar, sensing and metrology. Entanglement is generated between two modes where one is employed as the signal while the other, the idler, forms part of the receiver.

3.3 The quantum illumination potential

3.3.1 Initial proposal

QI, the use of non-classical states to enhance detection of potentially remote objects, was first outlined in 2008 when Lloyd [18] designed a qubit-based protocol showing how entanglement may enhance the detection probability of a low-reflectivity target embedded in a bright background. In his work, two protocols were considered and compared: in the first, the beam was composed on N unentangled single-photon states and, in the second, two entangled beams (labelled signal and idler) were generated. In both scenarios, the optical transmitter illuminated a region of space in which a weakly-reflecting target was equally likely to be present or absent, immersed, in either case, in a thermal background. In both the entangled and unentangled cases, the assumptions made were as follows:

- Signal comprising N high time-bandwidth product $M = TW \gg 1$, single-photon pulses. Here, T is the detection time window and W is the bandwidth such that the detector can distinguish between M modes per detection event.
- Round-trip transmissivity $0 < \kappa \ll 1$ when the target is present. $\kappa = 0$ when the target is absent.
- Background noise $N_B \ll 1$.
- For each transmitted signal pulse, at most one photon is detected at the receiver such that $MN_B \ll 1$.

Under these assumptions, two regimes, "good" and "bad", were identified for the operation of each of the single-photon and entangled sources based on their quantum Chernoff bounds (QCB). In their good regimes, the probability of making an error after N trials was found as

$$P_{\text{err}}^{\text{SP}} = \frac{1}{2}e^{-\kappa N},\ \kappa \gg N_B, \tag{3.1}$$

and

$$P_{\text{err}}^{\text{QI}} = \frac{1}{2}e^{-\kappa N},\ \kappa \gg \frac{N_B}{M}, \tag{3.2}$$

showing that the QI case afforded a much larger region of validity. In their bad regimes, these bounds are given by

$$P_{\text{err}}^{\text{SP}} = \frac{1}{2}e^{-\frac{\kappa^2 N}{8N_B}},\ \kappa \gg N_B, \tag{3.3}$$

and

$$P_{\text{err}}^{\text{QI}} = \frac{1}{2} e^{-\frac{\kappa^2 NM}{8N_B}}, \kappa \gg \frac{N_B}{M}, \tag{3.4}$$

yielding, again, an enhancement in the region of validity for QI with the error probability drastically reducing for $M \gg 1$ in comparison to unentangled single-photon sources.

These results rely on various, typically unrealistic, assumptions. Firstly, one requires the existence of a source of entangled high time-bandwidth product photons to probe the target region. Upon their eventual return, one demands that the receiver is an optimal one, performing an optimal joint measurement on each returning photon with its corresponding idler, all the while ensuring that the idler storage system was completely lossless throughout the signal's round-trip time. These limitations have been the subject of much debate regarding how realistic a practical QI-based quantum radar would be and will be explored in further detail later in this chapter.

Of course, it is important to note that Lloyd's initial comparison was not entirely comparing a quantum scheme to a classical one. In fact, it simply compared one using entanglement to one that did not. The use of single photons as a source for target detection, while not being entangled at all, still requires the use of quantum photo-detection theory in order to process the data and formulate a decision. Indeed, this is simply a form of Type 1 quantum sensor described in Sec. 3.2.

In 2009, Shapiro and Lloyd [52] provided a comparison between entanglement-based QI and what currently forms the classical benchmark, at least in the optical domain, the coherent state. Coherent states, see Sec. 2.2.3 for details, are minimum-uncertainty classical states that may be produced as the output of an ideal laser. In their comparison, the single-photon transmitter was replaced with a coherent state transmitter with N pulses, each with average photon number of unity. In this case, the QCB was found to be

$$P_{\text{err}}^{\text{CS}} \leq \frac{1}{2} e^{-\kappa N(\sqrt{N_B+1}-\sqrt{N_B})^2}, \tag{3.5}$$

applicable for all values of $0 \leq \kappa \leq 1$ and $N_B \geq 0$. In the regime of low-background, i.e., $N_B \ll 1$, this reduces to

$$P_{\text{err}}^{\text{CS}} \leq \frac{1}{2} e^{-\kappa N}, \tag{3.6}$$

matching Lloyd's previous "good" regime QI performance while substantially outperforming QI in its "bad" regime.

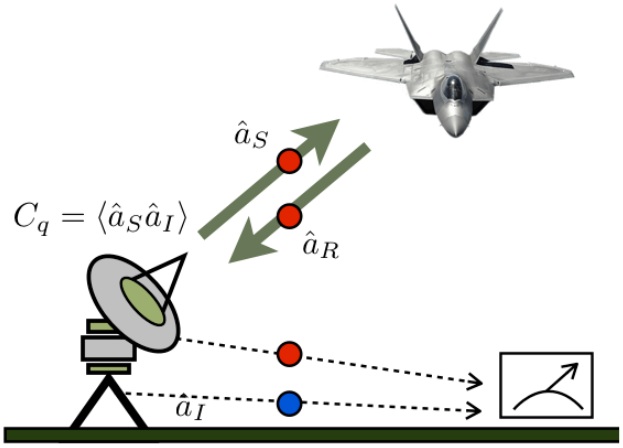

FIG. 3.1: Schematics of quantum illumination protocol.

3.3.2 Gaussian quantum illumination

Shapiro and Lloyd's results [52], while proving that the potential of QI at that point was limited, did not end research in the field. At around the same time period, Tan *et al.* [19] published their own version of QI involving the use of a more practical model under the Gaussian state formalism. This version, alongside the mathematical preliminaries of Chap. 2, will be the one primarily studied in this thesis.

Consider a resource state modelled as a two-mode squeezed vacuum (TMSV) Gaussian state comprising a signal mode sent out to some target region and an idler mode retained at the source for later joint measurement, each with N_S photons per mode[1]. The theory of Gaussian QI assumes the following conditions:

- Low-brightness signal, $N_S \ll 1$.
- High time-bandwidth product, $M = TW \gg 1$.
- Low target reflectivity, $0 \leq \kappa \ll 1$ (with $\kappa = 0$ when the target is absent).
- High-brightness thermal background, $N_B \gg 1$.

Two alternate hypotheses exist for the experiment's outcome. The first, H_0, with the target absent, where the returning signal is just a noisy background modelled as a thermal state

[1] A more in-depth mathematical description of Gaussian QI is included in Chap. 4 for the study of a generically-correlated (not necessarily maximally-entangled) Gaussian source.

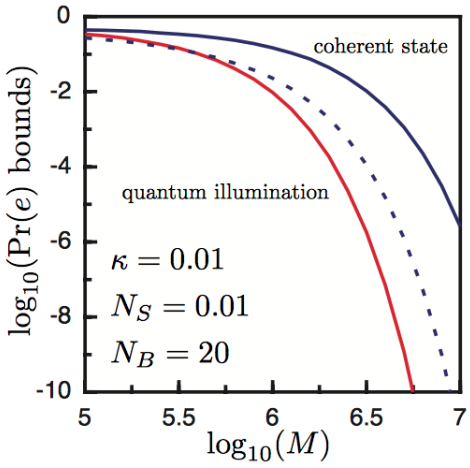

FIG. 3.2: Tan *et al.*'s bounds for QI and coherent-state transmitters [19], plotted for $\kappa = 0.01, N_S = 0.01, N_B = 20$. QBB for the QI radar (red) is lower than the QCB of the coherent-state transmitter (blue, dashed). Also shown is the (weaker) QBB of the coherent-state transmitter (blue, solid).

with mean number of photons per mode $N_B \gg 1$ (note the difference here to previous works where the assumption was that $N_B \ll 1$ and $MN_B \ll 1$). The second case, H_1, corresponds to a weakly reflective target being present in the region with reflectivity, $\kappa \ll 1$, giving the proportion of signal modes reflected back towards the source, physically representing a high loss regime. This is combined with a very strong background, now with mean photons per mode of the return given by $N_B/(1-\kappa)$. In either case, the returning signal and the retained idler are no longer entangled.

The decision problem is reduced to one of being able to distinguish between the two conditional states and our ability to do this is quantified by the computation of various bounds. Our choice of such bound depends on how we wish to weight the associated costs for error types and are reduced to the consideration of symmetric or antisymmetric costing procedures.

Tan *et al.* [19] followed this Gaussian state procedure using a symmetric cost quantum hypothesis testing (QHT) setting and found that the quantum Bhattacharyya bound (QBB) for the QI source takes the asymptotic form

$$P_{\text{err}}^{\text{QI}} \leq \frac{1}{2} e^{-M\kappa N_S/N_B}, \tag{3.7}$$

in the limits $0 < \kappa \ll 1$, $N_S \ll 1$ and $N_B \gg 1$.

Meanwhile, it was found [19,52] that the corresponding coherent state (yielding an optimal

classical benchmark, see Sec. 1.1.4) whose operation involves the transmittance of M pulses, as described previously, has a QCB given by

$$P_{\text{err}}^{\text{CS}} \leq \frac{1}{2} e^{-M\kappa N_S\left(\sqrt{1+N_B}-\sqrt{N_B}\right)^2}. \tag{3.8}$$

Imposing the same limitations used in the derivation of Eq. (3.7), that is, for $0 < \kappa \ll 1$, $N_S \ll 1$ and $N_B \gg 1$ the coherent-state transmitter QCB is given by

$$P_{\text{err}}^{\text{CS}} \leq \frac{1}{2} e^{-M\kappa N_S/4N_B}. \tag{3.9}$$

The performance of these bounds is shown in Fig. 3.2. In contrast to earlier results, the QI transmitter's error exponent in this regime has a factor of 4 (equivalent to 6 dB) advantage over the corresponding coherent-state transmitter. In other words, a QI-based approach with optimal reception offers a 6 dB enhancement over the effective signal-to-noise ratio (SNR) of coherent light illumination.

It has been shown that this 6 dB advantage is theoretically maximal [53] under the consideration of optimal collective quantum measurements, reducing to 3 dB (see also Ref. [2] and Chap. 5) when restricting one's receiver to local operations and classical communications (LOCCs) alone. Further, the two-mode Gaussian state considered in achieving these bounds has been shown to be the optimal quantum state [54], in other words, no other, more exotic, configurations of quantum state such as ones exhibiting multi-mode (> 2) entanglement can improve target detection under asymmetric QHT (the scenario considered in Ref. [54]). The same work also showed that in the absence of a quantum memory, i.e., no ability to store an idler, the coherent state forms the optimal source. More recent work has shown that, in fact, this well-known benchmark can strictly be outperformed by considering a squeezed-based protocol where both displacement and squeezing are jointly optimised, subject to a global energy constraint [55].

3.3.3 Microwave quantum illumination

The main findings of QI by Lloyd and Tan *et al.* presumed operation at optical wavelengths. In the optical domain, the necessary tools for QI implementation are well-known and widespread including spontaneous parametric down-conversion (SPDC) sources for signal generation (which naturally produce low-energy modes $N_S \ll 1$) and high fidelity single-photon detectors which are largely quantum-limited in noise associated with their operation. While this assumption poses no issue for the findings of Lloyd, the result of a 6 dB quantum advantage in effective SNR by Tan *et al.* was found under the assumption that the ambient

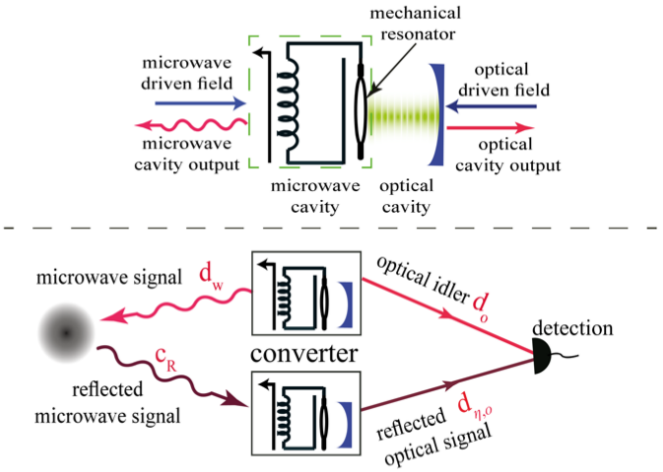

FIG. 3.3: Schematic of electro-optomechanical (EOM) converter of [20] (top) and its use in QI (bottom). Driven microwave and optical cavities are coupled by a mechanical resonator such that it may convert the optical signal of an entangled optical signal-idler mode pair to a microwave signal, and the reverse.

background mean number of photons per mode $N_B \gg 1$. This final constraint simply does not occur naturally at optical wavelengths where, in fact, $N_B \sim 10^{-6}$ and smaller.

A natural solution to this issue would be to extend the theory of QI to the microwave domain where the naturally occurring cosmic microwave background (CMB) would provide the necessary $N_B \gg 1$ for the QI advantage. Barzanjeh *et al.* [20] successfully did this in 2015 where they considered a standard SPDC photon source to generate entangled signal-idler optical mode pairs. The protocol proceeded with the employment of an electro-optomechanical (EOM) converter, see Figure 3.3, to down-convert the optical signal into a microwave mode which was then transmitted to the target region of interest. Upon the signal's return, a further EOM converter was used to reverse the process, up-converting back to the optical region to undergo a phase-conjugated $(PC)^2$ joint measurement with the retained optical idler. It is this microwave extension to QI which led to it becoming of great interest in the wider community as a potential quantum-mechanical alternative to the classical radar, potentially enabling one to detect a stealth target, while hiding a weak signal in a naturally occurring,[3]

[2]Such a receiver, is in fact, sub-optimal with respect to the theoretically optimal quantum joint measurement and thus only achieves a 3 dB quantum advantage in effective SNR [2, 60]. This is because it is based on heterodyne detection of the individual signal-idler modes, which is itself a classical measurement. This receiver is discussed in more detail, along with others, in Sec. 3.4.3

[3]For the purposes of radar detection one could also view this as "artificially-occurring" due to, for example,

strong background.

3.4 The quantum illumination challenges

3.4.1 Source generation at the microwave

QI relies on the generation of maximally-entangled mode pairs with high time-bandwidth product. Typically, the required entanglement may be achieved through methods such as SPDC. SPDC is a quantum process in which a crystal possessing non-linear properties, after being pumped with a laser of frequency ω_p, outputs a twin beam of photons with frequencies ω_s, ω_i, satisfying the relation $\omega_p = \omega_s + \omega_i$. This conservation of energy forms the basis of one example of means through which the photon pair's entanglement may be displayed: their frequency.

In the optical domain, such sources can reliably output the required photon numbers needed in order to perform QI - this, however, is not the case in the microwave. Implementation in the microwave domain comes with a host of technical difficulties of which source generation is just one example. While the EOM converter could provide a solution here by means of frequency conversion, it is still yet to be experimentally implemented, and low conversion rates between frequencies of operation would mean that the initial optical SPDC sources would have to be very intense.

An alternative method is one using a Josephson parametric amplifier [56, 57] which is exactly the method employed in recent prototypical experiments for microwave QI (see Sec. 3.5 for further details).

3.4.2 Idler storage

Idler storage poses a crucial problem for QI if one wishes to attain the maximum 6 dB enhancement in effective SNR. This performance gain hinges on the ability to perform an optimal joint measurement between the returning signal and idler beams; losses during idler storage will hinder the amount of information attainable through the process and their recombination at a specific point in time is necessary for any successful joint measurement.

Suppose one chooses a method of idler storage with an efficiency η_{I} quantifying the pro-

the process of active jamming.

portion of idlers successfully stored for later recombination with the returning signal. Then, the QCB for QI would be modified as

$$P_{\text{err}}^{\text{QI}} \leq \frac{1}{2} e^{-\frac{M\kappa\eta_I N_S}{N_B}}. \tag{3.10}$$

Possible means of idler storage are through optical fibre delay lines and quantum memories [58]. The latter method, while potentially more efficient, is still a technology very much in its infancy.

A further technique includes one carried out in a prototypical microwave QI experiment [59] where one performs measurements of the idler and stores the classical data digitally for later post-processing with measurement outcomes. While removing the need for idler storage and, in turn, any problems arising from this, the storage is of classical data arising from classical measurements which limits one's potential error exponent advantage.

3.4.3 Designing a quantum illumination receiver

After creating the large number of quantum-correlated or entangled photon pairs in order to implement quantum radar, particularly at long-range, and successfully storing the idlers during the experiment, the important question then is how to design the receiver in order to harness the QI advantage. After all, the quantum enhancement resides in the phase-sensitive cross-correlation terms existing between two different photonic modes thus both must be measured simultaneously. While it is relatively easy to individually measure quadratures through homodyne detection, measuring both at the same time through a heterodyne detection scheme cannot be done without introducing additional noise, owing to Heisenberg's uncertainty principle.

Guha and Erkmen [60] introduced the optical parametric amplifier (OPA) receiver, physically realisable by an SPDC crystal, which mixed input return and idler modes $\hat{a}_R^{(k)}$ and $\hat{a}_I^{(k)}$, $1 \leq k \leq M$, producing output mode pairs

$$\hat{c}^{(k)} = \sqrt{G}\hat{a}_I^{(k)} + \sqrt{G-1}\hat{a}_R^{\dagger(k)}, \tag{3.11}$$

and

$$\hat{d}^{(k)} = \sqrt{G}\hat{a}_R^{(k)} + \sqrt{G-1}\hat{a}_I^{\dagger(k)}, \tag{3.12}$$

where we have introduced the OPA gain $G > 1$. Then by assuming optimal photon counting on idler-output modes, they found that the receiver's QBB is given by

$$P_{\text{err}}^{\text{QI,OPA}} \leq \frac{1}{2} e^{-\frac{M\kappa N_S}{2N_B}}, \tag{3.13}$$

under the usual limits $0 < \kappa \ll 1$, $N_S \ll 1$ and $N_B \gg 1$, yielding half of the ideal QI error exponent advantage, Eq. (3.7), over coherent states, equivalent to 3 dB.

Despite its efforts in closing the gap between the performances of a physically realisable QI set-up and the theoretical ideal, the OPA receiver has proven to be sub-optimal. This is primarily due to the fact that it demands an optimal measurement on pairs of modes constituting a mixed-state, physically done through Gaussian local operations with photon-number resolving measurements. These measurements belong to the class of LOCCs, known to be sub-optimal for such a mixed-state procedure [61] hence the associated receiver designs' sub-optimality follows naturally.

Zhuang *et al.* [62] showed that exploiting sum-frequency generation (SFG), is capable of saturating QI's QCB. Equipping the proposed receiver architecture with a feed-forward (FF) mechanism was shown to push its performance to the Helstrom bound in the limit of low signal brightness. SFG is the inverse process to SPDC; the signal-idler photonic mode pairs are combined into a single photon with frequency $\omega_P = \omega_S + \omega_I$, the sum of the two individual frequencies and, after multiple SFG cycles and FF, this signal is subjected to photon counting measurements. This particular receiver design was later used in the determination of QI's receiver operating characteristic (ROC) which gives the detection probability as a function of the false alarm probability [63]. Nevertheless, despite its theoretical capability of saturating the QI QCB, such a receiver remains physically out of reach due to limitations on current technology.

3.4.4 Quantum target ranging

Classical radars are capable of carrying out tasks outside of simple target detection. Through measurement of arrival times, a target's range may be inferred and, through detection of Doppler shift and the way a target's motion shifts the frequency of the returning signal, its velocity may be determined. The extension of QI from a problem of detection to one of measurement is still an open question, partly relating to the issue with idler storage mentioned in Sec. 3.4.2. When the range of the target is unknown, in this case, the quantity to be determined, the correct time for successful signal-idler recombination is also unknown. Potential solutions to these are discussed later in this thesis in Chap. 9.

3.5 Prototypical experiments on quantum illumination

The first QI experiment was carried out by Lopaeva *et al.* [64] using an SPDC source and photon counting to detect a target modelled by a 50:50 beam splitter. They demonstrated that a QI-like advantage in effective SNR compared to a correlated thermal state may be achieved in a thermal background when the channel used was entanglement-breaking. However, as we have already seen, photon counting SPDC outputs is a sub-optimal detection scheme. Further, their chosen classical benchmark was not the optimal one based on coherent light. The same is true for a similar, more recent, experiment by England *et al.* [65].

Shortly after, Zhang *et al.* [66] and later [67] implemented the Gaussian QI protocol of Tan *et al.* using an OPA receiver. Their experiment demonstrated a sub-optimal 20% improvement (equivalent to 0.8 dB in comparison to the 3 dB available with OPA receivers) in effective SNR relative to the optimal classical scheme.

More recently there have been demonstrations of initial microwave QI experiments [59, 68, 69]. All three employ a Josephson parametric converter (JPC) for entanglement generation of microwave modes with low-brightness and compared the performance to a classically-correlated radar. After JPC generation, both modes were amplified and the signal was sent to the target region while the idler was immediately heterodyne detected. The classical outcome of this heterodyne detection was stored digitally to be compared with the outcome of the heterodyne detected returning signal in post-processing. In all experiments, a QI-like advantage was displayed over their chosen classical comparison cases which was a classically-correlated noise radar. Additionally, the Barzanjeh *et al.* [59] experiment compared to a coherent state source subject to the same heterodyne and post-processing receiver utilised for their entangled source.

3.6 Conclusion and further reading

The aim of this chapter has been to provide a broad overview of the current state of quantum target detection, particularly relating to QI, focusing on aspects specifically relating to this thesis and its contents. As a result, the content of this chapter is by no means exhaustive so the author would point the reader to a plethora of other reviews on the topic. Firstly, a book [13] and a recent review on QI [70] which focuses on QI-based target detection. For a recent review of quantum sensing in general, to provide a broader scope on the field see Ref. [11]. The author would also like to point to other articles published within the 2020

IEEE Aerospace and Electronic Systems Magazine special issue on quantum radar, e.g., Refs. [71, 72]. Finally, a recent review in quantum radar which explores protocols outside of QI, particularly the Maccone-Ren protocol [73], is given in Ref. [74].

4 Quantum illumination with a generic Gaussian source

Abstract

With the aim to loosen the entanglement requirements of quantum illumination, we study the performance of a family of Gaussian states at the transmitter, combined with an optimal and joint quantum measurement at the receiver. We find that maximal entanglement is not strictly necessary to achieve a quantum advantage over the classical benchmark of a coherent-state transmitter, in both settings of symmetric and asymmetric hypothesis testing. While performing this quantum-classical comparison, we also investigate a suitable regime of parameters for potential short range radar (or scanner) applications.

Relevant Publications Content from the following publications is used in this chapter:

[1] A. Karsa, G. Spedalieri, Q. Zhuang and S. Pirandola, *Quantum illumination with a generic Gaussian source*, Phys. Rev. Res. **2**, 023414 (2020). doi: 10.1103/PhysRevResearch.2.023414.

Modelling of the receiver operating characteristic was aided by G. Spedalieri. Q. Zhuang provided insight into the receiver operating characteristic for homodyne detection on coherent states.

4.1 Introduction

Hypothesis testing (HT) [16] and quantum hypothesis testing (QHT) [37] play crucial roles in information [17] and quantum information theory [38]. HT has fundamental links to both communication and estimation theory, ultimately underlying the task of radar detection [12] which has been extended to the quantum realm by the protocol of quantum illumination (QI) [18, 19] and, more precisely, by the model of microwave QI [20] (see Ref. [11] for a recent review on these topics). The simplest scenario of both HT and QHT is that of a binary decision, so that they are reduced to the statistical discrimination between just two hypotheses (null, H_0, and alternative, H_1).

At its most basic level, a quantum radar is a task of binary QHT. The two alternate hypotheses are encoded in two quantum channels through which a signal mode is sent. Depending on the presence or not of a target, the initial state of signal mode undergoes different transformations which result in two different quantum states at the output. Final detection is then reduced to distinguishing between these two possible quantum states. The ability to do this accurately, with a low probability of error, directly relates to an ability to determine the correct result. This fundamental mechanism can then be easily augmented with geometrical ranging arguments which account for the quantification of the round-trip time from the target, i.e., its distance.

While QI-based radars may potentially achieve the best performances [62], they require the generation of a large number of entangled states which may be a demanding task, especially if we consider the microwave regime. At the same time, the definition itself of quantum radar may be generalised beyond QI to any model that exploits a quantum part or device to beat the performance of a corresponding classical radar in the same conditions of energy, range etc. Driven by these ideas, we progressively relax the entanglement requirements of QI and we study the corresponding detection performances to the point where the source becomes just-separable, i.e., a maximally-correlated separable state. It is worth noting that, although Gaussian entanglement is the main resource of QI, previous literature has also considered the use of separable non-Gaussian sources with non-positive P-representations, finding an advantage over a restricted classical benchmark [64]. More generally, quantum correlations beyond entanglement have also been considered for a number of other quantum information and computation tasks [75–78]. However, this chapter is specifically focused on Gaussian states because they are, so far, the only sources showing a quantum advantage over the best classical benchmark. The analysis is done in the setting of symmetric and asymmetric QHT.

In particular, we show how a quantum advantage can still be achieved with less entangled sources, especially in a scenario of very short range target detection.

4.2 General quantum-correlated source

Following Gaussian QI, we consider a source modelled as a two-mode Gaussian state [10], comprising a signal (S) mode, sent out to some target region, and an idler (I) mode, retained at the source for later joint measurement. Each of these modes has N_S mean number of photons. However, instead of using a two-mode squeezed vacuum (TMSV) state [10] as in QI, we can employ a generic zero-mean Gaussian state whose covariance matrix (CM) takes the following block form

$$\mathbf{V}_{SI}^{\text{gen}} = \begin{pmatrix} \nu\mathbf{1} & c\mathbf{Z} \\ c\mathbf{Z} & \nu\mathbf{1} \end{pmatrix}, \tag{4.1}$$

where $\mathbf{1}$ is the 2×2 identity operator and Z is the Pauli Z-matrix. The terms in the leading diagonal, $\nu := 2N_S + 1$, quantify the amount of thermal noise within each of the local modes, S and I, while the covariance, c, quantifying the correlations between these two modes, may take any value within the range, $0 \leq c \leq 2\sqrt{N_S(N_S+1)}$ where the upper bound arises from the uncertainty principle 2.25. Mathematically, these are the second-order statistical moments of the quantum state (see Ref. [10] for more details).

At maximal quantum correlations we have $c = c_q := 2\sqrt{N_S(N_S+1)}$, corresponding to the TMSV state, while the case $c = c_d := 2N_S$ renders the state just-separable [79]. From here, we can see the effect that signal strength has on quantum correlations: writing $c_q = 2N_S\sqrt{1+1/N_S}$, for large N_S, $c_q \to 2N_S = c_d$.

At this border point, $c = c_d$, the state is not entangled but it still has quantum correlations [80]. In fact, its quantum discord is maximal among the states within the range $c \leq c_d$ and is equal to its Gaussian discord [81] (therefore computable using Refs. [82, 83]). This kind of source separable but discordant source has already played a non-trivial role in other problems of quantum information theory, e.g., as candidate separable state in relative entropy bounds for the two-way quantum capacities of bosonic Gaussian channels [84]. In this chapter, the QI model will be progressively relaxed of its entanglement requirements allowing the study of the performance of the two-mode Gaussian source in Eq. (4.1), up to the border case of $c = c_d$.

Considering the output state at the receiver, two hypotheses exist for the experiment's

outcome:

H_0 : Target is absent, so that the return signal is a noisy background modelled as a thermal state with mean number of photons per mode $N_B \gg 1$.

H_1 : Target is present with reflectivity $\kappa \ll 1$, so that a proportion of signal modes is reflected back to the transmitter. In this high-loss regime, the return signal is combined with a very strong background with mean photons per mode $N_B/(1-\kappa)$.

Under H_1, this physically represents a very lossy return from the target, combined with a very strong background contribution which is independent of the target's presence or absence. When $\kappa \ll 1$, there is little difference between the values of $\langle \hat{a}_B^\dagger \hat{a}_B \rangle$ under H_0 and H_1, so this ensures that there is no passive signature, i.e., a non-vacuum transmitter must be used in order to detect the target. Then the joint state of our returning (R) mode and the retained idler is given by, under H_0 and H_1, respectively:

$$\mathbf{V}_{RI}^0 = \begin{pmatrix} \omega \mathbf{1} & 0 \\ 0 & \nu \mathbf{1} \end{pmatrix}, \tag{4.2}$$

$$\mathbf{V}_{RI}^1 = \begin{pmatrix} \gamma \mathbf{1} & \sqrt{\kappa} c \mathbf{Z} \\ \sqrt{\kappa} c \mathbf{Z} & \nu \mathbf{1} \end{pmatrix}, \tag{4.3}$$

where $\omega := 2N_B + 1$ and $\gamma := 2\kappa N_S + \omega$. For an arbitrary Gaussian state with leading diagonal entries a and b, separability corresponds to the off-diagonal term $c \leq c_d := \sqrt{(a-1)(b-1)}$ [84]. For each of these output quantum states, conditional on H_0 and H_1, we have that $0 \leq 2\sqrt{N_B N_S}$ and $\sqrt{\kappa} c \leq 2\sqrt{(\kappa N_S + N_B) N_S}$, for small κ, respectively. Thus the separability criterion is always satisfied and neither of these states are entangled.

In the absence of the idler, the best strategy is to use coherent states. This is a semi-classical design which is used as a classical benchmark in quantum information to evaluate the effective performance of quantum-correlated sources [11, 19]. Let us work within the formalism of creation, $\hat{a}^\dagger$, and annihilation, $\hat{a}$, operators for bosonic modes defined by

$$\hat{a}^\dagger |n\rangle = \sqrt{n+1}\, |n+1\rangle, \tag{4.4}$$

$$\hat{a} |n\rangle = \sqrt{n}\, |n-1\rangle, \tag{4.5}$$

where $|n\rangle$ is a Fock state (an eigenstate of the photon number operator $\hat{n} = \hat{a}^\dagger \hat{a}$). Letting $\hat{a}_S$ be the annihilation operator for the signal mode prepared in the coherent state $|\sqrt{N_S}\rangle$

(satisfying the eigenvalue equation $\hat{a}_s |\sqrt{N_S}\rangle = \sqrt{N_S} |\sqrt{N_S}\rangle$), we send such a mode to some target region. Under H_0 the return signal, with annihilation operator $\hat{a}_R$, is equal to that of the background which is in a thermal state with mean photons per mode N_B, i.e., $\hat{a}_R = \hat{a}_B$. The state has mean vector of zero and CM $(2N_B + 1)\mathbf{1}$. Under H_1 the target is present and reflects a small proportion of our signal back. This is mixed with the background radiation such that our return takes the form $\hat{a}_R = \sqrt{\kappa}\hat{a}_S + \sqrt{1-\kappa}\hat{a}_B$, where $\kappa \in (0, 1)$ and the background has mean photons per mode $N_B/(1-\kappa)$. This corresponds to a displaced thermal state with mean vector $(\sqrt{2\kappa N_S}, 0)$ and CM $(2N_B + 1)\mathbf{1}$.

4.3 Quantum radar detection with generic Gaussian source

Using the generic quantum-correlated Gaussian source of Sec. 4.2 and the tools for symmetric and asymmetric QHT of Sec. 2.3, we study the performance of a relaxed QI protocol, clarifying how much entanglement is needed to beat the semi-classical benchmark of the coherent-state transmitter under symmetric testing. Then, in the setting of asymmetric testing, we repeat the study in terms of the receiver operating characteristic (ROC), where the mis-detection probability is plotted versus the false alarm probability.

4.3.1 Symmetric detection with generic Gaussian source

Using the generic quantum-correlated Gaussian source defined in Sec. 4.2 along with formulae and tools for symmetric QHT described in Sec. 2.3.1 of Chap. 2, one can compute the exact form of the quantum Bhattacharyya bound (QBB) for QI. The complete formula is too long to be displayed however, imposing parameter constraints, one can achieve a closed-form for the asymptotic performance in specified limits.

We begin by assuming the typical conditions of QI, which are low-reflectivity $\kappa \ll 1$, high thermal-noise $N_B \gg 1$ and low photon number per mode $N_S \ll 1$. Then, using numerical techniques, one can confirm that using a TMSV state, the minimum error probability satisfies [19]

$$P_{\text{err}}^{\text{TMSV}} \leq e^{-M\kappa N_S/N_B}/2, \tag{4.6}$$

which is exponentially tight in the limit of large M and is valid under the parameter constraints previously defined. Further, it is also known to be achieved by the sum-frequency-generation receiver of Ref. [62]. Its error-rate exponent has a factor of 4 advantage over the same bound computed over a coherent-state transmitter in the same conditions, for which

we have [19]

$$P_{\text{err}}^{\text{CS}} \leq e^{-M\kappa N_S/4N_B}/2. \tag{4.7}$$

In order to extend Eq. (4.6) to the error probability for a generic Gaussian source, we first note that as we only vary the value of cross-correlation parameter c the variation in the bound will be entirely dependent on this parameter. We also note that the parameter c is constrained by the terms on the leading diagonal such that

$$0 \leq c \leq 2\sqrt{N_S(N_S+1)} := c_q, \tag{4.8}$$

where the upper bound corresponds to the maximally-entangled TMSV state yielding Eq. (4.6). Since the just-separable state corresponds to $c = c_d := 2N_S$ it is clear that $c = c(N_S)$, i.e., it is a function of N_S alone.

The form of Eq. (4.6) is not surprising; the error exponent is directly proportional to the single-use SNR, $\gamma = \kappa N_S/N_B$, and one would expect the same for our generic source. Starting with single probing, $M = 1$, and subject to the limits $\kappa \ll 1$, $N_B \gg 1$ and $N_S \ll 1$, we can write the QBB for our generic source as

$$P_{\text{err}}^{\text{gen}} \leq e^{-\kappa N_S g_c(N_S)/N_B}/2, \tag{4.9}$$

where we define the function $g_c(N_S)$ as a constant of proportionality, entirely dependent on the parameter c and thus N_S. In particular, we demand the equivalence of exponents in the TMSV limit $c \to c_q$ such that $g_{c_q}(N_S) = 1$, recovering the bound given by Eq. (4.6).

To determine the form of $g_c(N_S)$ we use a numerical program to perform an asymptotic expansion of our generic source's exact QBB for small $\kappa \ll 1$. Keeping terms to first-order, we obtain an equation of the form

$$2P_{\text{err}}^{\text{gen}} \leq 1 - x\kappa + \mathcal{O}(\kappa^2) \simeq e^{-x\kappa}, \tag{4.10}$$

where the last equality holds when $x = \frac{N_S}{N_B} g_c(N_S)$, from Eq. (4.9), is small, i.e., $N_S \ll 1$ and $N_B \gg 1$.

Numerical analysis shows that the coefficient x is exactly proportional to c^2, independent of N_S and N_B, thus we can write $g_c(N_S) \propto c^2$ and, imposing the condition that $g_{c_q}(N_S) = 1$ determine that

$$g_c(N_S) = c^2/c_q^2. \tag{4.11}$$

Fig. 4.1 plots the function $g_c(N_S)$ as a function of cross-correlation parameter c for two sets of parameter values: (a) $N_S = 10^{-2}$, $N_B = 20$ and (b) $N_S = 10^{-4}$, $N_B = 200$. It shows

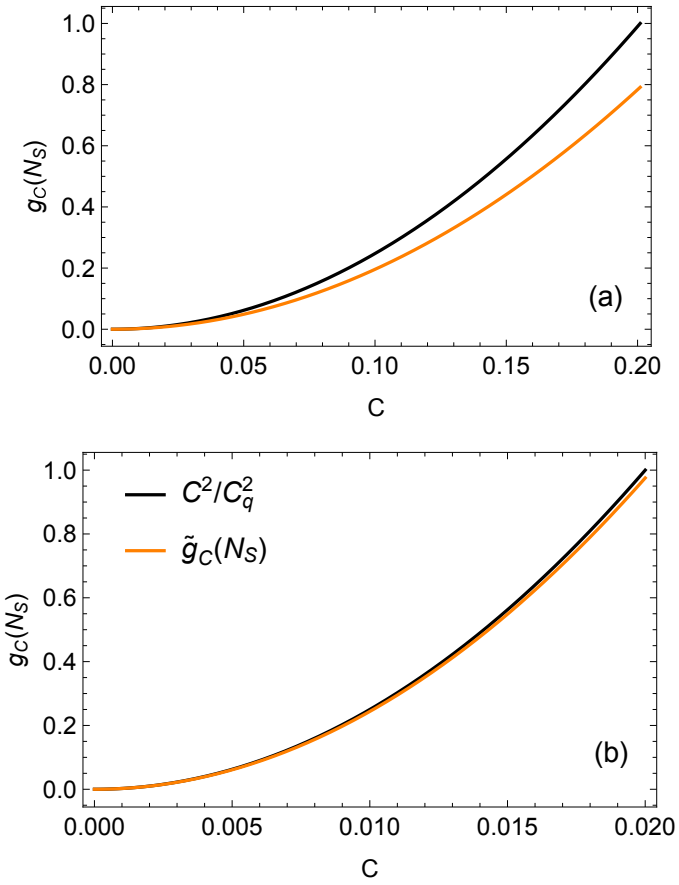

FIG. 4.1: Numerical study of generic Gaussian source's QI error exponent for parameter values: (a) $N_S = 10^{-2}$, $N_B = 20$ and (b) $N_S = 10^{-4}$, $N_B = 200$. The plots confirm that for small N_S and large N_B we have that $\tilde{g}_c(N_S) \to g_c(N_S) = c^2/c_q^2$ and our formula for generic Gaussian QI holds in this regime.

that in the regime of low brightness and high background the function $\tilde{g}_c(N_S) \to g_c(N_S)$, given by Eq. (4.11), and we can write that the QBB for a generic Gaussian source is given by

$$P_{\text{err}}^{\text{gen}} \leq e^{-M\kappa N_S c^2/N_B c_q^2}/2. \tag{4.12}$$

Note that the extension from $M = 1$ to generic M just follows from the structure of the QCB and QBB in Eq. (2.56).

By comparing Eqs. (4.12) and (4.7), we see that a quantum-correlated transmitter outperforms the coherent state transmitter in target detection if $P_{\text{err}}^{\text{gen}} \leq P_{\text{err}}^{\text{CS}}$ which is satisfied

when

$$\frac{c^2}{c_q^2} \geq \frac{1}{4} \Rightarrow c \geq \sqrt{N_S(N_S+1)}. \tag{4.13}$$

Thus, according to the QBB, the quadrature correlations required to outperform the semi-classical benchmark is half the value of those of a TMSV state. At the separable limit $c = 2N_S$ the relation is only satisfied for $N_S \geq 1/3$ which contradicts the assumption $N_S \ll 1$ (a similar analysis holds if we relax the assumption of $N_S \ll 1$). Therefore, according to the QBB, the employment of a source at the separable limit is not capable of achieving a quantum advantage over coherent states under symmetric testing.

4.3.2 Asymmetric detection with general source

Let us compute the QRE and the QREV for the quantum-correlated transmitter of Eq. (4.1). Though the full expressions for these quantities are far too long to display here, they are evaluated to first-order in N_B by taking an asymptotic expansion for large N_B while keeping N_S fixed, obtaining

$$D_{\text{gen}} := D\left(\hat{\rho}_{RI}^{(0)} || \hat{\rho}_{RI}^{(1)}\right) = \frac{\kappa c^2}{N_B} \ln\left(1 + \frac{1}{N_S}\right) + \mathcal{O}\left(N_B^{-2}\right), \tag{4.14}$$

$$V_{\text{gen}} := V\left(\hat{\rho}_{RI}^{(0)} || \hat{\rho}_{RI}^{(1)}\right) = \frac{\kappa c^2 (2N_S+1)}{N_B} \ln^2\left(1 + \frac{1}{N_S}\right) + \mathcal{O}\left(N_B^{-2}\right). \tag{4.15}$$

For coherent states, these quantities take the form

$$D_{\text{CS}} := D\left(\hat{\rho}_{\text{CS}}^{(0)} || \hat{\rho}_{\text{CS}}^{(1)}\right) = \kappa N_S \ln\left(1 + \frac{1}{N_B}\right), \tag{4.16}$$

$$V_{\text{CS}} := V\left(\hat{\rho}_{\text{CS}}^{(0)} || \hat{\rho}_{\text{CS}}^{(1)}\right) = \kappa N_S (2N_B+1) \ln^2\left(1 + \frac{1}{N_B}\right), \tag{4.17}$$

which hold for all values of N_S, N_B and κ. For comparative purposes we evaluate again to first-order in N_B while keeping N_S fixed to obtain the simple expressions

$$D_{\text{CS}} \simeq \gamma + \mathcal{O}\left(N_B^{-2}\right), \tag{4.18}$$

$$V_{\text{CS}} \simeq 2\gamma + \mathcal{O}\left(N_B^{-2}\right), \tag{4.19}$$

where

$$\gamma := \frac{\kappa N_S}{N_B} \tag{4.20}$$

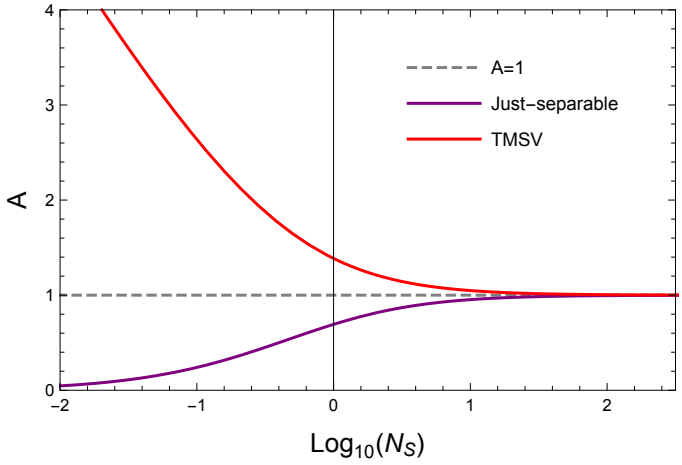

FIG. 4.2: Error exponent ratio A of Eq. (4.22) is shown as a function of number of signal photons per mode, N_S. The just-separable discordant source quickly approaches the coherent-state transmitter ($A = 1$) and the TMSV source, already at $N_S \simeq 20$ photons. For increasing N_S, the ratio A asymptotically approaches 1 independent of the source specification.

is the single-use signal-to-noise ratio (SNR), usually expressed in decibels (dB) via $\gamma_{\rm dB} = 10 \log_{10} \gamma$.

Together, the QRE and QREV may be combined (see Sec. 2.3.2 for details) to find that the optimal Type II error probability, for sample size M, takes the exponential form

$$\exp\left[MD\left(\hat{\rho}_0||\hat{\rho}_1\right) + \sqrt{MV\left(\hat{\rho}_0||\hat{\rho}_1\right)}\Phi^{-1}(\epsilon) + \mathcal{O}(\log M)\right]. \tag{4.21}$$

In the limit of very large M, we can approximately neglect the variance contribution and just consider the relative entropy in the Type II (mis-detection) error probability of Eq. (2.73) which simply becomes $P_{\rm md} \simeq \exp\left[-MD\left(\hat{\rho}_0, \hat{\rho}_1\right)\right]$. Then, we can deduce that, for large M and a very high background $N_B \gg 1$, the error exponent of a quantum-correlated source [Eq. (4.14)] has the following ratio with respect to a coherent state source [Eq. (4.18)]

$$A(c, N_S) := \frac{D_{\rm gen}}{D_{\rm CS}} = \frac{c^2}{N_S} \ln\left(1 + \frac{1}{N_S}\right). \tag{4.22}$$

Fig. 4.2 plots the ratio A for a just-separable discordant source ($c = N_S$) and that for a TMSV state, for varying N_S. The ultimate benefits of employing maximal entanglement for QI are exhibited only for very small energies, i.e., when N_S is of the order of units or less. For increasing N_S, the ratio A tends to the same asymptotic value, irrespective of source specification. This also means that the just-separable source quickly approaches the performance

of QI at as little as about 20 photons per mode. As seen in Sec. 1.1.2, for a given range R the radar equation imposes a $1/R^4$ loss factor in received signal-power and necessitates high overall photon numbers, particularly at long range, regardless of the underlying detection protocol. Our results show that at long range there is little-to-no advantage in using a QI-based radar over a coherent state protocol due to the need for large signal-power (N_S). QI is thus limited to applications where losses are relatively small so N_S may, in turn, take small values, for example, at short ranges.

4.3.3 Receiver operating characteristic

In the asymmetric setting, we now study the mis-detection probability versus the false alarm probability of the generic Gaussian source with respect to the classical benchmark of coherent states. For the latter, we consider the performance achievable by coherent states and homodyne detection at the output. This is the best-known measurement design which can be used when the phase of the optical field is perfectly maintained in the interaction with the target, so that one can adopt a coherent integration of the pulses (i.e., the quadrature outcomes can be added before making a classical binary test on the total value). If the phase of the field is deterministically changed to some unknown value but it is still coherently maintained among the pulses, then the typical choice is the heterodyne detection, followed by coherent integration of the outcomes from both the quadratures. If the coherence is lost among the pulses, then the classical strategy is to use heterodyne and perform a non-coherent integration of the pulses, which means to sum the recorded intensities (squared values of the quadratures). In this case, the performance (for non-fluctuating targets) is given by the Marcum's Q-function [85], an approximation of which is known as Albersheim's equation [12, 86]. An overestimation of the Marcum benchmark can be simply achieved by assuming a single coherent pulse with mean number of photons equal to MN_S.

In mathematical terms, the ROC (see also Sec. 1.1.2) $P_{\rm md} = P_{\rm md}(P_{\rm fa})$ of the generic Gaussian source can be upper-bounded $P_{\rm md} \leq \tilde{P}_{\rm md}$ by combining Eqs. (4.21), (4.14) and (4.15). For sufficiently large M (e.g., $\gtrsim 10^7$), the second-order asymptotics is a good approximation, and for large N_B (e.g., $\gtrsim 10^2$) the expansions in Eqs. (4.14) and (4.15) are valid. Therefore,

under these assumptions, we may write

$$\tilde{P}_{\rm md}^{\rm gen} = \exp\left\{-\left[\sqrt{\frac{M\gamma}{N_S}}\Lambda C \ln\left(1+\frac{1}{N_S}\right)+\mathcal{O}(N_B^{-1},1)\right]\right\}, \tag{4.23}$$

$$\Lambda := \left(\sqrt{\frac{M\gamma}{N_S}}c+\sqrt{2N_S+1}\Phi^{-1}(P_{\rm fa})\right). \tag{4.24}$$

In the case of coherent states and homodyne detection (followed by coherent integration and binary testing), the ROC is given by combining the following expressions

$$P_{\rm fa}^{\rm hom}(x) = \frac{1}{2}\,{\rm erfc}\left[\frac{x}{\sqrt{M(2N_B+1)}}\right], \tag{4.25}$$

$$P_{\rm md}^{\rm hom}(x) = \frac{1}{2}\,{\rm erfc}\left[\frac{M\sqrt{2\kappa N_S}-x}{\sqrt{M(2N_B+1)}}\right], \tag{4.26}$$

where ${\rm erfc}(z) := 1-2\pi^{-1/2}\int_0^z \exp(-t^2)dt$ is the complementary error function. Therefore we can invert Eq. (4.25) and replace in Eq. (4.26) to derive the corresponding ROC.

Finally, as already mentioned, we can also write a lower bound to Marcum's classical radar performance by assuming a single coherent state with mean number of photons MN_S so that the total SNR is given by $M\gamma$. This can be expressed as follows

$$P_{\rm md}^{\rm Marcum} = 1-Q\left(\sqrt{2M\gamma},\sqrt{-2\ln P_{\rm fa}}\right), \tag{4.27}$$

where the Marcum Q-function is defined as

$$Q(x,y) := \int_y^\infty dt\; te^{-(t^2+x^2)/2}I_0(tx), \tag{4.28}$$

with $I_0(.)$ being the modified Bessel function of the first kind of zero-order [85].

Before comparing the ROCs of the various transmitters, let us choose a suitable regime of parameters for potential short range applications (of the order of 1m, e.g., for security or biomedical applications), where N_S need not be too large and a quantum advantage may be observed. By fixing some specific radar frequency ν and the temperature T of the environment, we automatically fix the mean number of photons N_B of the thermal background. Thus, for $\nu = 1$GHz (L band) and $T = 290$K (room temperature), we get $N_B \simeq 6\times 10^3$ photons (bright noise). Assume broadband pulses, with 10% bandwidth (100MHz), so that their individual duration is about 10ns. If we use $M = 10^8$ pulses then we have an integration time of the order of 1s, which is acceptable for slowly-moving or still objects. Since we are

interested in low-energy applications, assume $N_S = 1$ mean photon per pulse. What is left is an estimation of the SNR γ which comes from the overall transmissivity/reflectivity κ.

This remaining quantity can be estimated using the radar equation (see Sec. 1.1.2 for details). This equation expresses the power $P_{\rm r}$ of the return signal in terms of the signal-power $P_{\rm tx}$ at the transmitter, the cross-section σ of the target, the range R of the target, and other parameters, such as the transmit antenna gain $G_{\rm tx}$, the receive antenna collecting area $a_{\rm r}$ and the form factor F which describes the transmissivity of the space between the radar and the target. It takes the form [14]

$$P_{\rm r} = \frac{G_{\rm tx} F^4 a_{\rm r} \sigma}{(4\pi)^2 R^4} P_{\rm tx}. \tag{4.29}$$

Here the factor $(4\pi)^{-2} R^{-4}$ accounts for the loss due to the pulse propagating as a spherical wave (back and forth). This is partly mitigated by the gain $G_{\rm tx}$ which introduces anisotropies from the spherical wave description, accounting for the directivity of the actual outgoing beam. In fact $G_{\rm tx}$ describes the ratio between the power irradiated in the direction of the target over the power that would have been irradiated by an isotropic antenna [14]. For a pencil beam, $G_{\rm tx}$ can be much higher than 1 (which is the value of an isotropic antenna).

It is clear that κ also provides the ratio between received and transmitted power, so that Eq. (4.29) leads to

$$\kappa = \frac{P_{\rm r}}{P_{\rm tx}} = \frac{G_{\rm tx} F^4 a_{\rm r} \sigma}{(4\pi)^2 R^4}, \tag{4.30}$$

which is also easy to invert, so as to express the range R in terms of κ and the other parameters. Assume $F = 1$ (no free-space loss) and an ideal pencil beam, such that its solid angle δ is exactly subtended by the target's cross-section σ (valid assumption at short ranges). This means that gain is ideally given by

$$G_{\rm tx} = \frac{4\pi}{\delta} = \frac{4\pi R^2}{\sigma}, \tag{4.31}$$

which fully compensates the loss in the forward propagation. Therefore, we find

$$\kappa = \frac{a_{\rm r}}{(4\pi R)^2}, \quad R = \frac{1}{4\pi}\sqrt{\frac{a_{\rm r}}{\kappa}}. \tag{4.32}$$

By fixing the receiver's collecting area $a_{\rm tx}$, we have a one-to-one correspondence between range R and transmissivity κ. Assuming $a_{\rm r} = 0.1{\rm m}^2$ and short range $R \simeq 1{\rm m}$, we get $\kappa \simeq 6 \times 10^{-4}$ which leads to $\gamma_{\rm dB} = -70{\rm dB}$ when we account for the values of N_S and N_B.

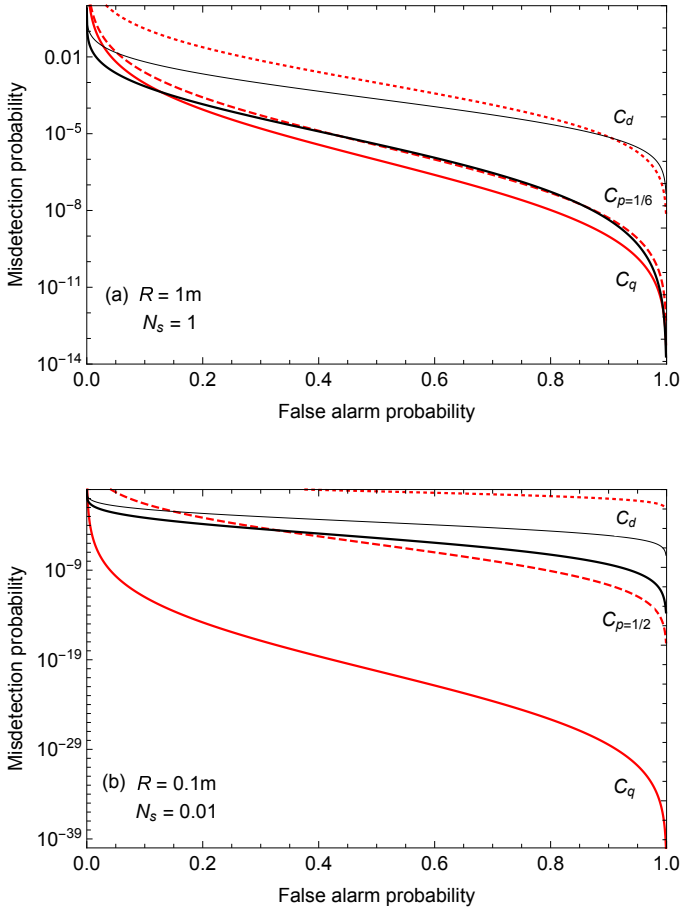

FIG. 4.3: Receiver operating characteristics (ROCs) of the various setups. We show the upper bound $\tilde{P}_{\rm md} = \tilde{P}_{\rm md}(P_{\rm fa})$ for quantum illumination based on a generic Gaussian state with off-diagonal correlation parameter $c(p)$ ranging from the maximally-entangled state (red solid) to the just separable state (red dotted). Between these two extremal curves, there are all the Gaussian states with intermediate correlations. In particular, we show the performance for an intermediate value of p (red dashed). For comparison, we plot the ROC $P_{\rm md} = P_{\rm md}(P_{\rm fa})$ of the classical benchmark of coherent states plus homodyne detection (black thick) and the lower bound to Marcum's classical performance (black thin). Parameters are: $\nu = 1$GHz and $T = 290$K (so that $N_B \simeq 6 \times 10^3$), $M = 10^8$ pulses and $\gamma_{\rm dB} = -70$dB. Upper panel (a): $N_S = 1$, corresponding to a range $R \simeq 1$m with intermediate $p = 1/6$; lower panel (b): $N_S = 0.01$ corresponding to a range $R \simeq 0.1$m with intermediate $p = 1/2$ and an integration time of about 1s at 10% bandwidth (100MHz) in both cases.

Considering this regime of parameters, we generate the ROCs plotted in Fig. 4.3. In particular, we show the performance of a generic Gaussian source with correlation parameter $c(p) = pc_d + (1-p)c_q$ between the extremal points given by the just-separable source $c_d = 2N_S$

and the maximally-entangled source (at that energy) $c_q = 2\sqrt{N_S(N_S+1)}$[1]. We perform the comparison for two scenarios while maintaining the same SNR, background characteristics and total number of uses: the first with $N_S = 1$ and the second with $N_S = 0.01$ corresponding to ranges $R = 1$m and $R = 0.1$m, respectively. From the figure, we can see that intermediate values of entanglement are able to beat the classical benchmark given by coherent states and homodyne detection. The potential advantage is greater at lower signal energy N_S or, equivalently, shorter range R and additionally, the intermediate level of entanglement required in order to attain such an advantage reduces. In the upper panel, we consider our suggested upper limit for both range and signal energy: $R = 1$m and $N_S = 1$. This plot shows that though maximal entanglement is not strictly necessary for a quantum advantage, the scope for such an advantage is limited with the minimum intermediate level at $p = 1/6$, i.e., very close to the maximally-entangled case. The lower panel highlights the benefits afforded to QI by limiting applications to short range and low signal energy, plotting results for $R = 0.1$m and $N_S = 0.01$. Here the minimum intermediate level is given by $p = 1/2$ which yields a large range of source specifications capable of achieving a quantum advantage with potential performances several orders of magnitude greater than the optimal classical protocol. This effect becomes greater still at progressively shorter ranges and lower energies. It is precisely in these cases where we find that QI is most suited and, in the likely scenario that there are inefficiencies associated with source generation, enhanced detection performance is still achievable to a potentially very high degree.

4.4 Conclusion

In this chapter, we have investigated how to loosen the transmitter requirements of QI, from the usual maximally-entangled TMSV source to a more general quantum-correlated Gaussian source, which may become just-separable. At the same time, we maintain the optimal quantum joint measurement procedure at the receiver side. We perform this investigation in both scenarios of symmetric and asymmetric testing where we test the quantum performance with respect to suitable classical benchmarks. Our results show that we can still find a quantum advantage by using Gaussian sources which are not necessarily maximally entangled. In particular, this is an advantage which appears at short ranges, so that the spherical beam spreading does not involve too many dBs of loss, a major killing factor for any quantum radar

[1] another study of the ROC of the maximally-entangled case can be found in Ref. [63] but for the regime $N_S \ll 1$.

design based on the exploitation of quantum correlations.

Note that there exists a discrepancy between the parameter values used in this chapter's analysis and what is physically possible. Our choice of source with frequency 1GHz means a wavelength of 30cm, meanwhile a pulse duration of 10ns yields a 3m pulse length. This renders the physical situation near-field, such that standing waves would form within the system giving rise to spatial resonances and the signal's behaviour would not follow the radar equation. Nevertheless, the qualitative description and behaviours observed are still valid regardless of the physical implications of our choices of parameter values.

A short range low-power radar is potentially interesting not only as a non-invasive scanning tool for biomedical applications but also for security and safety purposes, e.g., as a scanner for metallic objects or as a proximity sensor for obstacle detection. Once a quantum advantage in detection is achieved at a fixed target distance, it can be extended to variable distances to enable measurement of the range. For instance, this could be done by sending signal-idler pulses at different carrier frequencies and interrogating their reflection at different round-trip times. For slowly moving objects at short ranges, the total interrogation time would be small and the effective distance of the object could be well-resolved by sweeping a reasonable number of frequencies. In a static setting, e.g., biomedical, detection is naturally associated with a fixed depth, which is then gradually increased so as to provide a progressive scan of the target region. This quantum scanner would investigate the presence of the target at different layers, e.g., of a tissue while irradiating small energies. In conjunction with standard Doppler techniques, it could also extract information about the local velocity of the target within a layer of the tissue. Such a quantum scanner would then realise an ideal non-invasive diagnostic tool.

5 Noisy receivers for quantum illumination

Abstract

Quantum illumination (QI) promises unprecedented performances in target detection but there are various problems surrounding its implementation. Where target ranging is a concern, signal and idler recombination forms a crucial barrier to the protocol's success. This could potentially be mitigated if performing a measurement on the idler mode could still yield a quantum advantage. In this chapter, we investigate the QI protocol for a generically correlated Gaussian source and study the phase-conjugating (PC) receiver, deriving the associated SNR in terms of the signal and idler energies, and their cross-correlations, which may be readily adapted to incorporate added noise due to Gaussian measurements. We confirm that a heterodyne measurement performed on the idler mode leads to a performance which asymptotically approaches that of a coherent state with homodyne detection. However, if the signal mode is subject to added noise due to a heterodyne measurement but the idler mode is maintained clean, the performance asymptotically approaches that of the PC receiver without any added noise.

Relevant Publications

Content from the following publications is used in this chapter:

[2] A. Karsa and S. Pirandola, *Noisy receivers for quantum illumination*, IEEE Trans. Aerosp. Electron. Syst. Magazine 35(**11**), 22–29 (2021). doi: 10.1109/MAES.2020.3004019.

5.1 Introduction

To date, the specifics of an optimum receiver for QI remains unknown without access to a quantum computer. There have, however, been several proposals for practical receiver designs, the best of which are the sub-optimal optical parametric amplifier (OPA) and phase-conjugating (PC) receivers [60], achieving up to 3 dB in performance advantage. The 3 dB performance deficit is owing to the fact that these receivers operate based on Gaussian local operations which are known to be not optimal for general mixed-state discrimination [61,87]. Employing nonlinear operations, Zhuang *et al.* [62, 63, 88] used sum-frequency generation (SFG) alongside a feed-forward (FF) mechanism to show that the full QI advantage could theoretically be attained, however, the physical implementation of the FF-SFG receiver is yet out of reach.

Even though low signal energy is one of the key ingredients for QI's advantage, this inherent property of microwave photons make their detection difficult such that single photon counting forms a great obstacle for any experiment in the microwave domain. This is despite the fact that this task is generally quite straightforward in other regimes with efficient optical photon counters being widely available [89]. The actual measurement procedure forms a crucial and fundamental design aspect of any QI receiver, particularly in the microwave domain, with interesting progress being demonstrated by recent experiments [59, 69].

Further to questions regarding receiver design, idler storage poses another issue particularly with respect to target-ranging problems. In QI an entangled photon pair is created with one forming the signal and the other, the idler, stored for later joint measurement. In scenarios where the range, and thus return time of the signal, is unknown or even a measure to be determined, idler storage forms a crucial aspect of the protocol necessary for its success.

A potential solution is to perform a measurement on the idler photon, mitigating issues associated with its storage, and combine the result with that of the returning signal. In microwave QI, these measurement results take the form of quadrature voltages which may be used to reconstruct the annihilation operators of the modes; in turn, these may be post-processed to simulate potential receivers for QI, such as the digital PC receiver [59]. Despite the fact that the collected data can be used in this way, real-time implementation of such a strategy cannot beat the optimal performance of coherent states, as already discussed in Ref. [59] and further investigated here.

This chapter considers the QI protocol using a generic source modelled as a two-mode

Gaussian state with arbitrary quadrature correlations. Keeping in the domain of Gaussian linear operations, we study the PC receiver in terms of its effective signal-to-noise ratio (SNR) for our generic source. We consider various cases of added noise from, for example, the application of a heterodyne measurement on one or both of the source's modes, comparing their performances of these various receivers and determine their absolute performance capabilities relative to the optimal classical method using coherent states with homodyne detection.

5.2 Basics of the quantum illumination protocol

Consider the production of M independent signal-idler mode pairs, $\{\hat{a}_S^{(k)}, \hat{a}_I^{(k)}\}$; $1 \leq k \leq M$, with mean number of photons per mode given by N_S and N_I for the signal and idler modes, respectively. The signal (S) mode is sent out to some target region while the idler (I) mode is retained at the source for later joint measurement. Their joint state, $\hat{\rho}_{S,I}$, is modelled as a two-mode, zero mean Gaussian state [1] with covariance matrix (CM) given by

$$\mathbf{V}_{S,I} = \begin{pmatrix} \nu\mathbf{1} & c\mathbf{Z} \\ c\mathbf{Z} & \mu\mathbf{1} \end{pmatrix}, \quad \begin{cases} \mathbf{1} := \mathrm{diag}(1,1), \\ \mathbf{Z} := \mathrm{diag}(1,-1), \end{cases} \tag{5.1}$$

where $\nu := 2N_S + 1$, $\mu := 2N_I + 1$ and c quantifies the quadrature correlations between the two modes such that $0 \leq c \leq 2\sqrt{N_S(N_I+1)}$. In the case where the signal-idler mode pairs are maximally entangled we have $c = c_q := 2\sqrt{N_S(N_I+1)}$ while the case $c = c_d := 2\sqrt{N_S N_I}$ renders the state just-separable [79, 80]. Recall that, for $c = c_q$, the state is known as two-mode squeezed vacuum (TMSV) state [10].

Under hypothesis H_0, the target is absent so that the returning mode $\hat{a}_R = \hat{a}_B$, where $\hat{a}_B$ is in a thermal state with mean number of photons per mode $N_B \gg 1$. Under hypothesis H_1, the target is present such that $\hat{a}_R = \sqrt{\kappa}\hat{a}_S + \sqrt{1-\kappa}\hat{a}_B$, where $\kappa \ll 1$, and $\hat{a}_B$ is in a thermal state with mean number of photons per mode $N_B/(1-\kappa)$, so that the total mean photon number is equal under both hypotheses (when $\kappa \ll 1$ there is no passive signature such that a non-vacuum source must be used to detect the target's presence). The conditional joint state, $\hat{\rho}_{R,I}^{i}$ for $i = 0, 1$, of the returning (R) mode and the retained idler is given by

$$\mathbf{V}_{R,I}^{0} = \begin{pmatrix} \omega\mathbf{1} & 0 \\ 0 & \mu\mathbf{1} \end{pmatrix}, \tag{5.2}$$

[1] Note that here we assume the variance of vacuum noise to be equal to 1/2.

$$\mathbf{V}_{R,I}^{1} = \begin{pmatrix} \gamma\mathbf{1} & \sqrt{\kappa}c\mathbf{Z} \\ \sqrt{\kappa}c\mathbf{Z} & \mu\mathbf{1} \end{pmatrix}, \tag{5.3}$$

under hypotheses H_0 and H_1, respectively, where we set $\omega := 2N_B + 1$ and $\gamma := 2\kappa N_S + \omega$.

At this point the binary decision between target absence and presence is reduced to the discrimination of the two quantum states $\hat{\rho}_{R,I}^{i}$ with $i = 0, 1$ [90–92]. The total error in such a discrimination is given by a linear combination of two error types, $P_{\min} = \pi_0 P(1|H_0) + \pi_1 P(0|H_1)$, where π_0 and π_1 can be interpreted as the a priori probabilities that we assign to the occurrence of each hypothesis.

Due to analytical difficulty, the Helstrom bound based on an optimal POVM may be upper-bounded by the quantum Chernoff bound (QCB) [40] (see Sec. 7.2.2 for details),

$$\begin{aligned} P_{\min} \leq P_{\mathrm{QCB}} &:= \frac{1}{2}\left(\inf_{0\leq s\leq 1} C_s\right), \\ C_s &:= \mathrm{Tr}\left[(\hat{\rho}_{R,I}^{0})^{s}(\hat{\rho}_{R,I}^{1})^{1-s}\right], \end{aligned} \tag{5.4}$$

where the minimisation of the s-overlap C_s occurs over all $0 \leq s \leq 1$. For the problem under study, the minimum is achieved for $s = 1/2$ that corresponds to the simpler quantum Bhattacharyya bound (QBB) [10]

$$P_{\mathrm{QBB}} := \frac{1}{2}\,\mathrm{Tr}\left[\sqrt{\hat{\rho}_{R,I}^{0}}\sqrt{\hat{\rho}_{R,I}^{1}}\right]. \tag{5.5}$$

In particular, there is a closed analytical formula for computing C_s for the QCB between two arbitrary multimode Gaussian states (see Sec. 2.3.1). Using this formula, we can certainly compute the QCB between the two possible output states given in Eqs. (5.2) and (5.3), but the expression is too long to be exhibited here.

In the absence of an idler the best strategy is to use coherent states. The signal is prepared in the coherent state $\left|\sqrt{2N_S}\right\rangle$ which is then sent out to some target region. Under H_0, the received returning mode is in a thermal state with mean photon number N_B and covariance matrix equal to $\omega\mathbf{1}$, i.e., $\hat{a}_R = \hat{a}_B$. Under H_1, the signal is mixed with the background such that $\hat{a}_R = \sqrt{\kappa}\hat{a}_S + \sqrt{1-\kappa}\hat{a}_B$ with $\kappa \in (0, 1)$, corresponding to a displaced thermal state with mean vector $(\sqrt{2\kappa N_S}, 0)$ and covariance matrix $\omega\mathbf{1}$. The QCB of such a coherent state transmitter may be readily computed and takes the exact form [19]

$$P_{\mathrm{err}}^{\mathrm{CS,QCB}} \leq \frac{1}{2}e^{-M\kappa N_S\left(\sqrt{N_B+1}-\sqrt{N_B}\right)^2}. \tag{5.6}$$

Achieving Eq. (5.6) requires the use of an optimal receiver whose structure is not known. The best practical strategy for the reception of coherent states is homodyne detection whose

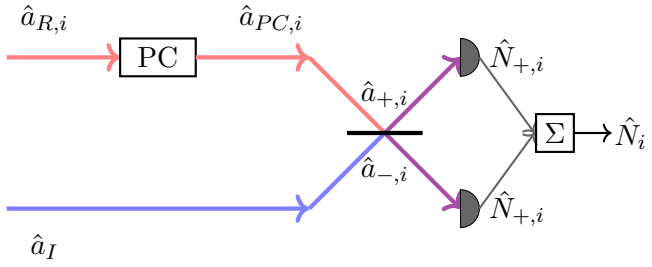

FIG. 5.1: The phase-conjugating (PC) receiver used to calculate the SNR of the QI protocol. Each of the M copies of the returning signal modes are phase-conjugated before being mixed with each of the individual corresponding retained idler modes in a 50-50 beam splitter. These outputs are photodetected with the difference between the two detectors' outputs corresponding to an outcome equivalent to that of the total photon number operator. This is used as input to a threshold detector which makes the binary decision: target absent or target present.

measurement operators are projectors over the quadrature basis. It is best used when the optical field phase is maintained across the detection protocol so that each of the M pulses may be coherently integrated before a binary test can be carried out on the outcome. In such a case the false-alarm probability, $P_{\text{fa}} = P(1|H_0)$, and mis-detection probability, $P_{\text{md}} = P(0|H_1)$, are given by

$$P_{\text{fa}}^{\text{CS,hom}}(x) = \frac{1}{2}\,\text{erfc}\left(\frac{x}{\sqrt{M(2N_B+1)}}\right), \tag{5.7}$$

$$P_{\text{md}}^{\text{CS,hom}}(x) = \frac{1}{2}\,\text{erfc}\left(\frac{M\sqrt{2\kappa N_S}-x}{\sqrt{M(2N_B+1)}}\right), \tag{5.8}$$

where $\text{erfc}(z) := 1 - 2\pi^{-1/2}\int_0^z \exp(-t^2)dt$ is the complementary error function. For equally-likely hypotheses, Eqs. (5.7) and (5.8) may be combined and minimised over x to give the minimum average error probability for homodyne detection and coherent integration

$$P_{\text{err}}^{\text{CS,hom}} = \frac{P_{\text{fa}}^{\text{CS,hom}} + P_{\text{md}}^{\text{CS,hom}}}{2} = \frac{1}{2}\,\text{erfc}\left(\sqrt{\frac{M\kappa N_S}{4N_B+2}}\right). \tag{5.9}$$

5.3 The phase-conjugating receiver

The phase-conjugating (PC) receiver [60] is one possible practical detector for QI. As depicted in Fig. 5.1, this receiver phase-conjugates all M returning modes $\hat{a}_{R,i}^{(k)}$, where $1 \leq k \leq M$ and $i = 0, 1$ (corresponding to the two hypotheses H_0 and H_1), according to

$$\hat{a}_{PC,i} = \sqrt{2}\hat{a}_v + \hat{a}_{R,i}^{\dagger}, \tag{5.10}$$

where $\hat{a}_v$ is the vacuum operator. Since the creation and annihilation operators are defined in terms of quadratures, $\hat{q}$ and $\hat{p}$, via $\hat{a} = (\hat{q} + i\hat{p})/\sqrt{2}$ and $\hat{a}^\dagger = (\hat{q} - i\hat{p})/\sqrt{2}$, respectively, we may recast Eq. (5.10) for $\hat{X} = (\hat{q}, \hat{p})^T$. Thus the PC receiver transforms quadratures as

$$\hat{X}_{PC,i} = \sqrt{2}\hat{X}_v + \mathbf{Z}\hat{X}_{R,i}, \tag{5.11}$$

and the corresponding conditional covariance matrices of the return-idler states are given by

$$\mathbf{V}^0_{PC,I} = \begin{pmatrix} (\omega+1)\mathbf{1} & 0 \\ 0 & \mu\mathbf{1} \end{pmatrix}, \tag{5.12}$$

and

$$\mathbf{V}^1_{PC,I} = \begin{pmatrix} (\gamma+1)\mathbf{1} & \sqrt{\kappa}c\mathbf{Z} \\ \sqrt{\kappa}c\mathbf{Z} & \mu\mathbf{1} \end{pmatrix}, \tag{5.13}$$

under hypotheses H_0 and H_1, respectively.

The individual phase-conjugated signal modes are then mixed with the corresponding retained idler modes on a 50-50 beam splitter whose outputs are given by

$$\hat{a}_{\pm,i} = \frac{\hat{a}_{PC,i} \pm \hat{a}_I}{\sqrt{2}}, \tag{5.14}$$

or, equivalently,

$$\hat{X}_{\pm,i} = \frac{\hat{X}_{PC,i} \pm \hat{X}_I}{\sqrt{2}}. \tag{5.15}$$

These modes with output conditional covariance matrices $\mathbf{V}^i_\pm$, for $i = 0, 1$, are then photodetected yielding photon counts equivalent to measurement outcomes of the number operator $\hat{N}_{\pm,i} = \hat{a}^\dagger_{\pm,i}\hat{a}_{\pm,i}$.

We construct the output conditional covariance matrices $\mathbf{V}^i_\pm$, for $i = 0, 1$, by considering the individual components, e.g., for H_0:

$$\begin{aligned} \langle \hat{X}^2_{+,0} \rangle &= \langle \hat{X}^2_{PC,0} \rangle + \langle \hat{X}^2_0 \rangle + 2\langle \hat{X}_{PC,0}\hat{X}_0 \rangle \\ &= (\omega+1)\mathbf{1} + \mu\mathbf{1} \\ &= \left(\frac{\omega+1+\mu}{2}\right)\mathbf{1} = \langle \hat{X}^2_{-,0} \rangle \end{aligned} \tag{5.16}$$

$$\begin{aligned} \langle \hat{X}_{+,0}\hat{X}_{-,0} \rangle &= \langle \hat{X}^2_{PC,0} \rangle - \langle \hat{X}^2_0 \rangle \\ &= (\omega+1)\mathbf{1} - \mu\mathbf{1} \\ &= \left(\frac{\omega+1-\mu}{2}\right)\mathbf{1}, \end{aligned} \tag{5.17}$$

and similarly for H_1:

$$\begin{aligned}\langle \hat{X}^2_{+,1}\rangle &= \langle \hat{X}^2_{PC,1}\rangle + \langle \hat{X}^2_I\rangle + 2\langle \hat{X}_{PC,1}\hat{X}_I\rangle \\ &= (\gamma+1)\mathbf{1} + \frac{1}{2}\mu\mathbf{1} + \sqrt{\kappa}c\mathbf{1} \\ &= \left(\frac{\gamma+1+\mu}{2} + \sqrt{\kappa}c\right)\mathbf{1}, \end{aligned} \tag{5.18}$$

$$\begin{aligned}\langle \hat{X}^2_{-,1}\rangle &= \langle \hat{X}^2_{PC,1}\rangle + \langle \hat{X}^2_I\rangle - 2\langle \hat{X}_{PC,1}\hat{X}_I\rangle \\ &= \left(\frac{\gamma+1+\mu}{2} - \sqrt{\kappa}c\right)\mathbf{1}, \end{aligned} \tag{5.19}$$

$$\begin{aligned}\langle \hat{X}_{+,1}\hat{X}_{-,1}\rangle &= \langle \hat{X}^2_{PC,1}\rangle - \langle \hat{X}^2_I\rangle \\ &= \left(\frac{\gamma+1-\mu}{2}\right)\mathbf{1}. \end{aligned} \tag{5.20}$$

Thus the output conditional covariance matrices $\mathbf{V}^i_\pm$ are given by

$$\mathbf{V}^0_\pm = \begin{pmatrix} \alpha_+\mathbf{1} & \alpha_-\mathbf{1} \\ \alpha_-\mathbf{1} & \alpha_+\mathbf{1}\end{pmatrix}, \tag{5.21}$$

$$\mathbf{V}^1_\pm = \begin{pmatrix} \beta_+\mathbf{1} & \gamma^*\mathbf{1} \\ \gamma^*\mathbf{1} & \beta_-\mathbf{1}\end{pmatrix}, \tag{5.22}$$

where $\alpha_\pm = (\omega+1\pm\mu)/2$, $\beta_\pm = (\gamma+1+\mu\pm 2\sqrt{\kappa}c)/2$ and $\gamma^* = (\gamma+1-\mu)/2$. It is these modes which are then photodetected yielding photon counts equivalent to measurement outcomes of the number operator $\hat{N}_{\pm,i} = \hat{a}^\dagger_{\pm,i}\hat{a}_{\pm,i}$. The binary decision is made by computing the difference between the two detectors' outputs [20], equivalent to the measurement outcome of the operator

$$\hat{N}_i = \hat{N}_{+,i} - \hat{N}_{-,i}. \tag{5.23}$$

Since the QI protocol uses a very large number of copies, M, of the signal-idler mode pairs the central limit theorem applies to our measurements. That is, the measurement $\hat{N}_i$ yields a Gaussian-distributed random variable, conditioned on the hypothesis. Thus we can write that the QI receiver's signal-to-noise ratio (SNR), for hypotheses with equal prior probabilities, satisfies [60]

$$\mathrm{SNR} = \frac{\left(\langle \hat{N}_1\rangle - \langle \hat{N}_0\rangle\right)^2}{2\left(\sqrt{\langle \Delta\hat{N}^2_1\rangle} + \sqrt{\langle \Delta\hat{N}^2_0\rangle}\right)^2}, \tag{5.24}$$

where $\langle \hat{O}_i\rangle$ and $\langle \Delta\hat{O}^2_i\rangle$, for $i = 0, 1$, are the conditional means and variances of measurement $\hat{O}_i$, respectively, and the notation $\langle \dots \rangle$ denotes an average over all M copies.

To evaluate the PC receiver's SNR for the QI protocol we begin by considering the number operator in terms of quadrature operators, $\hat{N} = \hat{a}^\dagger \hat{a} := (\hat{q}^2 + \hat{p}^2 - 1)/2$. Thus we can write the mean number of photons as

$$\langle \hat{N} \rangle = \frac{\langle \hat{q}^2 \rangle + \langle \hat{p}^2 \rangle - 1}{2}. \tag{5.25}$$

Applying this to the conditional covariance matrices given by Eqs. (5.21) and (5.22), we can compute the numerator of the SNR, Eq. (5.24) for the QI PC receiver as

$$\begin{aligned}\Big(\langle \hat{N}_1 \rangle - \langle \hat{N}_0 \rangle\Big)^2 &= \Big(\langle \hat{N}_{+,1} \rangle - \langle \hat{N}_{-,1} \rangle - \langle \hat{N}_{+,0} \rangle + \langle \hat{N}_{-,0} \rangle\Big)^2 \\ &= (\beta_+ - \beta_-)^2 \\ &= 4\kappa c^2. \end{aligned} \tag{5.26}$$

Considering the photon number variance, we have that

$$\begin{aligned}\langle \Delta \hat{N}^2 \rangle &:= \langle \hat{N}^2 \rangle - \langle \hat{N} \rangle^2 \\ &= \langle (\hat{N}_+ - \hat{N}_-)^2 \rangle - \langle \hat{N}_+ - \hat{N}_- \rangle^2 \\ &= \langle \Delta \hat{N}_+^2 \rangle + \langle \Delta \hat{N}_-^2 \rangle + \underbrace{2\Big[\langle \hat{N}_+ \rangle \langle \hat{N}_- \rangle - \langle \hat{N}_+ \hat{N}_- \rangle\Big]}_{(*)}. \end{aligned} \tag{5.27}$$

For the first two terms we begin by considering the form of the photon number variance in terms of quadrature operators using Eq. (5.25)

$$\begin{aligned}\langle \Delta \hat{N}_\pm^2 \rangle &:= \langle \hat{N}_\pm^2 \rangle - \langle \hat{N}_\pm \rangle^2 \\ &= \frac{1}{4}(\langle \hat{q}_\pm^4 \rangle - \langle \hat{q}_\pm^2 \rangle^2 + \langle \hat{p}_\pm^4 \rangle - \langle \hat{p}_\pm^2 \rangle^2) \\ &= \frac{1}{2}(\langle \hat{q}_\pm^2 \rangle^2 + \langle \hat{p}_\pm^2 \rangle^2), \end{aligned} \tag{5.28}$$

where we have used the following identity for higher-order Gaussian moments for even n

$$\langle \hat{O}^n \rangle = \sigma^n (n-1)!!\,, \tag{5.29}$$

where $\sigma = \sqrt{\langle \hat{O}^2 \rangle}$ is the standard deviation and $!!$ denotes the double factorial.

Rewriting the final term $(*)$ in terms of quadrature components, Eq. (5.25), we find that

$$\begin{aligned}(*) &= \frac{1}{2}(\langle \hat{q}_+^2 \rangle \langle \hat{q}_-^2 \rangle - \langle \hat{q}_+^2 \hat{q}_-^2 \rangle + \langle \hat{q}_+^2 \rangle \langle \hat{p}_-^2 \rangle - \langle \hat{q}_+^2 \hat{p}_-^2 \rangle \\ &\quad + \langle \hat{p}_+^2 \rangle \langle \hat{p}_-^2 \rangle - \langle \hat{p}_+^2 \hat{p}_-^2 \rangle + \langle \hat{q}_-^2 \rangle \langle \hat{p}_+^2 \rangle - \langle \hat{q}_-^2 \hat{p}_+^2 \rangle) \\ &= -(\langle \hat{q}_+ \hat{q}_- \rangle^2 + \langle \hat{q}_+ \hat{p}_- \rangle^2 + \langle \hat{p}_+ \hat{p}_- \rangle^2 + \langle \hat{q}_+ \hat{p}_+ \rangle^2), \end{aligned} \tag{5.30}$$

where we have used the following identity for multivariate higher-order Gaussian moments,

$$\langle \hat{O}_i^2 \hat{O}_j^2 \rangle = \langle \hat{O}_{ii}^2 \rangle \langle \hat{O}_{jj}^2 \rangle + 2 \langle \hat{O}_i \hat{O}_j \rangle^2, \tag{5.31}$$

where $\langle \hat{O}_i \hat{O}_j \rangle$ denotes the covariance of the zero-mean Gaussian variables $\hat{O}_i$ and $\hat{O}_j$.

Computing the required variances and covariances we find

$$\begin{aligned}
&\langle \hat{q}_{+,0}^2 \rangle^2 = \langle \hat{q}_{-,0}^2 \rangle^2 = \langle \hat{p}_{+,0}^2 \rangle^2 = \langle \hat{p}_{-,0}^2 \rangle^2 = \alpha_+^2, \\
&\langle \hat{q}_{+,0} \hat{q}_{-,0} \rangle^2 = \langle \hat{p}_{+,0} \hat{p}_{-,0} \rangle^2 = \alpha_-^2 \\
&\langle \hat{q}_{+,1}^2 \rangle^2 = \langle \hat{p}_{+,1}^2 \rangle^2 = \beta_+^2, \\
&\langle \hat{q}_{-,1}^2 \rangle^2 = \langle \hat{p}_{-,1}^2 \rangle^2 = \beta_-^2, \\
&\langle \hat{q}_{+,1} \hat{q}_{-,1} \rangle^2 = \langle \hat{p}_{+,1} \hat{p}_{-,1} \rangle^2 = \gamma^{*2}.
\end{aligned} \tag{5.32}$$

Inserting these into Eqs. (5.27), (5.28) and (5.30), we obtain the photon number variances,

$$\langle \Delta \hat{N}_0^2 \rangle = 2 \left(\mu(1+\omega) \right), \tag{5.33}$$

$$\langle \Delta \hat{N}_1^2 \rangle = 2 \left(\kappa c^2 + \mu(1+\gamma) \right). \tag{5.34}$$

Finally, we find that the single-mode SNR, Eq. (5.24) of the PC receiver is given by

$$\mathrm{SNR}_{\mathrm{PC}} = \frac{\kappa c^2}{\left(\sqrt{\kappa c^2 + \mu(1+\gamma)} + \sqrt{\mu(1+\omega)} \right)^2}, \tag{5.35}$$

which directly relates to its error probability after M uses, for equally-likely hypotheses, satisfying [60]

$$P_{\mathrm{PC}}^{(M)} = \frac{1}{2} \mathrm{erfc} \left(\sqrt{M \mathrm{SNR}_{\mathrm{PC}}} \right). \tag{5.36}$$

5.4 Comparison between receivers with added noise

It is easy to modify the final formula in Eq. (5.35) to include the presence of extra noise on the idler mode ($\hat{a}_I$) and returning signal mode ($\hat{a}_R$) *before* the action of the PC receiver. Assuming that this extra noise is Gaussian added noise with variances ε_I (for the idler) and ε_R (for the returning signal), we may write the same SNR in Eq. (5.35) up to the following replacement

$$\mu \to \mu' = \mu + \varepsilon_I, \tag{5.37}$$

and

$$\begin{aligned}
&\omega \to \omega' = \omega + \varepsilon_R, \text{ under } H_0, \\
&\gamma \to \gamma' = \gamma + \varepsilon_R, \text{ under } H_1.
\end{aligned} \tag{5.38}$$

Suppose that this added noise is the same amount you would get from the application of a heterodyne measurement, so that $\varepsilon_{I(R)} = 1$. Besides the standard configuration of an entangled TMSV source and the PC receiver that we denote QI+PC, consider the case where both idler and returning signal modes are affected by the extra noise $\varepsilon_I = \varepsilon_R = 1$ before the PC receiver, a configuration that we denote QI+Het+PC. Then, consider the hybrid case where only the returning signal is affected while the idler is noiseless or "calibrated", i.e., $\varepsilon_R = 1$ and $\varepsilon_I = 0$, that we denote QI+Cal+PC.

Considering now another scenario: for the case where both idler and returning signal modes have added noise ($\varepsilon_I = \varepsilon_R = 1$), let us assume this is indeed the effect of heterodyne detections. If we assume that the outcomes are processed in the optimal way so that we may apply the classical Chernoff bound (CCB) [40]. Recall that, for two probability distributions, $p_0(i)$ and $p_1(i)$, the CCB is given by

$$\xi_{\text{CCB}} = -\log\left(\min_{0\leq s\leq 1}\sum_i p_0(i)^s p_1(i)^{1-s}\right). \tag{5.39}$$

The outcomes of the heterodyne detections are distributed according to Gaussian probability densities that are directly related to the Wigner functions of the states. In fact, we have

$$\xi_{\text{CCB}} = \pi^2 \int d^4\mathbf{x}\; W^s_{\mathbf{V}^0+\mathbf{1}}(\mathbf{x}) W^{1-s}_{\mathbf{V}^1+\mathbf{1}}(\mathbf{x}). \tag{5.40}$$

where we have the two modes' quadrature components $\mathbf{x} := (q_R, p_R, q_I, p_I)^T$, $W_{\mathbf{V}^0}(\mathbf{x})$ is the Wigner function of $\hat{\rho}^0_{R,I}$ and $W_{\mathbf{V}^1}(\mathbf{x})$ is that of $\hat{\rho}^1_{R,I}$. Here we have

$$W_{\mathbf{V}^i}(\mathbf{x}) = \frac{\exp\left[-\frac{1}{2}\mathbf{x}^T(\mathbf{V}^i)^{-1}\mathbf{x}\right]}{4\pi^2\sqrt{\det \mathbf{V}^i}}, \tag{5.41}$$

where $\mathbf{V}^i = \mathbf{V}^i_{R,I}$ is given in Eqs. (5.2) and (5.3) for $i = 0, 1$. Denoting this case by QI+Het+CCB, we find that

$$\xi_{\text{QI+Het+CCB}} = \frac{4(1+N_B)}{4+4N_B+\kappa N_S}. \tag{5.42}$$

We can compare the performances of these receivers to that given by the coherent state QCB (CS-QCB) and coherent state transmitter with homodyne detection (CS+Hom), given by Eqs. (5.6) and (5.9), respectively. Results are shown in Fig. 5.2 where we plot the error probability exponent, defined as $\log_{10} P$ where P is the error probability associated with the given receiver, as a function of M. We see that QI+Het+PC is outperformed by CS+Hom

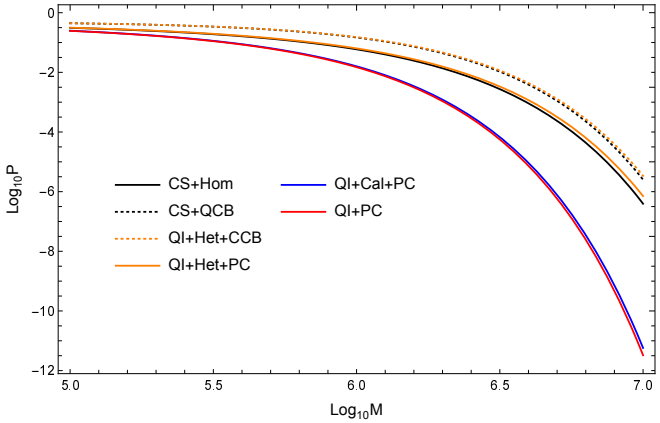

FIG. 5.2: Performance comparison of the various receivers in terms of error exponent versus (logarithmic) number of uses M. The results are computed for parameter values $N_S = N_I = 1/100$, $c = 2\sqrt{N_S(N_I+1)}$, $N_B = 20$ and $\kappa = 1/100$.

whose error probability exponent is always lower. Likewise, QI+Het+CCB does not surpass CS-QCB. However, it can be seen that the hybrid case QI+Cal+PC approaches the noiseless receiver QI+PC under optimal conditions: maximal entanglement, i.e., $c = 2\sqrt{N_S(N_I+1)}$, symmetric low-brightness $N_S = N_I \ll 1$, and large background $N_B \gg 1$. Performing an asymptotic expansion in the regime of large N_B, we find that

$$\mathrm{SNR}_{\mathrm{QI+Cal+PC}} \to \mathrm{SNR}_{\mathrm{QI+PC}} = \frac{(1+N_I)\kappa N_S}{2N_B(1+2N_I)}, \tag{5.43}$$

and

$$\mathrm{SNR}_{\mathrm{QI+Het+PC}} \to \mathrm{SNR}_{\mathrm{CS+Hom}} = \frac{\kappa N_S}{4N_B}. \tag{5.44}$$

The maximal advantage of QI+PC over CS+Hom is given by

$$\frac{\mathrm{SNR}_{\mathrm{QI+PC}}}{\mathrm{SNR}_{\mathrm{CS+Hom}}} = \frac{2(1+N_I)}{1+2N_I} \to 2 \text{ for } N_I \ll 1. \tag{5.45}$$

Our analysis above clearly shows that, whenever the idler mode is affected by an additive Gaussian noise that is equivalent to a heterodyne detection, the performance of coherent state transmitters cannot be beaten. There is indeed another argument to understand why this is the case. Performing a Gaussian measurement on the idler mode of a two-mode Gaussian state remotely prepares an ensemble of Gaussian states on the signal mode [81]. In particular, if the Gaussian state is a TMSV state and the idler mode is heterodyned, then the signal mode is projected onto an ensemble of coherent states, whose average state is thermal with mean number of photons equal to the signal energy of the TMSV state.

5.5 Conclusion

This chapter has investigated the QI protocol for a generically correlated Gaussian source, considering various receiver types. Keeping within the realms of Gaussian operations, we have paid attention to the PC receiver and studied its performance in various cases of added noise due to, for example, the action of a heterodyne measurement on one or both of the modes. The potential of performing a measurement on the idler, while still retaining a quantum advantage, would mitigate one of the major problems associated with QI implementation: idler storage and later recombination with the returning signal. This is of particular concern when the problem involves target ranging, where alternative strategies should be considered(see Refs. [3, 93] and Chap. 9).

Under these considerations, we have modelled the PC receiver for our generic source and have derived the associated SNR in terms of the signal and idler energies, and their cross-correlations. Our SNR may be readily adapted to include additional noise associated with Gaussian measurements. Our results confirm that a heterodyne measurement performed on the idler mode leads to a performance which asymptotically approaches that of a coherent state with homodyne detection, not surpassing it. Interestingly, if the signal mode is subject to added noise due to a heterodyne measurement but the idler mode is maintained clean, the performance asymptotically approaches that of the PC receiver without any added noise. In terms of future work, it would be interesting to investigate these aspects within the setting of unambiguous quantum discrimination [94].

6 Noiseless linear amplification for quantum target detection

Abstract This chapter studies the introduction of non-Gaussian protocols for quantum illumination (QI)-based quantum target detection by considering the action of a noiseless linear amplifier (NLA) at the detection stage. By transforming the problem of QI with an NLA at the receiver to an equivalent protocol with modified effective parameters, we compute the quantum Chernoff bound (QCB) and compare it to the classical benchmark of coherent states under the same NLA action. Our results show that, subject to certain parameter constraints where our analysis is valid, an NLA can significantly improve the performance of QI compared to the equivalent protocol without an NLA. Finally, we initiate a procedure for potentially implementing a measurement-based NLA through appropriate post-selection of heterodyne measurement outcomes.

Relevant Publications Content from the following publications is used in this chapter:

> [6] A. Karsa, M. Ghalaii and S. Pirandola, *Noiseless linear amplification in quantum target detection using Gaussian states*, under review, (2022), arXiv: 2201.02474.

M. Ghalaii provided insight and background of NLAs.

6.1 Introduction

Quantum mechanics, and the non-classical phenomena arising from it, have revolutionised many modern technologies including computation [95–97], communication [98–100] and sensing [11]. Quantum target detection forms a particular subset of quantum sensing protocols in which one's aim is to determine whether or not a target is present in some region of interest. Quantifying one's capability of doing so, and also confirming the benefits of using a quantum strategy, is carried out on the analysis of bounds on the probability of an error, in particular, comparing the upper bound to the lower bound of the corresponding, optimal classical method. Typically this classical benchmark will take the form of a coherent state, a classical state with minimum uncertainty, with homodyne detection at the receiver.

Attainment of the well-known 6 dB quantum advantage through QI relies on the use of an optimal joint measurement, however, the details of such a measurement remains unknown. Various receiver designs have been proposed for QI: the phase-conjugating (PC) and optical parametric amplification (OPA) [60] achieve, at most, a 3 dB performance enhancement over coherent states while a receiver based on sum-frequency generation with feed-forward (FF-SFG) [62] is capable of saturating the quantum Chernoff bound (QCB) for QI, though this receiver remains technologically out of reach. Experimentally, receivers are generally based on homodyne-type measurements carried out on the modes to determine the state's quadrature values. Owing to the uncertainty principle, such measurements necessarily introduce noise to the system. Further, homodyne statistics are described by marginals of the Wigner function of a state which is a classical probability distribution. As such, any homodyne-type measurement on a Gaussian state, whose Wigner function is positive, results in a description of quadratures which is realistic, i.e., not purely quantum-mechanical, and thus unable to demonstrate any violation of Bell inequalities. Nonetheless, Gaussianity offers straightforward means of experimental implementation, with tools associated with Gaussian state generation, transformation and detection readily available in optics labs. As such, one could consider as an alternative either using non-Gaussian measurements on Gaussian states or Gaussian measurements on non-Gaussian states.

While standard, Gaussian amplifiers can effectively recover losses in a classical signal, they necessarily add noise to the system (see Chap. 7 for an illustration of this on coherent states) rendering the resultant effective SNR bounded by the original such that no overall gains in performance can be achieved. Noiseless linear amplifiers (NLAs) offer a non-Gaussian means of non-deterministically amplifying a quantum state without the addition of noise, at the

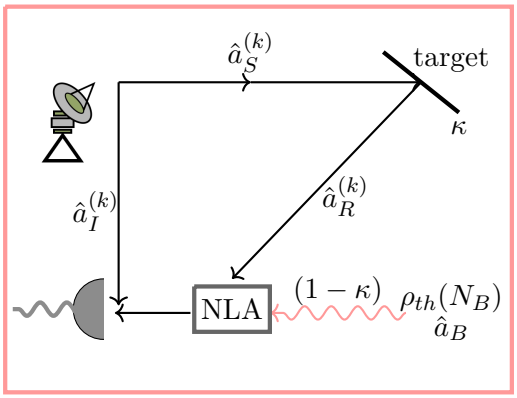

FIG. 6.1: Schematic of QI with the use of an NLA at the receiver. A TMSV state is generated with the signal mode (S) sent to probe the target region and the idler mode (I) sent to the receiver and stored. The target is modelled as a beam splitter with reflectivity κ. The receiver is equipped with an NLA which acts on the returning state which, when the target is present, is a portion κ of the original signal mixed with the background. When the target is absent, $\kappa = 0$ and only the background is received. The output of the NLA is then recombined with the idler in a joint measurement.

expense that when the procedure fails the signal is projected onto the vacuum state and completely lost [127–130] (interested readers are referred to Ref. [131] for a review). Experimentally, different NLA modules have been realised successfully [132–134]. Previously, NLAs have been shown to demonstrate increased robustness against loss and noise in continuous variable (CV) quantum key distribution (QKD) [135–138] and quantum repeater [139–141] protocols allowing for an increase in maximum transmission distance. They have also been shown to improve the performance of quantum distillation protocols [142, 143] and provide a quantum enhancement of the signal-to-noise ratio [144].

In this chapter we consider the use of an NLA at the detection stage of the QI protocol, effectively creating a non-Gaussian receiver for QI with a Gaussian probe. Then, by mapping the protocol of QI with a two-mode squeezed vacuum (TMSV) state with an NLA to one without an NLA but transformed Gaussian state input and quantum channel parameters, we compute the QCB. Considering the same procedure for the classical benchmark of coherent states, we show that under appropriate parameter constraints, an enhanced quantum advantage may be achieved. In particular, the resultant performance of a post-quantum channel NLA on a coherent state is always upper bounded by the performance of a coherent state without the NLA. On the other hand, the NLA acting on the received TMSV quantum channel output always yields an enhancement in detection capabilities.

6.2 Noiseless linear amplification for QI

6.2.1 The QI protocol

Consider the production of M independent signal-idler mode pairs, $\{\hat{a}_S^{(k)}, \hat{a}_I^{(k)}\}$; $1 \leq k \leq M$, with mean number of photons per mode N_S for each of the signal and idler modes, respectively. The signal (S) mode is sent out to some target region while the idler (I) mode is retained at the source for later joint measurement. Their joint state, $\hat{\rho}_{S,I}$, is modelled as a two-mode, zero mean Gaussian state [10] with covariance matrix (CM) given by

$$\mathbf{V}_{S,I} = \begin{pmatrix} \nu\mathbf{1} & c_q\mathbf{Z} \\ c_q\mathbf{Z} & \nu\mathbf{1} \end{pmatrix}, \quad \begin{cases} \mathbf{1} := \mathrm{diag}(1,1), \\ \mathbf{Z} := \mathrm{diag}(1,-1), \end{cases} \tag{6.1}$$

where $\nu := 2N_S + 1$ and $c_q = 2\sqrt{N_S(N_S+1)}$ quantifies the quadrature correlations between the two modes. The off-diagonal terms can in fact take any value such that $0 \leq c \leq 2\sqrt{N_S(N_S+1)}$. In the case where the signal-idler mode pairs are maximally entangled we have $c = c_q := 2\sqrt{N_S(N_S+1)}$ (the TMSV state [10]) while the case $c = c_d := 2N_S$ renders the state just-separable [79, 80].

Under hypothesis H_0, the target is absent so that the returning mode $\hat{a}_R = \hat{a}_B$, where $\hat{a}_B$ is in a thermal state with mean number of photons per mode N_B. Under hypothesis H_1, the target is present such that $\hat{a}_R = \sqrt{\kappa}\hat{a}_S + \sqrt{1-\kappa}\hat{a}_B$, where κ is the target reflectivity, incorporating all propagation losses associated with the channel, and $\hat{a}_B$ is in a thermal state with mean number of photons per mode $N_B/(1-\kappa)$, so that the mean noise photon number is equal under both hypotheses (no passive signature). The conditional joint state, $\hat{\rho}_{R,I}^i$ for $i = 0, 1$, of the returning (R) mode and the retained idler is given by, under hypotheses H_0 and H_1, respectively,

$$\mathbf{V}_{R,I}^0 = \begin{pmatrix} \omega\mathbf{1} & 0 \\ 0 & \nu\mathbf{1} \end{pmatrix}, \tag{6.2}$$

and

$$\mathbf{V}_{R,I}^1 = \begin{pmatrix} \gamma\mathbf{1} & \sqrt{\kappa}c_q\mathbf{Z} \\ \sqrt{\kappa}c_q\mathbf{Z} & \nu\mathbf{1} \end{pmatrix}, \tag{6.3}$$

where we set $\omega := 2N_B + 1$ and $\gamma := 2\kappa N_S + \omega$.

6.2.2 NLA action

An NLA provides a means to achieve phase-insensitive amplification without the addition of any noise at the expense of a probabilistic transformation. Ralph and Lund [129] illustrate this, which we will outline here. Consider the unitary operator $\hat{T}$ which, acting on a coherent state $|\alpha\rangle$ with complex amplitude α, yields the transformation

$$\hat{T}\,|\alpha\rangle = c\,|g\alpha\rangle \tag{6.4}$$

where g is a real number with $|g|> 1$ (i.e., the state is amplified) and c is a complex number with $|c|> 1$. Now consider the following

$$\hat{T}\hat{a}\,|\alpha\rangle = \hat{T}\hat{a}\hat{T}^{\dagger}\hat{T}\,|\alpha\rangle = \hat{T}\hat{a}\hat{T}^{\dagger}\,|g\alpha\rangle = \alpha\,|g\alpha\rangle\,, \tag{6.5}$$

where $\hat{a}$ is the annihilation operator for the coherent state $|\alpha\rangle$ obeying the usual commutation relations $\left[\hat{a},\hat{a}^{\dagger}\right] = 1$. The final equality here implies that coherent state $|g\alpha\rangle$ is an eigenstate of the operator $\hat{b} = \hat{T}\hat{a}\hat{T}^{\dagger}$ with eigenvalue α. However, this in turn implies that $\hat{b} = 1/g\hat{a}$ which would mean that $\left[\hat{b},\hat{b}^{\dagger}\right] = 1/g^2$ while $\left[\hat{b},\hat{b}^{\dagger}\right] = \hat{T}\left[\hat{a},\hat{a}^{\dagger}\right]\hat{T}^{\dagger} = \hat{T}\hat{T}^{\dagger} = 1$, a contradiction.

This is typically rectified by the addition of a noise operator associated with the amplification, which would fix the commutation relations but render the transformation of Eq. (6.4) impossible since the output state would no longer be pure, but mixed. Alternatively, one can instead consider the operator $\hat{T}$ to be non-unitary, yielding a non-deterministic transformation

$$|\alpha\rangle\langle\alpha| \to P_{\text{succ}}^{\text{NLA}}\,|g\alpha\rangle\langle g\alpha| + (1 - P_{\text{succ}}^{\text{NLA}})\,|0\rangle\langle 0|\,, \tag{6.6}$$

where $P_{\text{succ}}^{\text{NLA}}$ is probability with which the NLA succeeds.

Note that on average, taking into account all successful and unsuccessful NLA outcomes, the distinguishability of the quantum states does not increase. However, a scheme where successful amplifications are heralded (see Ref. [129]) such that measurements are only performed on successfully amplified outputs can yield performance enhancements in various protocols [145].

Such a probabilistic transformation is given by the operator $g^{\hat{n}}$ where $\hat{n} = \hat{a}^{\dagger}\hat{a}$ is the number operator whose action on a coherent state is given by [129]

$$g^{\hat{n}}\,|\alpha\rangle = e^{\frac{|\alpha|^2}{2}(g^2-1)}\,|g\alpha\rangle\,. \tag{6.7}$$

6.2.3 Effective parameters for QI with an NLA

Consider the entanglement-based QI protocol where the source is two-mode squeezed vacuum (TMSV) state comprising signal and idler modes given by

$$|\lambda\rangle_{S,I} = \sqrt{1-\lambda^2}\sum_{n=0}^{\infty}\lambda^n |n\rangle_S |n\rangle_I , \tag{6.8}$$

with $\lambda^2 = \frac{N_S}{N_S+1} < 1$, where N_S is the average number of photons per mode. Its initial CM is equivalent to that in Eq. (6.1).

Consider the action of a generic Gaussian channel with transmittance T, and input equivalent excess noise ϵ on a single mode A of an arbitrary input TMSV state with CM $\gamma_{A,B}$. The output CM is given by

$$\gamma'_{A,B} = \begin{pmatrix} T(V(\lambda)+B+\epsilon)\mathbf{1} & \sqrt{T(V(\lambda)^2-1)}\mathbf{Z} \\ \sqrt{T(V(\lambda)^2-1)}\mathbf{Z} & V(\lambda)\mathbf{1} \end{pmatrix}, \tag{6.9}$$

where $V(\lambda) = \frac{1+\lambda^2}{1-\lambda^2}$ is the variance of the thermal state $\mathrm{Tr}_A |\lambda\rangle\langle\lambda|$ and $B = \frac{1-T}{T}$ is the input equivalent noise due to losses.

Now consider the implementation of a NLA to mode A prior to measurement, as shown in Fig. 6.1. It can be shown that the CM $\gamma'_{A,B}(\lambda, T, \epsilon, g)$ of the amplified state, post NLA action, is equivalent to the CM $\gamma'_{A,B}(\zeta, \eta, \epsilon^g, g=1)$ of an equivalent system with EPR parameter ζ, under action of a Gaussian channel with transmittance η and excess noise ϵ^g, without the use of an NLA. These effective parameters are given by

$$\zeta = \lambda\sqrt{\frac{(g^2-1)(\epsilon-2)T-2}{(g^2-1)\epsilon T-2}}, \tag{6.10}$$

$$\eta = \frac{g^2 T}{(g^2-1)T(\frac{1}{4}(g^2-1)(\epsilon-2)\epsilon T-\epsilon+1)+1}, \tag{6.11}$$

$$\epsilon^g = \epsilon - \frac{1}{2}(g^2-1)(\epsilon-2)\epsilon T. \tag{6.12}$$

For the above system of effective parameters to represent an actual physical system, the following constraints must be satisfied: $0 \le \zeta < 1$, $0 \le \eta \le 1$ and $\epsilon^g \ge 0$. The first is always satisfied when

$$0 \le \zeta < 0 \Rightarrow 0 < \lambda < \left(\sqrt{\frac{(g^2-1)(\epsilon-2)T-2}{(g^2-1)\epsilon T-2}}\right)^{-1}. \tag{6.13}$$

The second and third conditions are satisfied provided the excess noise $\epsilon < 2$ and the gain is smaller than a maximum value given by

$$g_{\max} = \sqrt{\frac{\epsilon(T(\epsilon-4)+2) + 4\sqrt{\frac{T(\epsilon-2)+2}{\epsilon}} - 2\sqrt{\epsilon(T(\epsilon-2)+2)} + 4T - 4}{T(\epsilon-2)^2}}. \tag{6.14}$$

Equivalences can be made between Eq. (6.9) and Eq. (5.3): For QI we consider a TMSV state with N_S mean photons per mode such that the variance $V(\lambda) = 2N_S+1$ and $\sqrt{V(\lambda)^2-1} = 2\sqrt{N_S(N_S+1)}$ while Gaussian channel transmittance $T \equiv \kappa$, the target reflectivity. Of course, for real-world target detection, this parameter would also incorporate other losses and gains given by the radar equation. In QI, a portion κ of the signal is mixed with the thermal background, which comprises $N_B/(1-\kappa)$ mean photons per mode. Taking into account this rescaling, when the target is present the returning signal mode (R) takes the form

$$\begin{aligned}\kappa(2N_S+1) + (1-\kappa)\left(\frac{2N_B}{1-\kappa}+1\right) &\equiv TV(\lambda) + BT\left(\frac{2N_B}{1-T}+1\right) \\ &= T\left(V(\lambda) + B + \frac{2N_B}{T}\right) \equiv T(V(\lambda)+B+\epsilon),\end{aligned} \tag{6.15}$$

where excess noise $\epsilon = \frac{2N_B}{T} \equiv \frac{2N_B}{\kappa}$. Thus by considering an equivalent system of effective parameters in place of the two conditional CMs for QI given in Eqs. (6.2) and (6.3), one can consider the additional action of an NLA on the returning signal modes at the receiver, before joint measurement with the retained idler.

Note that the constraint on excess noise to maintain the effective system's physicality means that $\epsilon = \frac{2N_B}{\kappa} < 2$, i.e., $N_B < \kappa$. Since $0 \leq \kappa \leq 1$, we have the global constraint $N_B < 1$ on the mean number of thermal photons associated with the background. Typically, for QI, the parameter constraints involve very high background, $N_B \gg 1$, which is naturally satisfied in the microwave domain at room temperature, and $\kappa \ll 1$. However, these are not strictly necessary for a quantum advantage to exist; provided $N_S \ll 1$ quadrature correlations c_q are maximised and it is from here where the quantum advantage arises. The new constraint on N_B introduced here means that, comfortably, at room temperature ($T = 300$K) applications the protocol described here is valid for frequencies $\gtrsim 4$THz, beginning at the higher end of the microwave. Lower frequencies can meet this requirement as long as the temperature of application is small enough, e.g., for operations at ~ 1GHz we require $T \lesssim 0.07$K.

Further, for a given environment (N_B) and target parameters (κ), Eq. (6.13) implies that the maximum value of signal energy, N_S, that may be employed given by

$$N_S^{\max}(g) = \frac{1 - N_B(g^2 - 1)}{\kappa(g^2 - 1)}, \tag{6.16}$$

which is maximised when $g = 1$, i.e., no amplification occurs and the protocol is equivalent to that of standard QI.

The action of the NLA is a non-deterministic one. That is, it provides a tool for heralded noiseless quantum amplification with probability of success for the transformation $|\alpha\rangle \to |g\alpha\rangle$ given by

$$P_{\text{succ}}^{\text{NLA}} = \frac{1}{g^2}, \tag{6.17}$$

where g is the NLA gain. In other words, under NLA action the number of probings used for the detection process transforms as $M \to M/g^2$ with the remaining $M(g^2 - 1)/g^2$ channel uses discarded.

Thus, with NLA action we are considering post-selected QI and the problem of hypothesis testing becomes one of two stages and four potential outcomes:

H_{00} : Target is absent, and the NLA is unsuccessful;

H_{01} : Target is absent, and the NLA is successful;

H_{10} : Target is present, and the NLA is unsuccessful;

H_{11} : Target is present, and the NLA is successful.

Post-selection essentially discards all events corresponding to hypotheses H_{00} and H_{10} and the problem is reduced to standard QI involving the discrimination of only two hypotheses H_{01} and H_{11}, subject to $M \to M/g^2$.

6.2.4 Classical benchmarking with coherent states

In the absence of an idler the best strategy is to use coherent states. The signal is prepared in the coherent state $|\sqrt{2N_S}\rangle$ which is then sent out to some target region. Under H_0, the received returning mode is in a thermal state with mean photon number N_B and CM equal to $\omega\mathbf{1}$, i.e., $\hat{a}_R = \hat{a}_B$. Under H_1, the signal is mixed with the background such that $\hat{a}_R = \sqrt{\kappa}\hat{a}_S + \sqrt{1-\kappa}\hat{a}_B$ with $\kappa \in (0, 1)$, corresponding to a displaced thermal state with mean vector $(\sqrt{2\kappa N_S}, 0)$ and CM $\omega\mathbf{1}$.

Consider the thermal state $\hat{\rho}_{\rm th}(\lambda_{\rm th})$ with Fock basis representation

$$\hat{\rho}_{\rm th}(\lambda_{\rm th}) = (1-\lambda_{\rm th}^2)\sum_{n=0}^{\infty}\lambda_{\rm th}^{2n}\,|n\rangle\langle n|\,, \tag{6.18}$$

displaced by complex β yielding the state $\hat{\rho} = \hat{D}(\beta)\hat{\rho}_{\rm th}(\lambda_{\rm th})\hat{D}(-\beta)$. Such a state can be written as an ensemble of coherent states,

$$\hat{\rho} = \int P(\alpha)\,|\alpha\rangle\langle\alpha|\,{\rm d}\alpha, \tag{6.19}$$

where $P(\alpha) = \frac{e^{|\alpha|^2}}{\pi^2}\int e^{|u|^2}\langle -u|\hat{\rho}|u\rangle e^{u^\star\alpha - u\alpha^\star}{\rm d}u$, is the P-function.

After successful amplification using operator $\hat{C} = g^{\hat{n}}$, where $\hat{n}$ is the Fock basis number operator, coherent state $|\alpha\rangle$ transforms as

$$\hat{C}\,|\alpha\rangle = e^{\frac{|\alpha|^2}{2}(g^2-1)}\,|g\alpha\rangle \tag{6.20}$$

such that the initial state after NLA action becomes

$$\hat{\rho}' = \hat{C}\hat{\rho}\hat{C} = \int P(\alpha)e^{|\alpha|^2(g^2-1)}\,|g\alpha\rangle\langle g\alpha|\,{\rm d}\alpha. \tag{6.21}$$

After change of variables it can be found that the resulting state after NLA action,

$$\hat{\rho}' \propto \hat{D}(\bar{g}\beta)\hat{\rho}_{\rm th}(g\lambda_{\rm th})\hat{D}(-\bar{g}\beta), \tag{6.22}$$

where $\bar{g} = g\frac{1-\lambda_{\rm th}^2}{1-g^2\lambda_{\rm th}^2}$. That is, as in the case for a TMSV source, result of a displaced thermal state acted on by an NLA is equivalent to a displaced thermal state with modified effective parameters without amplification, subject to the constraint that $g\lambda_{\rm th} < 1$ to ensure physicality.

For QI applications, the initial coherent state $|\sqrt{2N_S}\rangle$ is sent through a quantum channel with reflectivity/transmittance κ such that the displacement can be taken as, $\beta = \sqrt{2\kappa N_S}$. Meanwhile, the variance of the thermal state is given by

$$\frac{1+\lambda_{\rm th}^2}{1-\lambda_{\rm th}^2} = 2N_B + 1 = \omega \Rightarrow \lambda_{\rm th}^2 = \frac{N_B}{1+N_B}. \tag{6.23}$$

Thus, action of the NLA on the displaced thermal state with these parameters yields the following transformations: for the mean,

$$\begin{aligned}\sqrt{2\kappa N_S} &\to g\frac{1-\lambda_{\rm th}^2}{1-g^2\lambda_{\rm th}^2}\sqrt{2\kappa N_S}\\ &= \frac{g}{1+N_B(1-g^2)}\sqrt{2\kappa N_S} = \beta'.\end{aligned} \tag{6.24}$$

Then,

$$\lambda_{\rm th}^2 = \frac{N_B}{1+N_B} \to g^2 \frac{N_B}{1+N_B} = \lambda_{\rm th}'^2, \tag{6.25}$$

such that the effective variance becomes

$$\frac{1+\lambda_{\rm th}'^2}{1-\lambda_{\rm th}'^2} = \frac{1+N_B(1+g^2)}{1+N_B(1-g^2)} = \omega'. \tag{6.26}$$

6.2.5 Performance bounds for QI with NLA

TMSV state with NLA

Using the tools of Sec. 2.3.1 the QCB of the maximally-entangled TMSV source for QI may be computed. We compute the QCB for a single successful use of the QI protocol, where the probability of success is given by that of the NLA which in the ideal case is equal to $P_{\rm succ}^{\rm NLA} = 1/g^2$, where g is the NLA gain. Let us denote the QCB on the output of a successful NLA following QI as $\xi_{\rm QI+NLA}$. Then, for equally likely hypotheses, and after k uses, the QCB becomes

$$\frac{1}{2}\left(\xi_{\rm QI+NLA}\right)^k. \tag{6.27}$$

But, we must include the probabilistic nature of successful outcomes. Given a total of M uses of the entire QI protocol, that is M copies of the TMSV source, discrimination is carried out on the k successful outcomes where k follows a binomial distribution. Then, the total average error probability, for equally likely hypotheses, becomes

$$\begin{aligned} P_{\rm QI+NLA}^{\rm QCB} &= \frac{1}{2}\sum_{k=0}^{M}\left(\xi_{\rm QI+NLA}\right)^k \binom{M}{k} \left(P_{\rm succ}^{\rm NLA}\right)^k \left(1-P_{\rm succ}^{\rm NLA}\right)^{M-k} \\ &= \frac{1}{2}\left(1+P_{\rm succ}^{\rm NLA}(-1+\xi_{\rm QI+NLA})\right)^M \\ &= \frac{1}{2}\left(1+\frac{1}{g^2}(-1+\xi_{\rm QI+NLA})\right)^M, \end{aligned} \tag{6.28}$$

where in the last equality we have set the ideal case of $P_{\rm succ}^{\rm NLA} = 1/g^2$. Note that in the case of no successful NLA outcomes, i.e., $k = 0$, one simply chooses at random, bounding the maximum error to be $1/2$, such that regardless of how the NLA behaves a decision is always made as to whether or not the target is present. Further, all measurements, and thus the entirety of decision-making, are only based on the k successful NLA output states.

The computation is carried out using mathematical computational software and, while the full form too long to be exhibited here, its behaviour is plotted in Figs. 6.2 and 6.3 and discussed in the following sections.

Coherent state with NLA

As with the TMSV source, the tools of Sec. 2.3.1 may be used to compute the QCB of a coherent state with amplification by considering an equivalent protocol, without amplification, using modified effective parameters for mean and variance given by Eqs. (6.24) and (6.26), respectively. For equally-likely hypotheses, the single-use ($M = 1$) QCB for a coherent state with NLA amplification takes the exact form

$$P_{\text{CS+NLA}}^{\text{QCB},M=1} = \frac{1}{2}\exp\left(-\frac{g^2\kappa N_S\left(\sqrt{N_B+1}-g\sqrt{N_B}\right)^2}{(1+N_B-g^2N_B)^3}\right) = \frac{1}{2}\xi_{\text{CS+NLA}}. \tag{6.29}$$

Taking into account the probabilistic nature of our NLA procedure, the overall average error probability for the coherent state source follows the same behaviour as seen for the TMSV state for QI with an NLA. Explicitly, after M uses with k successes, the average error probability becomes

$$P_{\text{CS+NLA}}^{\text{QCB}} = \frac{1}{2}\left(1+\frac{1}{g^2}(-1+\xi_{\text{CS+NLA}})\right)^M, \tag{6.30}$$

Meanwhile, the QCB of such a coherent state transmitter, without amplification, may be readily computed and takes the exact form [19]

$$P_{\text{CS}}^{\text{QCB}} = \frac{1}{2}\exp\left(-M\kappa N_S\left(\sqrt{N_B+1}-\sqrt{N_B}\right)^2\right). \tag{6.31}$$

6.2.6 Benchmarking QI with NLA

Comparison of NLA protocols

Eq. (6.30) allows for the benchmarking of the TMSV with the use of an NLA for target detection as the coherent state forms the ideal, minimum-uncertainty state and serves as the theoretically optimal classical benchmark.

Taking into account constraints on effective parameters given by Eqs. (6.10), (6.11) and (6.12), Figs. 6.2 and 6.3 plot the performance of the TMSV state with NLA relative to that of a coherent state with NLA. Note that the full, exact forms of the QCB have been employed in the computation, that is, without any assumptions as to the relative magnitude of parameter values.

In Fig. 6.2, the error probability exponent is plotted as function of the NLA gain, g, up to and including $g_{\max}$, for fixed environmental parameters $N_B = 0.1$ and $\kappa = 0.2$ with the total

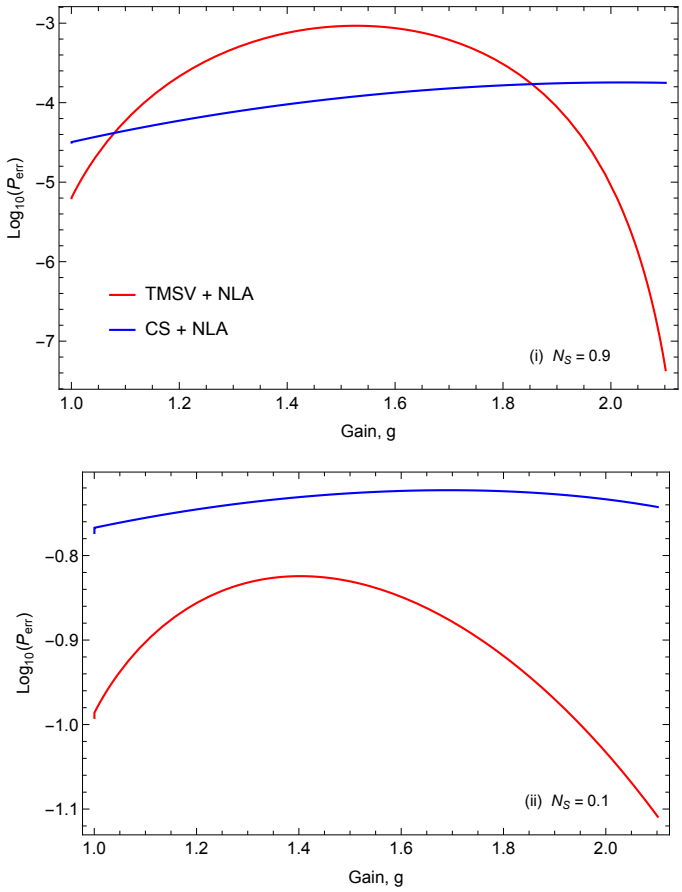

FIG. 6.2: Error probability exponents for QI using a maximally-entangled TMSV source with NLA (red) at the receiver, compared to a coherent state source with the same NLA (blue) as a function of NLA gain, g. In both panels, parameters are set such that $N_B = 0.1$, $\kappa = 0.2$ such that the maximum source energy applicable across the range, $N_S^{\max}(g_{\max}) \simeq 0.96$. Thus, values are plotted for (i) $N_S = 0.9$ and (ii) $N_S = 0.1$. The total number of probes $M = 100$.

number of probings $M = 100$. Based on these parameters it can be found that the maximum energy valid across all values of g, maintaining physicality, is given by $N_S^{\max}(g_{\max}) \simeq 0.96$ thus results are plotted for two values of N_S: 0.9 and 0.1. It can clearly be seen that an increase in the gain, g, has a much larger and more valuable effect on the TMSV state, compared to the same amplification of the returning coherent state. Note that where $g = 1$ the performance coincides with that of the standard QI protocol without any amplification. As expected, smaller values of source energy N_S are favoured by the QI with a TMSV source compared to the coherent state since it is for small N_S where cross-correlations, $c_q = 2\sqrt{N_S(N_S+1)}$, are maximised.

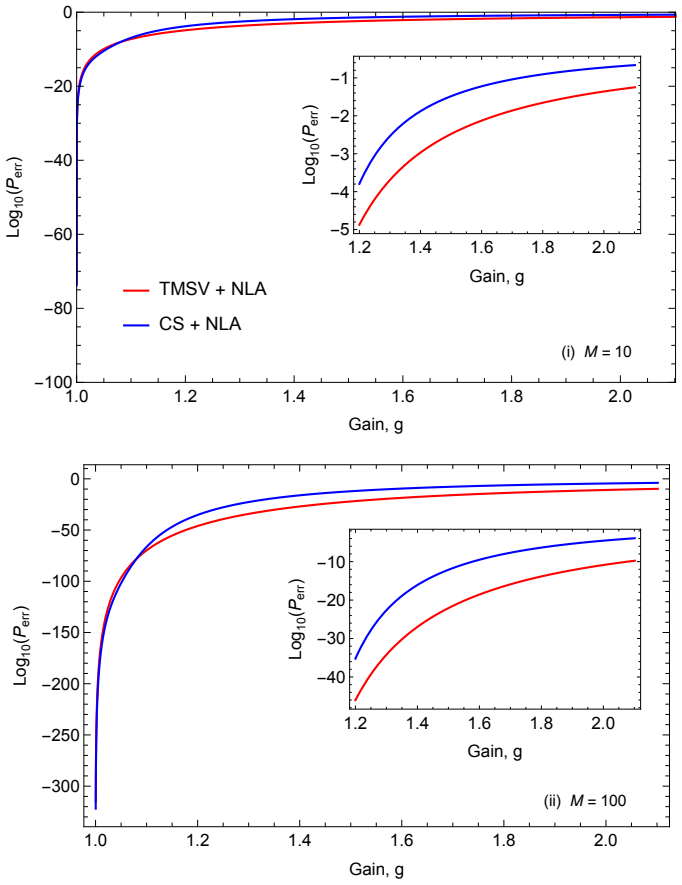

FIG. 6.3: Error probability exponents for QI using a maximally-entangled TMSV source with NLA (red) at the receiver, compared to a coherent state source with the same NLA (blue) as a function of NLA gain, g. In both panels, parameters are set such that $N_B = 0.1$, $\kappa = 0.2$, while for each value of g, the signal energy is set very close (99%) to its local maximum, i.e., $N_S = N_S^{\max(g)}$. Total number of probes is set to for (i) $M = 10$ and (ii) $M = 100$.

Fig. 6.3 plots the same function as Fig. 6.2 with much of the same parameters, however in this scenario rather than considering the global maximum of N_S, applicable across all values of g, up to and including $g_{\max}$, we consider a source whose energy is given by (99% of) the local maximum. That is, for each value of $g \in [0, g_{\max}]$, N_S is set such that $N_S = N_S^{\max}(g)$. Of course, $N_S^{\max}$ is a decreasing function of g, so the behaviour observed for $g \to 1$, where N_S is typically very large, sees the coherent state outperforming the TMSV. However small increases in g show a large quantum advantage can be achieved, even at the maximal N_S value. This quantum advantage may be amplified in cases where the source energy must be kept low, as in stealth surveillance or biomedical sensing where samples may be sensitive to

high energies, due to the freedom available in decreasing N_S below the value used in this comparison. Making use of such freedom will, of course, amplify entanglement benefits.

Comparison with non-NLA protocols

While Sec. 6.2.6 shows that the use of NLAs yields improvement in performance for TMSV protocols over coherent state protocols, there is, of course, a question as to whether or not their use is beneficial when one can simply forgo the NLA and keep all M channel uses in the detection. After all, successful amplification comes at the expense of a proportion, QCBs for target detection, both for QI with a TMSV source and coherent states (see Ref. [1] and Chap. 4 for full details), may be recovered by simply setting $g = 1$.

Figs. 6.4 and 6.5 plot the error probability exponents for QI using a maximally entangled TMSV source with an NLA at the receiver alongside that of a coherent state source using the same NLA. For comparison and to show that the NLA is of actual value, we plot the QCBs for the same protocols without the use of the NLA. In these protocols, all M probings are used at the receiver in decision-making. Results show that there exists a clear advantage in employing NLAs at the receiver compared to without.

Note that there is one difference in the results of Figs. 6.4 and 6.5. In the vast majority of operational regimes, the maximal advantage in employing the NLA is observed for maximum gain, given the regime's associated parameters. This is true for the regime considered in Fig. 6.4. However, at maximal gain, the regime of Fig. 6.5 shows no advantage in using the NLA at all. In this case, one can find that the minimum across the allowed range of g actually occurs at approximately half of the maximum. A possible explanation of this is that when the regime yields a maximum gain which is quite large, the probability of success for the NLA becomes too small. In these cases, while a given successful NLA outcome state can have a higher information content, over the course of the protocol there simply are not enough of them to achieve an overall improvement in target detection.

6.3 Virtual noiseless amplification and Gaussian post-selection

6.3.1 Emulation of noiseless amplification

While the concept of heralded noiseless quantum amplification enables one to probabilistically increase the amplitude of a coherent state with some probability, the physical realisation

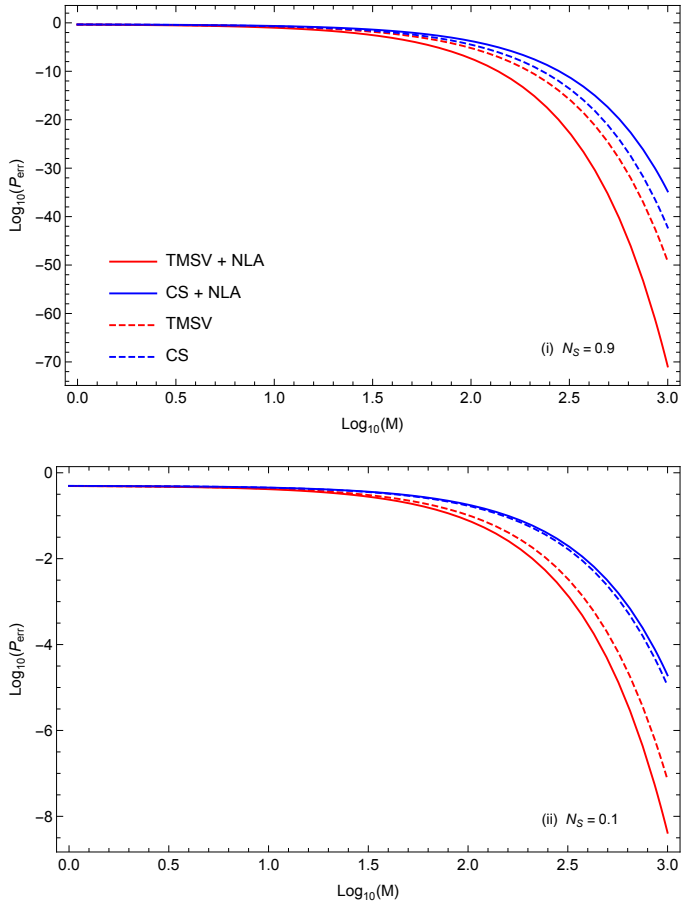

FIG. 6.4: Error probability exponents for QI using a maximally-entangled TMSV source with NLA (red, solid) at the receiver, compared to a coherent state source with the same NLA (blue, solid) as a function of the number of probes, M. Also included are performance bounds without the use of the NLA (dashed). In both panels, parameters are set such that $N_B = 0.1$, $\kappa = 0.2$ such that the maximum source energy applicable across the range, $N_S^{\max}(g_{\max}) \simeq 0.96$, with $g = g_{\max} \simeq 2.1$. Thus, values are plotted for (i) $N_S = 0.9$ and (ii) $N_S = 0.1$.

of such a tool is very demanding. Described by the non-unitary operator $g^{\hat{n}}$, where $\hat{n}$ is the photon number operator, it is unbounded for $g > 1$ so cannot be implemented exactly. Nonetheless, it maintains the Gaussian nature of input states yielding Gaussian outputs, effectively transforming the quantum channel of interest into one of higher associated performances. While implementation is challenging, it has been shown that faithful emulation of noiseless amplification is possible through classical post-processing [101, 149]. Such a virtual emulation of the NLA is possible through protocols where amplification is immediately followed by heterodyne detection.

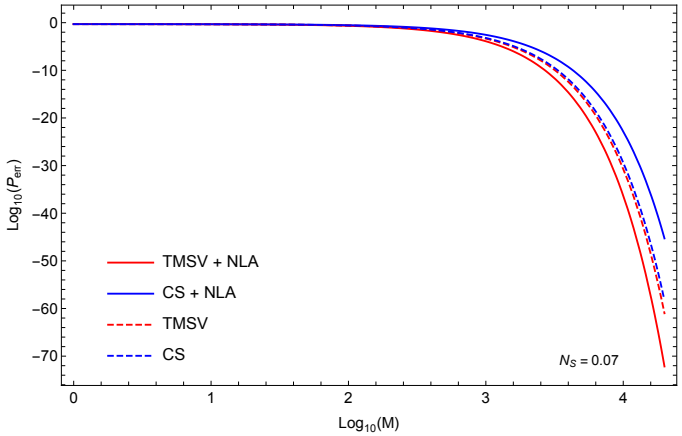

FIG. 6.5: Error probability exponents for QI using a maximally-entangled TMSV source with NLA (red, solid) at the receiver, compared to a coherent state source with the same NLA (blue, solid) as a function of the number of probes, M. Also included are performance bounds without the use of the NLA (dashed). In both panels, parameters are set such that $N_B = 0.005$, $\kappa = 0.1$ such that the maximum source energy applicable across the range, $N_S^{\max}(g_{\max}) \simeq 0.075$, with $g = g_{\max}/2 \simeq 5.5$. Values are plotted for $N_S = 0.07$.

Consider the quantum state $\hat{\rho}$ as output of the quantum channel $\mathcal{L}$. After amplification, one obtains the measurement outcome β with probability

$$\begin{aligned} p_g(\beta) &= \frac{1}{\pi} \langle \beta | \, g^{\hat{n}} \hat{\rho} g^{\hat{n}} \, | \beta \rangle \\ &= \frac{1}{\pi} e^{(g^2-1)|\beta|^2} \langle g\beta | \, \hat{\rho} \, | g\beta \rangle \, , \end{aligned} \tag{6.32}$$

where the identity $g^{\hat{n}} \, |\beta\rangle = e^{(g^2-1)|\beta|^2/2} \, |g\beta\rangle$ has been used. On the other hand, without prior amplification, the measurement outcome γ is obtained with probability

$$p_g(\gamma) = \frac{1}{\pi} \langle \gamma | \, \hat{\rho} \, | \gamma \rangle \, . \tag{6.33}$$

Comparing Eq. (6.33) with Eq. (6.32), one can emulate the NLA by rescaling each measurement outcome γ as $\beta = \gamma/g$ and assign to it a relative weight $Q(\gamma) = e^{(1-g^{-2})|\gamma|^2}$.

The relative weight of these new data points may be simulated in post-selection: each data point γ is accepted with some probability $p_{\text{acc}}(\gamma) \propto Q(\gamma)$. One possibility is to set

$$p_{\text{acc}}(\gamma) = e^{(1-g^{-2})(|\gamma|^2 - |\gamma_{\max}|^2)} \leq 1 \tag{6.34}$$

where $|\gamma_{\max}|$ is the maximum value of $|\gamma|$ within the entire sample of size M. Then, assuming a Gaussian distribution with variance V_γ of measurement outcomes γ,

$$p(\gamma) = \frac{1}{2\pi V_\gamma} e^{-\frac{|\gamma|^2}{2V_\gamma}} , \tag{6.35}$$

one finds that the number of accepted data points $M_{\rm acc} \propto M^k$ where k<1, i.e., $N_{\rm acc}$ grows sublinearly with M.

Alternatively, one can pick a fixed value for $|\gamma_{\rm max}|$ and set $p_{\rm acc}(\gamma) = 1$ for any $|\gamma| > |\gamma_{\rm max}|$. For example, suppose the distribution $p(\gamma)Q(\gamma)$ is expected to have variance V'_γ, then one can choose $|\gamma_{\rm max}| = c\sqrt{V'_\gamma}$ where c is some relatively large number, e.g., 10. Then, we have the lower bound

$$M_{\rm acc} \geq M \int_0^{2\pi} \int_0^{|\gamma_{\rm max}|} p(\gamma) p_{\rm acc}(\gamma) |\gamma| {\rm d}\gamma {\rm d}\phi, \tag{6.36}$$

where $\gamma = |\gamma| e^{i\phi}$. For the Gaussian distribution Eq. (6.35), this recovers a linear scaling of accepted data points

$$\frac{M_{\rm acc}}{M} \geq \frac{g^2}{g^2 + 2V_\gamma(1-g^2)} \left[e^{-(1-g^{-2})|\gamma_{\rm max}|^2} - e^{-\frac{|\gamma_{\rm max}|^2}{2V_\gamma}} \right]. \tag{6.37}$$

In this case the integral converges and emulation of noiseless amplification is possible provided $2(g^2-1)V_\gamma < g^2$.

6.3.2 Virtual noiseless amplification for entanglement-based target detection

Applying the process for emulating noiseless amplification from Sec. 6.3.1 demands a protocol in which amplification is immediately followed by heterodyne detection. Of course, it is not possible to achieve a quantum advantage in target detection using a TMSV state in which heterodyne is used prior to detection [2] since heterodyne of the idler mode immediately projects the signal mode onto an ensemble of coherent states with Gaussian-modulated amplitude. The inherent noise within such states renders them inferior for target detection in comparison to the pure coherent state followed by homodyne detection.

Nonetheless, one can consider a protocol whereby upon return of the signal, after probing the target region, two heterodyne measurements are carried out, first on the idler mode and subsequently the signal mode.

The process of carrying out measurements on two-mode Gaussian states is outlined as follows (see Ref. [81] for full details). Consider an arbitrary two-mode Gaussian state $\hat{\rho}_{AB}$ with mean value $\bar{\mathbf{x}}_{AB} = (\bar{\mathbf{x}}_A, \bar{\mathbf{x}}_B)^T$ and CM

$$\mathbf{V}_{AB} = \begin{pmatrix} \mathbf{A} & \mathbf{C} \\ \mathbf{C}^T & \mathbf{B} \end{pmatrix}, \tag{6.38}$$

where $\mathbf{A} = \mathbf{A}^T$, $\mathbf{B} = \mathbf{B}^T$ and $\mathbf{C}$ are 2×2 real blocks. By detecting mode B, the outcome $\mathbf{k}$ is obtained with probability

$$p(\mathbf{k}) = \frac{\exp\left[\frac{1}{2}\mathbf{d}^T(\mathbf{B}+\mathbf{V}_0)^{-1}\mathbf{d}\right]}{2\pi\sqrt{\det(\mathbf{B}+\mathbf{V}_0)}}, \tag{6.39}$$

where $\mathbf{d} = \bar{\mathbf{x}}_B - \mathbf{k}$, which is Gaussian with classical CM $\mathbf{V_k} = \mathbf{B} + \mathbf{V_0}$. Then, mode A is projected onto a conditional Gaussian state $\hat{\rho}_{A|\mathbf{k}}$, with mean value

$$\bar{\mathbf{x}}_{A|\mathbf{k}} = \bar{\mathbf{x}}_A - \mathbf{C}(\mathbf{B}+\mathbf{V}_0)^{-1}\mathbf{d}, \tag{6.40}$$

and CM

$$\mathbf{V}_{A|\mathbf{k}} = \mathbf{A} - \mathbf{C}(\mathbf{B}+\mathbf{V}_0)^{-1}\mathbf{C}^T. \tag{6.41}$$

Now, consider heterodyne detection on the returning signal and idler mode after probing some target region. When the target is present, the returning state has zero mean and CM given by

$$\mathbf{V}_{R,I} = \begin{pmatrix} (2N_B + 2\kappa N_S + 1)\mathbf{1} & 2\sqrt{\kappa N_S(N_S+1)}\mathbf{Z} \\ 2\sqrt{\kappa N_S(N_S+1)}\mathbf{Z} & (2N_S+1)\mathbf{1} \end{pmatrix}. \tag{6.42}$$

Heterodyne detection of the idler mode yields outcome $\mathbf{k}$ which follows a Gaussian distribution $p(\mathbf{k})$, given by Eq. (6.39), with classical CM $\mathbf{V_k} = \mathbf{B} + \mathbf{V}_0 = (2N_S + 2)\mathbf{1}$, since for heterodyne measurements we have that $\mathbf{V}_0 = \mathbf{1}$. The resultant reduced state of the idler mode, $\hat{\rho}_I$ is in a thermal state with CM $(2N_S + 1)\mathbf{1}$.

Consequently, the signal mode is projected onto the conditional Gaussian state $\hat{\rho}_{S|\mathbf{k}}$ with mean value

$$\bar{\mathbf{x}}_{S|\mathbf{k}} = \sqrt{\frac{\kappa N_S}{N_S+1}}\mathbf{Z}\mathbf{k} \tag{6.43}$$

and CM

$$\mathbf{V}_{S|\mathbf{k}} = (2N_B + 1)\mathbf{1}. \tag{6.44}$$

Now consider an ideal heterodyne measurement of this conditional signal state with positive operator-valued measure (POVM) given by $\{|\boldsymbol{\alpha}\rangle\langle\boldsymbol{\alpha}|/\pi\}$. The overlap between two arbitrary n-mode Gaussian states $\hat{\rho}_1$ and $\hat{\rho}_2$, with covariance matrices $\mathbf{V}_1$ and $\mathbf{V}_2$ and vectors of first moments $\bar{\mathbf{x}}_1$ and $\bar{\mathbf{x}}_2$, is given by [24]

$$\mathrm{Tr}\left[\hat{\rho}_1\hat{\rho}_2\right] = \frac{2^n \exp\left[-\boldsymbol{\delta}^T(\mathbf{V}_1+\mathbf{V}_2)^{-1}\boldsymbol{\delta}\right]}{\sqrt{\det(\mathbf{V}_1+\mathbf{V}_2)}}, \tag{6.45}$$

where $\boldsymbol{\delta} = \bar{\mathbf{x}}_1 - \bar{\mathbf{x}}_2$. Then, letting $\hat{\rho}_1 = |\boldsymbol{\alpha}\rangle\langle\boldsymbol{\alpha}|$, a coherent state, and $\hat{\rho}_2 = \hat{\rho}_{S|\mathbf{k}}$, we find that measurement outcome $\boldsymbol{\alpha}$ is obtained with probability

$$p(\boldsymbol{\alpha}) = \frac{1}{\pi} \operatorname{Tr}\left[|\boldsymbol{\alpha}\rangle\langle\boldsymbol{\alpha}|\, \hat{\rho}_{S|\mathbf{k}}\right], \tag{6.46}$$

where

$$\operatorname{Tr}\left[|\boldsymbol{\alpha}\rangle\langle\boldsymbol{\alpha}|\, \hat{\rho}_{S|\mathbf{k}}\right] = \frac{1}{2(N_B+1)} \exp\left[-\frac{\left(\boldsymbol{\alpha} - \bar{\mathbf{x}}_{S|\mathbf{k}}\right)^T \left(\boldsymbol{\alpha} - \bar{\mathbf{x}}_{S|\mathbf{k}}\right)}{2(N_B+1)}\right]. \tag{6.47}$$

At this point, one's task is to reconcile Eqs. (6.46) and (6.47) with the theory of the measurement-based virtual NLA from Sec. 6.3.1 to determine the number of accepted data points that may be used in decision making. By doing so it is then possible to ascertain whether or not emulation of an NLA can be advantageous despite loss of events in a manner akin to what is observed with a real NLA when the number of events transform as $M \to M/g^2$ for NLA gain, g. While this would enable a true comparison of virtal NLAs with existing benchmarks, here this is left for future work.

6.4 Conclusion and future work

This chapter has explored the use of an NLA at the receiver for QI-based quantum target detection. Our results show that, in the regime where our considerations apply, it is advantageous to use an NLA on the joint-state of the received signal and retained idler after probing the target region compared to not using the NLA. The gains persist despite the fact that noiseless amplification comes at a cost of losing a portion of the data points.

While NLAs remain experimentally demanding to implement, it is possible to simulate the effect of an NLA via a measurement-based approach with appropriate post-processing of measurement outcomes. Sec. 6.3.1 outlined the process of determining a probabilistic filter and appropriate rescaling of heterodyne measurement data to obtain a new dataset which would match the heterodyne results if one had employed a real NLA of gain $g > 1$. After implementation of the virtual NLA, the decision making is based on processing of measurement outcomes. If we assume that the outcomes are processed optimally, we may apply the classical Chernoff bound (CCB) [40] (see also Chap. 5, Sec. 5.4). Then, if one determines that the number of accepted data points is M_{acc}, the CCB for that number of accepted data points would be just the M_{acc}th power of the single-use CCB. At this point one could also consider the implementation of a digital phase-conjugating (PC) receiver, as

studied in Chap. 5, to determine whether or not this version of data-processing, simulating the action of an NLA, is capable of achieving a quantum advantage over coherent states with homodyne detection.

7 Classical benchmarking for microwave quantum illumination

Abstract Quantum illumination (QI) theoretically promises up to a 6dB error exponent advantage in target detection over the best classical protocol. The advantage is maximised by a regime which includes a very high background, which occurs naturally when one considers microwave operation. Such a regime has well-known practical limitations, though it is clear that, theoretically, knowledge of the associated classical benchmark in the microwave is lacking. The requirement of amplifiers for signal detection necessarily renders the optimal classical protocol here different to that which is traditionally used, and only applicable in the optical domain. This work outlines what is the true classical benchmark for microwave QI using coherent states, providing new bounds on the error probability and closed formulae for the receiver operating characteristic (ROC), for both optimal (based on quantum relative entropy) and homodyne detection schemes. An alternative source generation procedure based on coherent states is also proposed which demonstrates potential to reach classically optimal performances achievable in optical applications. The same bounds and measures for the performance of such a source are provided and its potential utility in the future of room temperature quantum detection schemes in the microwave is discussed.

Relevant Publications

Content from the following publications is used in this chapter:

[4] A. Karsa and S. Pirandola, *Classical benchmarking for microwave quantum illumination*, IET Quant. Comm. 2(**4**), 246–257 (2021).
doi: 10.1049/qtc2.12025.

7.1 Introduction

Original work on QI typically assumed operation at optical wavelengths where experimental tools are more readily available. However, at these wavelengths, one of the criteria for an optimal quantum advantage is not realistic: a high background. The natural solution was the theoretical extension of QI's operation to the microwave domain [20], though practical difficulties here, including source-generation and signal-detection, are well-known [102]. Despite this, recent initial microwave QI experiments [59,69] have been carried out showing improved performances over their chosen classical comparison cases. This has been the subject of much debate, since these classical comparison cases are indeed different to the traditionally 'optimal' one based on coherent states and, as such, their performances may be viewed as sub-optimal. However, there are very few known methods for generating a low-energy semi-classical source for room temperature applications. Currently, there are three potential procedures:

1. Source is generated with an amplifier. A microwave coherent state at the single-photon level must first be generated at ultra-low temperature ($\sim$ 7mK). Due to detector limitations and free-space loss, the signal must first be passed through an amplifier prior to probing a target region at $\sim$ 300K. This process necessarily introduces noise to the state rendering the resultant source sub-optimal in the traditional sense.

2. Source is generated without an amplifier. Recently, solid-state devices have been shown to be able to produce 'microwave lasers', or masers, at room temperature [103, 104]. In QI applications, however, these sources must be heavily attenuated in order to achieve low enough photon numbers to form sensible comparisons with entanglement-based QI sources. In order to minimise noise and maintain an approximately coherent source, it is necessary to carry out this attenuation at cryogenic temperatures as will be seen in this work. Note that such a scheme has, as of yet, not been experimentally demonstrated but will be proposed as an alternative in this work with its efficacy studied.

3. Source is generated without an amplifier or cryogenic attenuation. Such a protocol would require reliable low-energy microwave coherent state generation in addition to quantum-limited microwave detectors robust to thermal noise. This would ultimately yield the theoretically 'optimal' classical source previously described, coinciding with what can be seen, as of yet, only in optical applications, however, there is no currently known way to realise this.

Note that the source generation method used in the prototypical experiment [59] was in fact

a hybrid between procedures (1) and (2): a room temperature microwave source generated a weak coherent tone followed by a chain of low temperature attenuators which was then amplified to enable returning signal detection. Further, despite the fact that procedure (3) is impossible to carry out with current experimental capabilities, it persists to be assumed as the classical benchmark in almost all literature pertaining to microwave QI when benchmarking performances. While it is certainly valid and optimal in the optical regime, this does not translate to the microwave where it simply does not exist. Knowledge of the true, regime-dependent, classical benchmark is crucial in order to ascertain the existence of a quantum advantage.

Regardless of the classical benchmarking procedure considered, limitations on detectors pose problems for realistic implementation of coherent state illumination. Irrespective of how the source is generated and transmitted, use of a quantum detector is needed in order to receive such low-energy returning signals since homodyne detection does not work; a quantum detector design is required such that even if the input is coherent (classical), the radar system, as a whole, is still in fact quantum.

This chapter outlines a true classical benchmark for microwave QI for room temperature applications, based on the fact that these techniques are, so far, the only known tools for generating an optimal classical source at the microwave. Sec. 7.2.1 outlines two protocols for microwave QI using coherent states: the first, for a source generated with amplification; the second, proposed by this work, based on the output of a room temperature maser followed by heavy cryogenic attenuation. The tools of quantum hypothesis testing (QHT) are used in Secs. 7.2.2 and 7.2.3 where formulae for the quantum Chernoff bound (QCB) and quantum relative entropy (QRE) are given, under symmetric and asymmetric considerations, respectively, yielding new error bounds for the microwave classical benchmark. In Sec. 7.2.4, a protocol involving homodyne detection of the returning signal is considered with the resulting receiver operating characteristic (ROC) computed. In all cases, the results for these new classical benchmarks are compared to the traditional one applicable only in the optical regime, constrained such that the total energy by which the target is irradiated is maintained. Up to here, this work's analyses are confined to regimes whereby the simultaneous study and comparison of classical benchmarks (1), (2) and (3) are possible. The sheer magnitude of the noise introduced by procedure (1) renders the signal energy per mode so large that any quantum advantage would be diminished owing to the fact that the two-mode, signal-idler, entanglement correlations enabling the QI advantage become irrelevant (see Sec. 4.2) at high brightness. Thus, in Sec. 7.3 the results of Sec. 7.2 are studied as the classical bench-

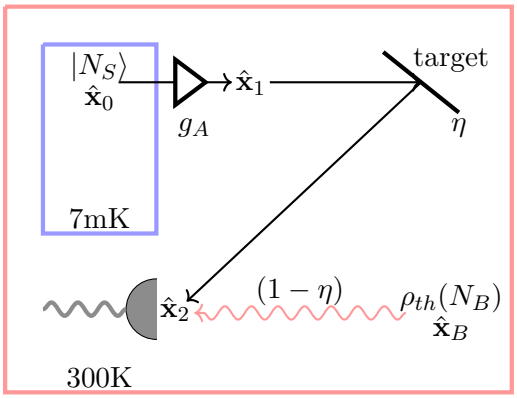

FIG. 7.1: Protocol for experimental microwave QI using a coherent state source generated with an amplifier. Each source mode is prepared in a coherent state $|N_S\rangle$ at 7mK which is passed through an amplifier of gain g_A to probe a target with reflectivity η residing at room temperature, 300K. The received signal is then mixed with the background which is in a thermal state $\rho_{th}(N_B)$.

mark and compared to the performance of a two-mode squeezed vacuum (TMSV) source for entanglement-based QI, within the regime where such a protocol may be applied.

7.2 Classical benchmark for microwave QI

7.2.1 Protocols for microwave QI using coherent states

Source generated with an amplifier

For microwave QI experiments, the classical benchmark is obtained by replacing the QI source with one for coherent states in a fridge operating at $\simeq$ 7mK. Amplifiers must be used to take the source out of this environment in order to probe and detect the presence or absence of a target existing at room temperature (300K), otherwise, the SNR at detection will be too low. Such a process necessarily changes the returning state at the detector to one whose properties are typically very different to those used so far in classical benchmarking for QI. The protocol itself, illustrated in Fig. 7.1, is outlined as follows:

- For the purpose of classical benchmarking, the input is prepared in a coherent state $|N_S\rangle^{\otimes M}$ with mean number of photons per mode, M, equal to N_S. Quadrature operators are given by $\hat{\mathbf{x}}_0 = (\hat{q_0}, \hat{p_0})^{\mathrm{T}}$ with mean $\bar{\mathbf{x}}_0 = (\sqrt{2N_S}, 0)$ and covariance matrix $\mathbf{V}_0 = \mathbf{1}$, the 2×2 identity matrix.

- Upon exiting the fridge to probe a target region at $T = 300\text{K}$, the source must pass through an amplifier characterised by gain $g_A \geq 1$ which, assuming phase-preserving quantum-limited amplification, transforms quadratures as

$$\hat{\mathbf{x}}_0 \to \hat{\mathbf{x}}_1 = \sqrt{g_A}\hat{\mathbf{x}}_0 + \sqrt{g_A - 1}\hat{\mathbf{x}}_A, \tag{7.1}$$

  where $\hat{\mathbf{x}}_A$ are the quadrature operators associated with the amplifier. Rescaling the input as $\hat{\mathbf{x}}_0 \to \hat{\mathbf{x}}_0/\sqrt{g_A}$ yields as output

$$\hat{\mathbf{x}}_1 = \hat{\mathbf{x}}_0 + \sqrt{g_A - 1}\hat{\mathbf{x}}_A \tag{7.2}$$

  with mean $\bar{\mathbf{x}}_1 = \bar{\mathbf{x}}_0$ and covariance matrix $\mathbf{V}_1 = N_A\mathbf{1}$ where $N_A = 2N_B + g_A$ is added number of photons added due to the amplifier, constituting classical noise. Note that $N_A \geq N_B$, where N_A is the mean number of photons associated with the ambient background given by Planck's law, with equality when $g_A = 1$, a minimum. This state constitutes the source seen by the target; the target is irradiated by a displaced thermal state with higher total energy due to the combined photons from the original coherent state *and* those added through the necessary use of an amplifier.

- The interaction of the source $\hat{\mathbf{x}}_1$ with the target may be modelled as a beam splitter[1] with transmissivity η. The returning signal at the receiver, $\hat{\mathbf{x}}_2$, is mixed with background photons constituting a thermal state $\rho_{th}(N_B)$ with $N_B/(1-\eta)$ average photons per mode and quadrature operators $\hat{\mathbf{x}}_B$ such that

$$\hat{\mathbf{x}}_2 = \sqrt{\eta}\hat{\mathbf{x}}_1 + \sqrt{1-\eta}\hat{\mathbf{x}}_B. \tag{7.3}$$

  This state has mean value $\bar{\mathbf{x}}_2 = (\sqrt{2\eta N_S}, 0)$ and variance,

$$\begin{aligned}\mathbf{V_2} &= \eta\left(1 + 2N_A\right)\mathbf{1} + (1-\eta)\left(1 + \frac{2N_B}{1-\eta}\right)\mathbf{1} \\ &= \left(1 + 2\eta N_A + 2N_B\right)\mathbf{1}.\end{aligned} \tag{7.4}$$

- Target detection is then reduced to discriminating between two hypotheses: H_0, target is absent and the received signal is just the thermal state $\hat{\mathbf{x}}_B$ with zero mean and covariance $\mathbf{V}_B = (2N_B + 1)\mathbf{1}$; and H_1, target is present and the received signal is $\hat{\mathbf{x}}_2$.

[1] Note that, while the modelling of the target as a beam splitter with transmissivity η is common within quantum optics and, specifically, its applications in quantum target detection, it is, in fact, a simplification. The transmissivity η would actually vary stochastically with each pulse.

Source generated without an amplifier

An alternative benchmark for microwave QI starts by generating a high energy microwave coherent state such as the output of a room temperature maser. By passing such a state through an ultra-cold beam splitter the source may be energetically diminished providing a suitable benchmark for QI. At the same time, the necessary introduction of environmental noise through the beam splitting process is minimised by ensuring the local ambient temperature, and thus the local ambient background, is small. The protocol, illustrated in Fig. 7.2, is outlined as follows:

- The input is prepared in coherent state $|N_S\rangle^{\otimes M}$ with mean number of photons per mode M equal to $N_S \gg 1$. Quadrature operators are given by $\hat{\mathbf{x}}_0 = (\hat{q_0}, \hat{p_0})^{\mathrm{T}}$ with mean $\bar{\mathbf{x}}_0 = (\sqrt{2N_S}, 0)$ and covariance matrix $\mathbf{V}_0 = \mathbf{1}$.
- The source initially passes through a beam splitter of transmissivity ϕ contained inside a fridge maintained at temperature T. Its specifications are such that $\phi \ll 1$ such that the resulting output state has a low energy suitable for use as a QI benchmark. The state transforms as $\hat{\mathbf{x}}_0 \to \hat{\mathbf{x}}_1$ with mean $\bar{\mathbf{x}}_1 = (\sqrt{2\phi N_S}, 0)$ and covariance matrix $\mathbf{V_1} = (2\bar{n}_T + 1)\mathbf{1}$, where $\bar{n}_T = (\exp[\hbar\nu/k_B T - 1])^{-1}$.
- As previously described, the interaction of the source $\hat{\mathbf{x}}_1$ with the target may be modelled as a beam splitter with transmissivity η such that, at the receiver, we have the return state $\hat{\mathbf{x}}_2$ with mean $\bar{\mathbf{x}}_2 = (\sqrt{2\eta\phi N_S}, 0)$ and covariance matrix $\mathbf{V_2} = (2N_B + 2\eta\bar{n}_T + 1)\mathbf{1}$ is the number of environmental photons per mode associated with the fridge operating at temperature T.
- As before, target detection is then reduced to discriminating between two hypotheses: H_0, target is absent and the received signal is just the thermal state $\hat{\mathbf{x}}_B$ with zero mean and covariance $\mathbf{V}_B = (2N_B + 1)\mathbf{1}$; and H_1, target is present and the received signal is $\hat{\mathbf{x}}_2$.

7.2.2 Classical benchmark for symmetric QHT

Under symmetric QHT one considers the minimisation of the average error probability in the discrimination of two quantum states. Applied to target detection, it provides a measure of the distinguishability of the returning states under each of the two alternative hypotheses: target present and target absent. The QCB provides an upper bound to the minimum

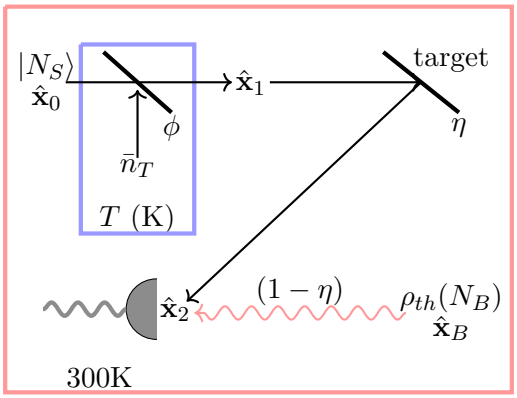

FIG. 7.2: Protocol for experimental microwave QI using a coherent state source generated without an amplifier. Each source mode is prepared in a coherent state $|N_S\rangle$ at 300K with $N_S \gg 1$, i.e., the output of a room temperature maser. Attenuation at temperature T (K) with a beam splitter with transmissivity ϕ mixes the source with environmental noise $\bar{n}_T$ yielding the final source which probes the target with reflectivity η residing at room temperature, 300K. The received signal is then mixed with the background which is in a thermal state $\rho_{th}(N_B)$.

error probability and, for Gaussian states, may be computed straightforwardly using closed formulae (see Sec. 2.3.1 for details).

Source generated with an amplifier

First considering the first protocol for microwave coherent state generation with amplification, we can compute the QCB for such a source. Using an algebraic computation program, it can be found that the QCB for target detection using amplified microwave coherent states is given by

$$P_{\text{err}}^{\text{CS,amp}} \leq \frac{1}{2\xi_1} e^{-M\eta N_S \xi_2}, \tag{7.5}$$

where

$$\begin{aligned}\xi_1 = \Big(&1 + 2N_B(1+N_B) + \eta(N_A + 2N_A N_B) \\ &- 2\sqrt{N_B(1+N_B)(\eta N_A + N_B)(1+\eta N_A + N_B)}\Big)^{1/2},\end{aligned} \tag{7.6}$$

and

$$\xi_2 = \frac{(\sqrt{N_B} - \sqrt{1+N_B})(\sqrt{\eta N_A + N_B} - \sqrt{1+\eta N_A + N_B})}{\sqrt{(1+N_B)(1+\eta N_A + N_B)} - \sqrt{N_B(\eta N_A + N_B)}}. \tag{7.7}$$

When amplifier noise $N_A \to 0$ the usual QI using coherent state bound is recovered which

is valid in, for example, the optical regime, where amplifiers are not required,

$$P_{\text{err}}^{\text{CS}} \leq \frac{1}{2} e^{-M\eta N_S(\sqrt{N_B+1}-\sqrt{N_B})^2}. \tag{7.8}$$

This coincides with the performance of procedure (3) detailed in Sec. 7.1.

Further, in the limit where the background is very large, $N_B \gg 1$ we have that

$$P_{\text{err}}^{\text{CS,amp}} = P_{\text{err}}^{\text{CS}} \approx \frac{1}{2} e^{-M\eta N_S/4N_B}, \tag{7.9}$$

valid for any value of N_A, over which QI using a TMSV state has the well-established factor of 4 error exponent advantage,

$$P_{\text{err}}^{\text{TMSV}} \lesssim \frac{1}{2} e^{-M\eta N_S/N_B}, \tag{7.10}$$

in the limit of large background, $N_B \gg 1$, and small reflectivity, $\eta \ll 1$.

Source generated without an amplifier

The second, alternative, protocol for the generation of low-energy microwave coherent sources for the purposes of QI benchmarking has not been experimentally demonstrated so far. It requires precise use of a room temperature maser (mas) alongside controlled beam splitting at cryogenic temperatures in order to create a suitable state for illumination. As done previously, using an algebraic computation program, it can be found that the QCB for target detection using microwave coherent states generated in this manner is given by

$$P_{\text{err}}^{\text{CS,mas}} \leq \frac{1}{2\chi_1} e^{-M\eta N_S \phi \chi_2}, \tag{7.11}$$

where

$$\begin{aligned} \chi_1 = \Big(&1 + 2N_B(1+N_B) + \eta(\bar{n}_T + 2\bar{n}_T N_B) \\ &- 2\sqrt{N_B(1+N_B)(\eta\bar{n}_T + N_B)(1+\eta\bar{n}_T + N_B)}\Big)^{1/2}, \end{aligned} \tag{7.12}$$

and

$$\chi_2 = \frac{(\sqrt{N_B} - \sqrt{1+N_B})(\sqrt{\eta\bar{n}_T + N_B} - \sqrt{1+\eta\bar{n}_T + N_B})}{\sqrt{(1+N_B)(1+\eta\bar{n}_T + N_B)} - \sqrt{N_B(\eta\bar{n}_T + N_B)}}. \tag{7.13}$$

Notice that the QCB for a room temperature generated source, Eq. (7.11), is a very similar form to that of one generated with amplification, Eq. (7.5). The change of parameters $\xi_{1(2)} \to \chi_{1(2)}$ is done by replacing the added noise due to amplification $N_A \to \bar{n}_T$, the number

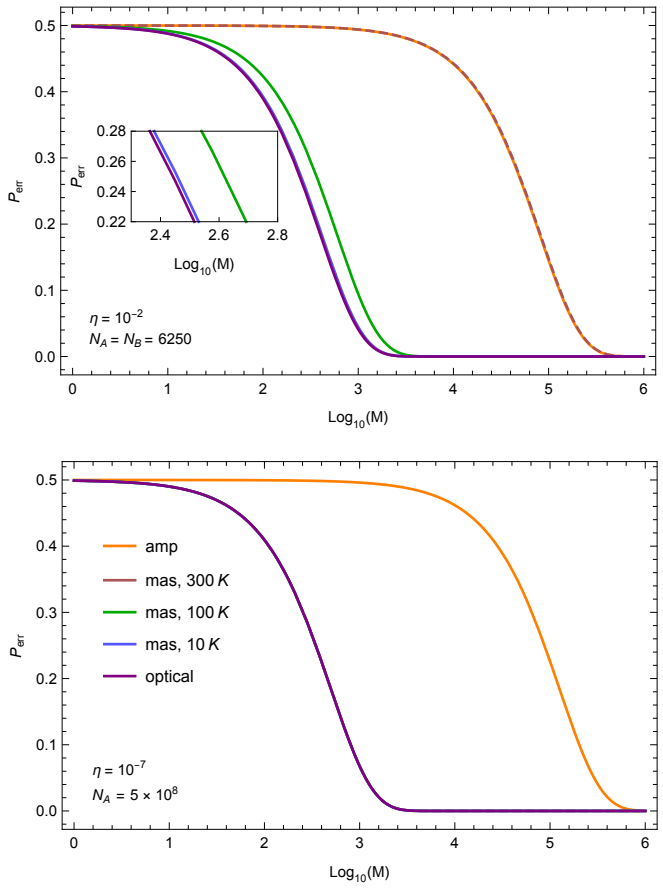

FIG. 7.3: QCB for microwave QI classical benchmarks: 1) with the source generated inside a fridge followed by amplification (amp), and 2) with the source generated by a room temperature maser (mas) followed by attenuation at temperature T (mas, T K), compared to the optical coherent state performance. For the latter two cases we make the substitutions $\phi N_S \to N_S + N_A - \bar{n}_T$ and $N_S \to N_S + N_A$, respectively, with $N_S = 10^{-2}$. We assume the target is maintained at temperature $T = 300$K, yielding $N_B = 6250$. Upper panel: $N_A = N_B = 6250$, the minimum, with reflectivity $\eta = 10^{-2}$ corresponding to a target range of 0.25m assuming receiver collecting area of 0.1m^2. Lower panel: $N_A = 5 \times 10^8$, a typical experimental value, with reflectivity $\eta = 10^{-7}$ corresponding to a target range $\simeq$ 80m. Note with lower N_A and thus signal energy, (mas, 300 K) overlaps with amp (dashed line) highlighting value of cryogenic attenuation. At higher N_A all of the (mas, T K) plots here overlap with that for the optical coherent state due to the magnitude of N_A and resultant energies.

of photons per mode associated to the fridge operating at temperature T K. Further, there is an additional factor ϕ, the transmissivity of the cryogenic beam splitter inside the fridge used to create the low-energy QI source in the error exponent, essentially modulating the SNR by that same amount.

As the fridge temperature $T \to 0$ K, the added noise $\bar{n}_T \to 0$ as well. Imposing this limit along with that for $N_B \gg 1$, the error probability becomes

$$P_{\text{err}}^{\text{CS,mas}} \simeq \frac{1}{2} e^{-M\eta\phi N_S/4N_B}, \tag{7.14}$$

and such a source generated at room temperature performs as the well-known classical benchmark for the optical regime. However, in this scenario, such a performance may be achieved providing the temperature at which attenuation takes place is suitably low.

Fig. 7.3 plots the total error probability, using the QCB, for the microwave QI classical benchmarks: (1) with the source generated inside a fridge followed by amplification (amp), and (2) with the source generated by a room temperature maser (mas) followed by attenuation at temperature T (mas, T K), compared to the un-amplified optical coherent state performance which would coincide with protocol (3) from Sec. 7.1 if it were possible (at the microwave). In order to maintain the overall energy by which the target is irradiated, the substitutions $\phi N_S \to N_S + N_A - \bar{n}_T$ and $N_S \to N_S + N_A$ are made for the latter two, un-amplified, cases. When the source is generated by a maser followed by cryogenic attenuation, the performance closely coincides with that of the coherent state operating in the optical domain at only 10K.

7.2.3 Classical benchmark for asymmetric QHT

Asymmetric QHT, rather than minimising the total average error probability, allows for some small, fixed type-I (false alarm) error, $P_{\text{fa}} < \epsilon$, in an attempt to further minimise the type-II (mis-detection) error, P_{md}. Following quantum Stein's lemma, the quantum relative entropy (QRE) and the quantum relative entropy variance (QREV) give the optimal decay rate of the type-II error in this scenario (see Sec. 2.3.2 for details). An alternative approach using the quantum Hoeffding bound [48, 49] is not considered here.

Source generated with amplification

It can be found that the QRE and QREV for the target detection using microwave coherent states generated with amplification are given by

$$D^{\mathrm{CS,amp}} = \frac{1}{2}\Bigg((1+2N_B+2\eta N_S)\ln\left(1+\frac{1}{\eta N_A+N_B}\right) - (1+2N_B)\ln\left(1+\frac{1}{N_B}\right) + \ln\left(\frac{(\eta N_A+N_B)(1+\eta N_A+N_B)}{N_B(1+N_B)}\right)\Bigg), \tag{7.15}$$

and

$$V^{\mathrm{CS,amp}} = N_B(1+N_B)\ln^2\left(1+\frac{1}{N_B}\right) - 2N_B(1+N_B)\ln\left(1+\frac{1}{N_B}\right)\ln\left(1+\frac{1}{\eta N_A+N_B}\right) + (N_B(1+N_B)+\eta N_S+2\eta N_S N_B)\ln^2\left(1+\frac{1}{\eta N_A+N_B}\right), \tag{7.16}$$

respectively. As in the symmetric case, when amplifier noise $N_A \to 0$, these expressions recover the known quantities for a coherent state transmitter [1, 105] given by

$$D^{\mathrm{CS}} = \eta N_S \ln\left(1+\frac{1}{N_B}\right), \tag{7.17}$$

and

$$V^{\mathrm{CS}} = \eta N_S(2N_B+1)\ln^2\left(1+\frac{1}{N_B}\right). \tag{7.18}$$

Source generated without amplification

Alternatively, for the coherent state source generated without amplification, the QRE and QREV for target detection are given by

$$D^{\mathrm{CS,mas}} = \frac{1}{2}\Bigg((1+2N_B+2\eta\phi N_S)\ln\left(1+\frac{1}{\eta\bar{n}_T+N_B}\right) - (1+2N_B)\ln\left(1+\frac{1}{N_B}\right) + \ln\left(\frac{(\eta\bar{n}_T+N_B)(1+\eta\bar{n}_T+N_B)}{N_B(1+N_B)}\right)\Bigg), \tag{7.19}$$

and

$$V^{\mathrm{CS,mas}} = N_B(1+N_B)\ln^2\left(1+\frac{1}{N_B}\right) - 2N_B(1+N_B)\ln\left(1+\frac{1}{N_B}\right)\ln\left(1+\frac{1}{\eta\bar{n}_T+N_B}\right) + (N_B(1+N_B)+\eta\phi N_S+2\eta\phi N_S N_B)\ln^2\left(1+\frac{1}{\eta\bar{n}_T+N_B}\right), \tag{7.20}$$

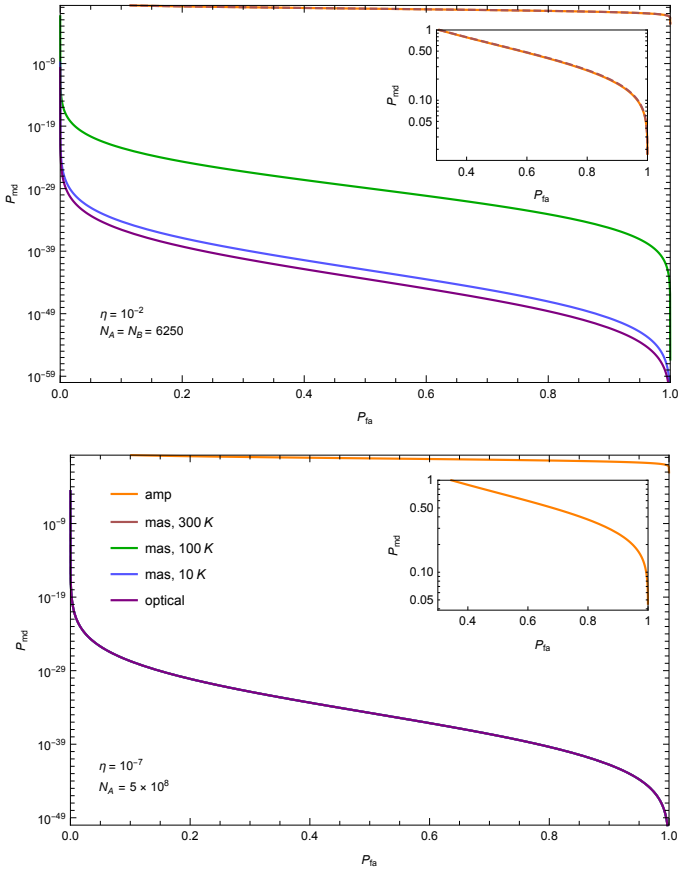

FIG. 7.4: ROC curves generated using the QRE and QREV for microwave QI classical benchmarks: 1) with the source generated inside a fridge followed by amplification (amp), and 2) with the source generated by a room temperature maser (mas) followed by attenuation at temperature T (mas, T K), compared to the optical coherent state performance. For the latter two cases we make the substitutions $\phi N_S \to N_S + N_A - \bar{n}_T$ and $N_S \to N_S + N_A$, respectively, with $N_S = 10^{-2}$. We assume the target is maintained at temperature $T = 300$K, yielding $N_B = 6250$. Upper panel: $N_A = N_B = 6250$, the minimum, with reflectivity $\eta = 10^{-2}$ corresponding to a target range of 0.25m assuming receiver collecting area of 0.1m^2. Lower panel: $N_A = 5 \times 10^8$, a typical experimental value, with reflectivity $\eta = 10^{-7}$ corresponding to a target range $\simeq 80$m. In all cases we set $M = 10^5$. Note with lower N_A and thus signal energy, (mas, 300 K) overlaps with amp (dashed line) highlighting value of cryogenic attenuation. At higher N_A all of the (mas, T K) plots here overlap with that for the optical coherent state due to the magnitude of N_A and resultant energies.

respectively. As in the case for the QCB, the forms of QRE and QREV for the two coherent state sources are very similar with the replacement $N_A \to \bar{n}_T$ and an additional factor $N_S \to \phi N_S$ due to the action of a beam splitter.

Together, combined with the constraint that $P_{\text{fa}} \leq \epsilon$, these can be used to compute the corresponding probability of mis-detection by

$$P_{\text{md}} = \exp\Big\{ -\Big[MD + \sqrt{MV}\Phi^{-1}(\epsilon) + \mathcal{O}(\log M)\Big]\Big\}, \tag{7.21}$$

enabling us to calculate the relevant receiver operating characteristic (ROC) curves.

Fig. 7.4 plots the ROCs, based on the QRE and QREV, for microwave QI classical benchmarks: (1) with the source generated inside a fridge followed by amplification (amp), and (2) with the source generated by a room temperature maser (mas) followed by attenuation at TK (mas, TK), compared to the optical coherent state performance which would coincide with protocol (3) from Sec. 7.1 if it were possible (at the microwave). For the latter two cases we make the substitutions $\phi N_S \to N_S + N_A - \bar{n}_T$ and $N_S \to N_S + N_A$, respectively, to ensure that the total energy by which the target is irradiated is maintained. As seen in the symmetric case with the QCB, attenuating the maser source at a cryogenic temperature achieves a ROC closely coinciding with that of the optical coherent state.

7.2.4 ROC with homodyne detection

In the case of coherent states with homodyne detection (combined with coherent integration and binary decision-making on the measurement results) the ROC is given by combining the following expressions

$$P_{\text{fa}}^{\text{hom}}(x) = \frac{1}{2}\,\text{erfc}\left[\frac{x}{\sqrt{2M\lambda_0}}\right], \tag{7.22}$$

$$P_{\text{md}}^{\text{hom}}(x) = \frac{1}{2}\,\text{erfc}\left[\frac{M\sqrt{2\eta N_S} - x}{\sqrt{2M\lambda_1}}\right], \tag{7.23}$$

where $\text{erfc}(z) := 1 - 2\pi^{-1/2}\int_0^z \exp(-t^2)dt$ is the complementary error function [1].

Regardless of means of source generation, and in both optical and microwave applications, the mean value of the returning signal, in the case where the target is present, is the same and equal to $(\sqrt{2\eta N_S}, 0)$. Further, in the case of a null hypothesis, for Eq. (7.22) we have that $\lambda_0 = 2N_B + 1$ which holds in all considered classical benchmarking protocols. However, the effect of both the amplification and attenuation in the two protocols considered is to

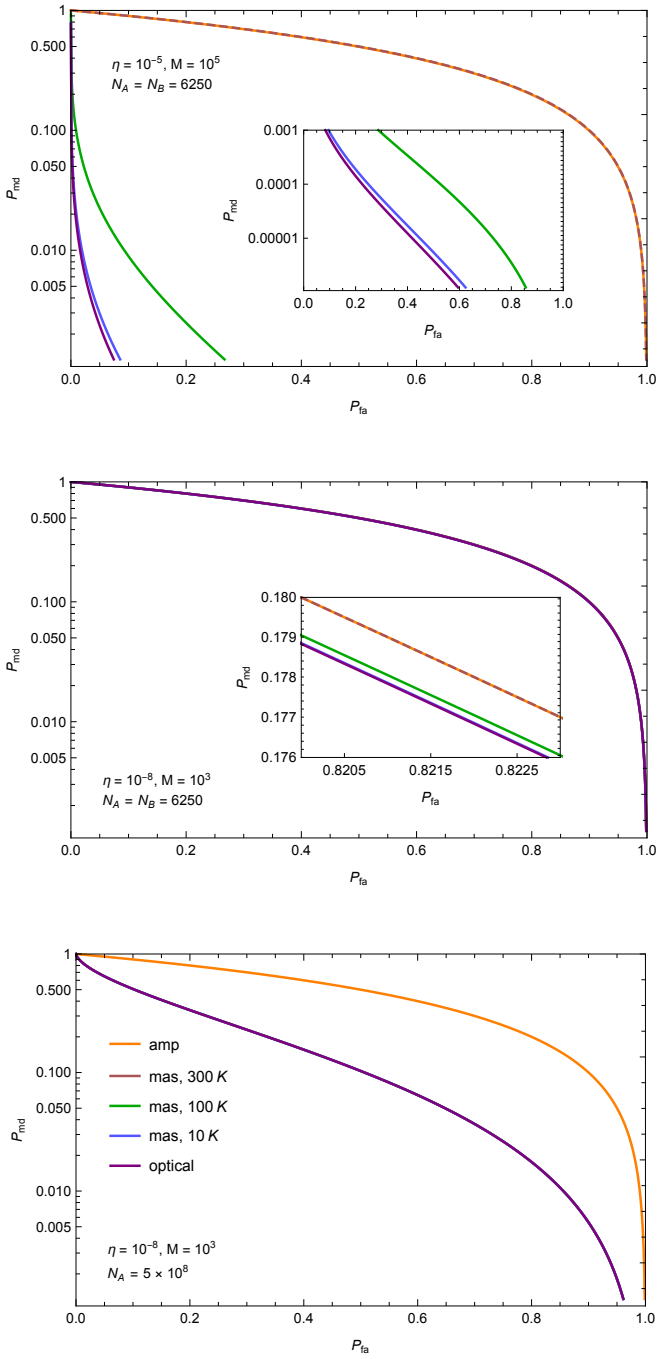

FIG. 7.5: ROCs for coherent state microwave illumination with homodyne detection with: 1) the source generated inside a fridge followed by amplification (amp), and 2) the source generated by a room temperature maser (mas) followed by attenuation at temperature T (mas, T K), compared to the optical coherent state. We set $N_S = 10^{-2}$ and assume target is maintained at temperature $T = 300$K, yielding $N_B = 6250$. Upper panel: $N_A = N_B = 6250$, the minimum, with $\eta = 10^{-5}$ (corresponding to a target range $\simeq$ 8m assuming receiver collecting area of 0.1m^2) and $M = 10^5$. Middle and lower panel: $N_A = N_B = 6250$ and $N_A = 5 \times 10^8$, respectively, with $\eta = 10^{-8}$ ($\simeq$ 250m) and $M = 10^3$.

introduce additional noise to the system prior to target illumination. Thus for Eq. (7.23) we have that $\lambda_1 \to \lambda_{\text{amp}} = 2\eta N_A + 2N_B + 1$ in the amplified case, $\lambda_1 \to \lambda_{\text{mas}} = 2\eta\bar{n}_T + 2N_B + 1$ in the case of the cryogenically attenuated maser, and $\lambda_1 \to \lambda_{\text{opt}} = 2N_B + 1$ in the (optimal) optical case. Then, using the appropriate values for variances, Eq. (7.22) can be inverted and substituted into Eq. (7.23) to derive the corresponding ROC in each of the considered protocols.

For these two panels, with lower N_A and thus signal energy, (mas, 300 K) overlaps with amp (dashed line) highlighting the value of cryogenic attenuation. Note that all of the (mas, T K) plots here overlap with that for the optical coherent state due to the magnitude of N_A and resultant energies.

Fig. 7.5 plots the ROC curves for coherent state microwave illumination with homodyne detection: (1) with the source generated inside a fridge followed by amplification (amp), and (2) with the source generated by a room temperature maser (mas) followed by attenuation at temperature T (mas, T K), compared to the optical coherent state performance would coincide with protocol (3) from Sec. 7.1 if it were possible (at the microwave). For the latter two cases we make the substitutions $\phi N_S \to N_S + N_A - \bar{n}_T$ and $N_S \to N_S + N_A$, respectively, to maintain the total energy incident on the target. As seen with previous results, the proposed technique for source generation based on the output of a room temperature maser performs very closely to the optimal, optical coherent state as long as the attenuating temperature is low.

7.3 Using the new classical benchmark

The purpose of the comparisons seen in Figs. 7.3, 7.4 and 7.5 is to allow for the proper comparison of the three classical benchmarks first outlined in Sec. 7.1 by constraining the total energy by which the target is irradiated. Procedure (1) is responsible for setting this constraint due to the magnitude of the noise introduced by the room temperature amplifier. At a minimum, this is equal to the ambient background which, for room temperature applications ($T = 300$ K), is given by $N_A = N_B \simeq 6250$. This further determines the necessary values of other parameters such as reflectivity η which corresponds to target range, to ultimately allow for the performance comparison.

Of course, such high signal energies per mode are not a valid regime for entanglement-based QI since the correlations which quantify the amount of entanglement are maximised

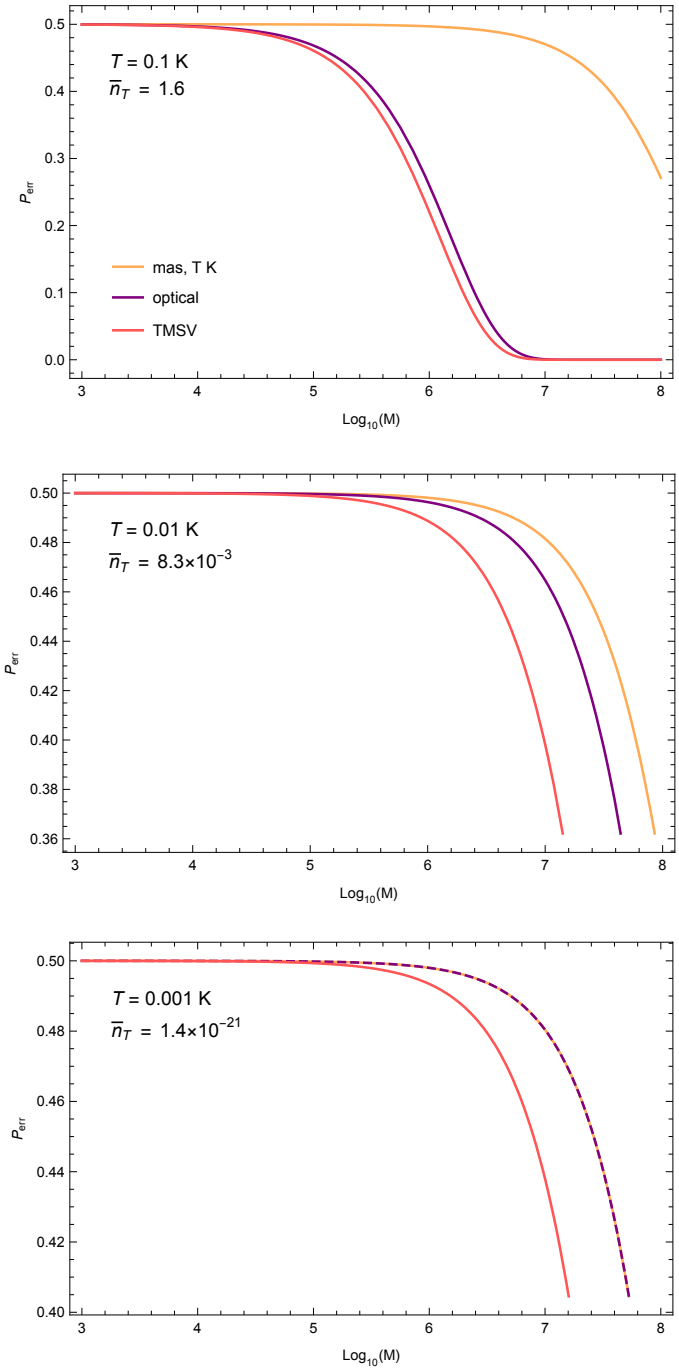

FIG. 7.6: QCB for TMSV microwave QI compared with the new classical benchmarks. Considered are 1) the source generated by a room temperature maser (mas) followed by attenuation at temperature T (mas, T K), 2) comparison with to the optical coherent state performance, and 3) the TMSV. For the latter two cases we make the substitutions $N_S \rightarrow N_S + \bar{n}_T$ with $N_S = 10^{-2}$. We assume the target is maintained at temperature $T = 300$K, yielding $N_B = 6250$. Upper panel: $T = 0.1$ K $\Rightarrow \bar{n}_T = 1.6$. Middle panel: $T = 0.01$ K $\Rightarrow \bar{n}_T = 8.3 \times 10^{-3}$. Lower panel: $T = 0.001$ K $\Rightarrow \bar{n}_T = 1.4 \times 10^{-21}$. We set $\eta = 10^{-2}$ corresponding to a target range of 0.25m assuming receiver collecting area of 0.1m^2.

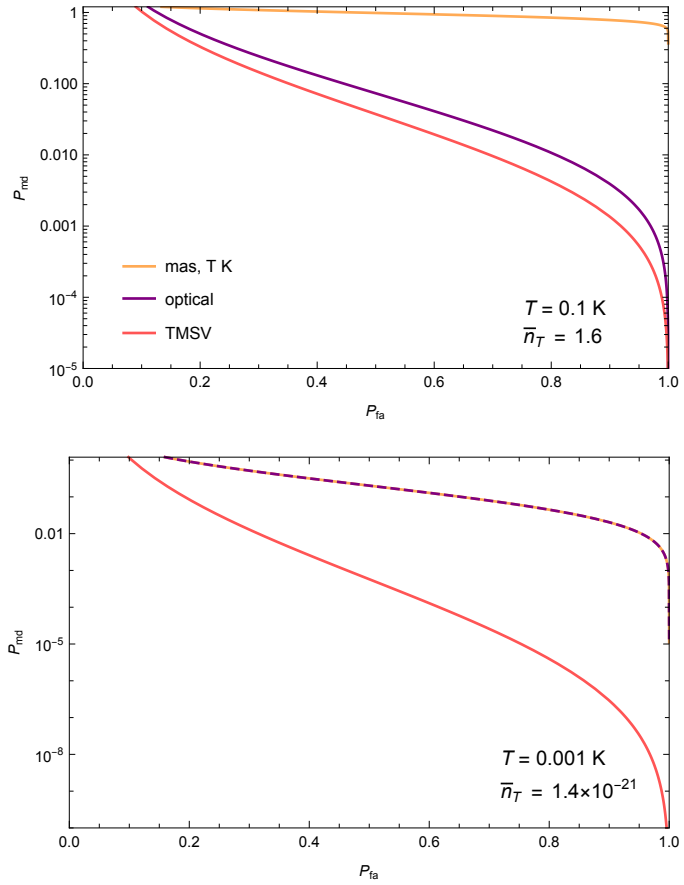

FIG. 7.7: ROCs for TMSV microwave QI compared with the new classical benchmarks. Considered are 1) the source generated by a room temperature maser (mas) followed by attenuation at temperature T (mas, T K), 2) comparison with to the optical coherent state performance, and 3) the TMSV. For the latter two cases we make the substitutions $N_S \to N_S + \bar{n}_T$ with $N_S = 10^{-2}$. We assume the target is maintained at temperature $T = 300$K, yielding $N_B = 6250$. Upper panel: $T = 0.1$ K $\Rightarrow \bar{n}_T = 1.6$. Lower panel: $T = 0.001$ K $\Rightarrow \bar{n}_T = 1.4 \times 10^{-21}$. We set $\eta = 10^{-2}$ corresponding to a target range of 0.25m assuming receiver collecting area of 0.1m^2.

for $N_S \ll 1$; they become irrelevant for $N_S \gg 1$ [1]. Limiting our attention to only procedures (2), room temperature maser source followed by cryogenic attenuation, and (3), currently only possible in the optical domain, a final comparison can be made to the entanglement-based QI using a TMSV source.

Fig. 7.6 plots the QCBs as a function of total number of probings M for the classical benchmark (2) (mas, T K) the optical coherent state (3) and the TMSV QI protocol (see Ref. [1] for full details). Energetic constraints are determined by (mas, T K) whereby the

amplification process alters the total energy by which the target is irradiated as $N_S \to N_S + \bar{n}_T$, and these are the substitutions made for energy in the latter two cases. Note that the values plotted for the TMSV source are exact and valid for all parameter values, i.e., no assumptions have been made as to their relative magnitudes.

Fig. 7.7 shows the ROCs, based on the QRE and QREV (see Ref. [1] for full details), for the same sources and under the same energetic constraints as Fig. 7.6. As for the TMSV QCB, here we use the exact expressions for QRE and QREV in the computation of the ROC such that it is valid for any choice of parameter values.

Results show, as expected, that provided attenuation occurs at small enough T, added noise may be diminished such that the practical coherent state source generation (2) may achieve performances coinciding with the 'optimal' classical benchmark (3), currently only achievable at the microwave. Further, in the regimes considered the TMSV state retains its quantum advantage.

7.4 Concluding remarks

The aim of this work is to outline a true classical benchmark for microwave QI. Current experimental abilities (also limitations) mean that the only way to generate an 'optimal' classical state in the microwave regime is also one which ultimately renders the source 'sub-optimal' compared to traditional notions of the term, though these are based on optical applications where the impeding issues do not exist.

As of yet, the only readily available technique for generating microwave coherent states for room temperature applications (for the purposes of QI benchmarking) requires the use of amplifiers to enable detection of a transmitted signal from low temperature source environment to the target region. Here we have outlined the practical protocol for microwave QI using coherent states, and computed the appropriate performance metrics, which may be used for comparisons, in terms of the total noise added due to the necessary use of amplifiers in the protocol. A new bound on the error probability for classical benchmarking in the microwave regime is given, alongside closed formulae for the ROCs using both the QRE for optimal performances and with homodyne detection, showing the inherent sub-optimality of such a procedure.

A further method is proposed based on a source generated via cryogenically attenuating the output of a room temperature maser. Then, by choosing appropriate levels of attenuation

within a cold enough environment one could potentially generate any appropriately specified source for the given detection problem, taking into account detector limitations, forgoing the need for amplification.

Bounds on the target detection error probability using the QCB are given alongside ROCs based on the QRE and a scheme based on homodyne detection. Results show that such a protocol shows promise in being able to act as an 'optimal' one in the microwave, demonstrating a performance coinciding with optical coherent states provided the attenuation occurs at a low enough temperature to minimise added noise.

Recent developments in continuous-wave room temperature masers using optically pumped nitrogen-vacancy (NV^-) defect centres in diamond [103] and a pentacene-doped crystal [104] give promise to the eventual realisation of such a procedure. Operating at 1.45 GHz and reporting a peak output power of ~ -90dBm and -25dBm, respectively, yielding a rate of $\sim 10^{12}$ and $\sim 10^{18}$ photons per second, such devices could potentially be used for microwave coherent state source generation provided their noise temperatures are kept low.

In Sec. 7.3 the results from preceding sections were employed as the classical benchmark to compare with TMSV performances, verifying that results hold even in regimes where a quantum advantage exists. Explicitly, this regime is one of low brightness ($N_S \ll 1$), high background ($N_B \gg 1$), naturally satisfied in the microwave domain, and low reflectivity ($\eta \ll 1$). There is, however, a trade-off between the first and last requirements - particularly with respect to the fact that η determines to what problems QI may be applied as it incorporates the target range which is, by far, the most dominant loss factor. Confined to a single-use protocol, there is no theoretical limitation to the coherent state signal energy such that propagation losses may be overcome to still yield a result. For a protocol based on entanglement, having to keep N_S small means that the burden of overcoming such losses is shifted to the number of uses M, rendering the value so large that, at least in the near-term, may be experimentally unfeasible.

Although this work's focus has been on classical benchmarking for microwave QI, the proposed alternative method which may prove optimal, as in the optical regime, relies on technologies which are fundamentally quantum. The underlying process in these room temperature maser devices is the optical pumping of quantum spin states that are engineered to exist within the relevant material. Furthermore, for this to be effective and have signal states with quantum-limited noise at the microwave, the use of cryogenic temperature appears to be essential. Yet, any illumination device comprises two distinct components: the

source generator and the signal detector. The enhancement of either or both of these through quantum means would ultimately yield a quantum-enhanced device. Thus one could argue that the classical benchmark for microwave QI proposed here could play two roles: first, at short ranges depending on experimental capabilities, as an optimal classical benchmark for evaluating a quantum advantage; and second, at medium-long ranges, a potential QI device which simply does not use entanglement.

8 Quantum channel position finding using single photons

Abstract Channel position finding is the task of determining the location of a single target channel amongst an ensemble of background channels. It has many potential applications, including quantum sensing, quantum reading and quantum spectroscopy. In particular, it could allow for simple detection protocols to be extended to ones of measurement, for example, target ranging with quantum illumination. The use of quantum states and entanglement in such protocols have shown to yield quantum advantages over their optimal classical counterparts. Here we consider quantum channel position finding using sources specified by at most one single photon on average per mode, using the discrete variable formalism. By considering various quantum sources it is shown through the derivation of performance bounds that a quantum enhancement may be realised.

Relevant Publications

Content from the following publications is used in this chapter:

[5] A. Karsa, J. Carolan, and S. Pirandola, *Quantum channel position finding using single photons*, Phys. Rev. A (**105**), 023705 (2022). doi: 10.1103/PhysRevA.105.023705.

J. Carolan provided knowledge and background of the biphoton state via integrate quantum photonics suggesting its potential use in a discrete variable channel position finding problem.

8.1 Introduction

Quantum hypothesis testing (QHT) [37, 90] is a fundamental tool of quantum sensing where the goal is to distinguish between two alternate hypotheses with applications in quantum reading [11, 106], quantum illumination [1, 19] and spectroscopy [107]. These are problems of quantum channel discrimination (QCD) [50] whereby the different scenarios to be distinguished are characterised by different physical processes modelled as quantum channels of varying parameters. By employing sources which are sensitive to these parameters as channel inputs, the outputs may be analysed in order to make a decision. Determining the optimal strategy for such a task becomes an optimisation problem over both input states and output measurements, typically subject to energetic constraints on the total number of probings and, in the bosonic case, mean number of photons employed.

Channel position finding (CPF) [93, 108] is a problem in multiple channel discrimination whereby given an array of quantum channels where all but one is different, the task is to locate the dissimilar one. It allows for QHT to be extended beyond well-studied binary problems. In the case of quantum illumination, a scenario may exist in which one is certain that the target is located within a region of interest but wishes to determine precisely where, as in quantum target finding [93] (on a plane) or quantum target ranging [3]. The protocol for such a task would involve probing each of the pre-defined locations a fixed number of times then collecting and performing suitable measurements on the returning states. Within the CPF framework, the differing pathways in terms of loss and target reflectivity may be encoded within the quantum channels under study.

Zhuang and Pirandola [93] formulated the general problem of CPF for the testing of multiple quantum hypotheses providing upper and lower bounds on the error probability. This was given for a classical CPF protocol using coherent state sources (minimum uncertainty states with positive P-representation, considered classically 'optimal') and compared to a specific quantum protocol employing maximally entangled two-mode squeezed vacuum (TMSV) states. It was shown that by using the generalised conditional-nulling (CN) receiver at the output a quantum advantage could be achieved.

The work presented in this chapter studies the problem of CPF subject to the constraint that the sources considered are comprised of *at most* one single photon. Remaining in the discrete variable setting, while works so far have been focused on continuous variables, we study the potential of quantum-enhanced CPF for various source specifications: Single-photon (Fock) state, GHZ state exhibiting multipartite entanglement across the channel array, bipar-

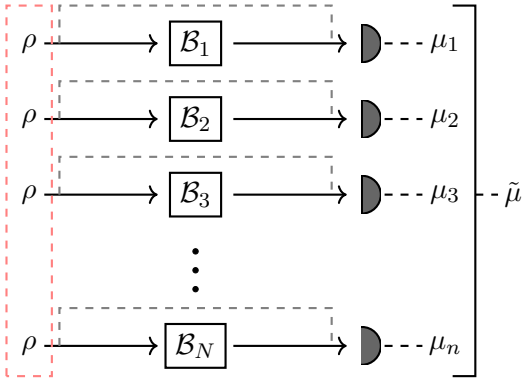

FIG. 8.1: Schematic diagram of channel position finding (CPF). For $i = 1, \ldots, N$ we have an ensemble of boxes B_i and the task is locate the single target channel amongst background channels using identically prepared sources, ρ, which may be specified in several ways. In the classical (coherent state) and single-photon strategies, the source is sent through the channel (black) with the output going straight to the receiver for post-processing. In the quantum strategy two scenarios exist: first, a maximally-entangled two-mode source comprising a signal (black), sent through the channel, and an idler (grey) which recombines with the output at the receiver; second, there are no idlers however the source comprises of multi-mode entanglement spanning the entire N-box array (red). In each case, outputs from boxes are combined to yield a final result, $\tilde{\mu}$, giving the target's location with some error probability.

tite (signal-idler) entanglement in a quantum illumination-style setup, and biphoton (Bell) states. In Section 8.2 we outline the problem of CPF describing the model and mathematical tools used to quantify performances with respect to the source. In Section 8.3 we consider the four quantum sources previously described providing formulae for fidelity and bounds on the CPF error probability. These are compared to the classical benchmark of a coherent state whose amplitude $\alpha = 1$. Finally, in Section 8.3.6 a simple receiver based on photon counting is outlined and applied to two cases: classical coherent state source and single-photon (Fock) state source.

8.2 Problem Specification

8.2.1 Basic model

Consider the basic model of quantum CPF comprised of $N \geq 2$ input-output black boxes as shown in Fig. 8.1. For $i = 1, 2, \ldots N$, the ith box $\mathcal{B}_i$ contains either a reference channel $\mathcal{R}$ or some target channel $\mathcal{E} \neq \mathcal{R}$ and the task is to locate $\mathcal{E}$. We assume the target channel only

occupies one box, such that joint probabilities of the form $\mathrm{P}(\mathcal{B}_i = \mathcal{E}, \mathcal{B}_j = \mathcal{E})$ are all zero, and the target channel is in one of the boxes with certainty, i.e., $\mathrm{P}(\mathcal{B}_i = \mathcal{R}\,\forall i) = 0$. Identification of the target channel is a problem of symmetric quantum hypothesis testing where the task is to discriminate between N hypotheses given by

$$H_i : \mathcal{B}_i = \mathcal{E} \quad \text{and} \quad \mathcal{B}_{j\neq i} = \mathcal{R}. \tag{8.1}$$

To carry out this task we employ a quantum state ρ as input into each of the boxes $\mathcal{B}_i$. Such a quantum system interacting with its environment unavoidably undergoes the quantum dynamical process of decoherence. Such a noisy process may be described by the CPT map $\mathcal{B}(\rho)$ acting on the quantum state ρ using the Kraus representation

$$\mathcal{B}(\rho) = \sum_{\mu} K_\mu \rho K_\mu^\dagger, \tag{8.2}$$

where K_μ are the Kraus operators satisfying $\sum_\mu K_\mu^\dagger K_\mu = \mathbb{1}$. The output state is then clearly dependent on the channel's specification: whether $\mathcal{B} = \mathcal{R}$, the reference channel, or $\mathcal{B} = \mathcal{E}$, the target channel.

We model the contents of each box $\mathcal{B}_i$ as a purely dissipative amplitude damping channel (ADC) with Kraus operators [7]

$$\mathbf{K}_{\mathrm{ADC}} = \{|0\rangle\langle 0| + \sqrt{1-\gamma}\,|1\rangle\langle 1|\,, \sqrt{\gamma}\,|0\rangle\langle 1|\}, \tag{8.3}$$

where γ is the damping rate. Of course, in the case where $\gamma = 0$ the channel reduces to the identity. Such a model allows us to also consider inefficient detectors which may themselves be modelled as ADCs with damping rate $\gamma = 1 - \eta$, where η is the efficiency.

The classical output at each detector takes a binary value $\mu_i \in \{0, 1\}$ corresponding to a decision on whether $\mathcal{B}_i = \mathcal{R}$ or $\mathcal{B}_i = \mathcal{E}$, respectively. All of these N outputs must then be post-processed to give a final decision $\tilde{\mu}$ on the target channel's position.

8.2.2 Quantum state discrimination

The task of quantum CPF may be reduced to one of quantum state discrimination [37, 90]. Our aim is, for a given input state ρ, to best distinguish between two possible channel outputs $\mathcal{E}(\rho)$ and $\mathcal{R}(\rho)$.

To determine whether or not a quantum advantage exists we must compute and compare the error probabilities $p_{\mathrm{err}}^{N,M}(\rho)$ for the N-box, M-use discrimination problem using a classical

state ρ_{C} and quantum state ρ_{Q} as input. Exact analytical forms of error probability are difficult to compute but may be replaced by upper and lower bounds [109, 110] such that for any input state ρ we may write

$$L(\rho) \leq p_{\mathrm{err}}^{N,M}(\rho) \leq U(\rho). \tag{8.4}$$

Then, establishing that the inequality $U(\rho_{\mathrm{Q}}) < L(\rho_{\mathrm{C}})$ holds is sufficient to prove that $p_{\mathrm{err}}^{N,M}(\rho_{\mathrm{Q}}) < p_{\mathrm{err}}^{N,M}(\rho_{\mathrm{C}})$.

We assume equiprobable hypotheses, so that $p_i = N^{-1}$ for any i. Suppose that the overall input state has a tensor product form over the N boxes such that $\rho = \sigma^{\otimes N}$, such that

$$\mathcal{E}_i^N(\sigma^{\otimes N}) = \bigotimes_{j \neq i} \mathcal{R}_j(\sigma) \otimes \mathcal{E}_i(\sigma). \tag{8.5}$$

Of course, Eq. (8.5) does not hold for more elaborate quantum systems such as GHZ states where multipartite entanglement is distributed across the entire arrangement of boxes (this will be studied in Section 8.3.3). Then, we have the following upper- and lower bounds [111–114], respectively, for the error probability

$$p_{\mathrm{err}}^{N,M}(\rho) \leq (N-1) F^{2M}\left(\mathcal{E}(\sigma), \mathcal{R}(\sigma)\right), \tag{8.6}$$

$$p_{\mathrm{err}}^{N,M}(\rho) \geq \frac{N-1}{2N} F^{4M}\left(\mathcal{E}(\sigma), \mathcal{R}(\sigma)\right), \tag{8.7}$$

where F is the Bures' fidelity [115, 116]

$$F(\rho, \sigma) := ||\sqrt{\rho}\sqrt{\sigma}||_1 = \mathrm{Tr}\sqrt{\sqrt{\rho}\sigma\sqrt{\rho}}. \tag{8.8}$$

8.3 Results

In the following, Eqs. (8.6), (8.7) and (8.8) are used to compute the fidelity-based upper- and lower bounds in error probability for the N-channel, M-use CPF protocol for the various sources under consideration. Namely, and in order of consideration, these are: the classical benchmark using coherent states; the single-photon (Fock) state; the GHZ state with multipartite entanglement; a two-mode (signal-idler) state with bipartite entanglement. For the final source type with bipartite entanglement an alternative, idler-free CPF protocol is provided. In all cases, the final performance bounds are computed and plotted in Figs. 8.4 and 8.5 at the end of Section 8.3.4.

8.3.1 Classical benchmark

For our classical benchmark we consider the classical input state $\rho_{\mathrm{C}} = \sigma_{\mathrm{C}}^{\otimes N}$ with $\sigma_{\mathrm{C}} = |\alpha\rangle\langle\alpha|$. This is a coherent state with Fock basis representation [10]

$$|\alpha\rangle = \exp\left(\frac{-|\alpha|^2}{2}\right) \sum_{n=0}^{\infty} \frac{\alpha^n}{\sqrt{n!}} |n\rangle\,, \tag{8.9}$$

with complex amplitude $\alpha = |\alpha|^2 e^{i\theta}$ where the magnitude $|\alpha|^2 = \bar{n}$ is the mean number of photons and θ is the phase. Under the action of an arbitrary ADC with damping rate γ, coherent state $|\alpha\rangle \to |\sqrt{\tau}\alpha\rangle$, where $\tau = 1 - \gamma$ is the transmissivity.

The squared-fidelity between the outputs of two ADCs, parametrised by rates γ_0 and γ_1, respectively, acting on $|\alpha\rangle$ is given by

$$F^2\left(|\sqrt{\tau_0}\alpha\rangle\,, |\sqrt{\tau_1}\alpha\rangle\right) = \exp\left(-\bar{n}(\sqrt{1-\gamma_0} - \sqrt{1-\gamma_1})^2\right), \tag{8.10}$$

yielding the classical lower bound benchmark

$$p_{\mathrm{err}}^{N,M}(\rho_{\mathrm{C}}) \geq \frac{N-1}{2N} \exp\left(-2M(\sqrt{1-\gamma_0} - \sqrt{1-\gamma_1})^2\right), \tag{8.11}$$

where we have set $\bar{n} = 1$.

8.3.2 Single-photon state

The first quantum source we will consider is the tensor product of single-qubit or single-photon states $\rho_{\mathrm{Q}} = \sigma_{\mathrm{Q}}^{\otimes N}$ with $\sigma_{\mathrm{Q}} = |1\rangle$ in the computational basis. Under action of the ADC we have that

$$\sigma_{\mathrm{Q}} \to \gamma\,|0\rangle\langle 0| + (1-\gamma)\,|1\rangle\langle 1|\,. \tag{8.12}$$

Computing the fidelity between two arbitrary ADC outputs we obtain

$$F\left(\rho_{\mathrm{Q},0}, \rho_{\mathrm{Q},1}\right) = \sqrt{(1-\gamma_0)(1-\gamma_1)} + \sqrt{\gamma_0\gamma_1}, \tag{8.13}$$

allowing us to write both the lower and upper bounds for error probability as

$$p_{\mathrm{err}}^{N,M}\left(\rho_{\mathrm{Q}}\right) \geq \frac{N-1}{2N}\left(\sqrt{(1-\gamma_0)(1-\gamma_1)} + \sqrt{\gamma_0\gamma_1}\right)^{4M}, \tag{8.14}$$

and

$$p_{\mathrm{err}}^{N,M}\left(\rho_{\mathrm{Q}}\right) \leq (N-1)\left(\sqrt{(1-\gamma_0)(1-\gamma_1)} + \sqrt{\gamma_0\gamma_1}\right)^{2M}. \tag{8.15}$$

8.3.3 Multipartite entanglement

Of course one may consider a quantum source with entanglement distributed across the N boxes. Such a source could take the form of a GHZ state, an entangled quantum state of $N > 2$ d-dimensional subsystems, given by

$$|\mathrm{GHZ}\rangle = \frac{1}{\sqrt{d}} \sum_{i=0}^{d-1} |i\rangle^{\otimes N}. \tag{8.16}$$

In the case of qubits ($d = 2$), it reads

$$|\mathrm{GHZ}\rangle = \frac{|0\rangle^{\otimes N} + |1\rangle^{\otimes N}}{\sqrt{2}}. \tag{8.17}$$

Consider now the action of an N-box system consisting of ADCs with damping rate γ_0 or γ_1 (for one of the N boxes) on the N-partite GHZ state $\Psi = |\mathrm{GHZ}\rangle\langle\mathrm{GHZ}|$. The resulting output state consists of all possible partial decays of constituent states $|1\rangle \to |0\rangle$. Clearly, such a state does not have a tensor product form across the N boxes so the fidelity must be computed across the entire N-partite system outputs

$$\mathcal{E}_i^N(\Psi) = \bigotimes_{j\neq i} \mathcal{R}_j \otimes \mathcal{E}_i(\Psi), \tag{8.18}$$

such that the error probability upper bound reads

$$p_{\mathrm{err}}^{N,M}(\rho) \leq (N-1) F^M \left(\mathcal{E}_i^N(\Psi), \mathcal{E}_k^N(\Psi)\right). \tag{8.19}$$

8.3.4 Bipartite (signal-idler) entanglement

An alternative, entanglement-based quantum source is given by a tensor product over all the boxes ($\otimes N$) where each signal S_i is coupled to an ancillary idler I_i. Only the signal probes the box while the idler is sent directly to the receiver to join the output. The total joint state $\Phi_{S,I}$ forms a Bell pair in the case where the two modes are maximally-entangled and the associated quantum channel takes the form

$$\mathcal{E}_i^N := \otimes_{j\neq i}(\mathcal{R}_{S_j} \otimes \mathcal{I}_{I_j}) \otimes (\mathcal{E}_{S_i} \otimes \mathcal{I}_{I_i}). \tag{8.20}$$

Consider as our two-mode source $\Phi_{S,I}$ a generic state with density operator given by

$$\begin{aligned} \rho_{\mathrm{gen}} = a\,|00\rangle\langle 00| + \sqrt{a(1-a)}\,(|00\rangle\langle 11| + |11\rangle\langle 00|) \\ + (1-a)\,|11\rangle\langle 11|, \end{aligned} \tag{8.21}$$

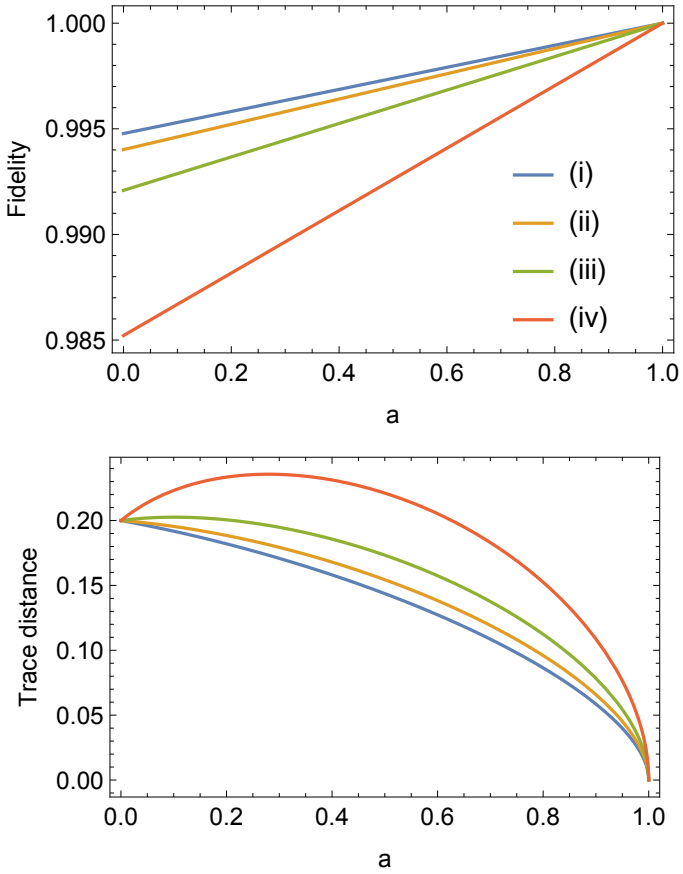

FIG. 8.2: Plots showing fidelity (upper) and trace distance (lower) as a function of a for varying values of damping rate $\gamma_0 = \gamma_1 + 0.1$ with (i) $\gamma_1 = 0.55$, (ii) $\gamma_1 = 0.65$, (iii) $\gamma_1 = 0.75$, and (iv) $\gamma_1 = 0.85$. Fidelity is always minimised for single qubit/photon states where $a = 0$. The trace distance is maximised in most cases by such a Fock state however the optimum value of a resides somewhere in between the two extremes considered, i.e., $0 < a < 1/2$ in regions where damping rates are both relatively high ($\gtrsim 0.75$).

where a is a parameter quantifying how close ρ_{gen} is to a Bell state. That is, when $a = 1/2$ the source is a maximally-entangled Bell state while when $a = 0$ (or $a = 1$) we have the single-qubit/single-photon state $|11\rangle$ (or vacuum state $|00\rangle$), which is clearly separable.

Upon action of an ADC with damping rate γ only on the signal (S) mode while performing

the identity on the reference idler (I) mode our output joint state reads

$$\begin{aligned}\rho_{\text{gen}} \to \rho'_{\text{gen}} =& a\,|00\rangle\langle 00| + (1-a)\gamma\,|01\rangle\langle 01| \\ &+ \sqrt{a(1-a)(1-\gamma)}(|00\rangle\langle 11| + |11\rangle\langle 00|) \\ &+ (1-a)(1-\gamma)\,|11\rangle\langle 11|\,.\end{aligned} \tag{8.22}$$

Computing the fidelity between two output states under differing ADCs with rates γ_0 and γ_1 we obtain

$$F\left(\rho'_{\text{gen},0}, \rho'_{\text{gen},1}\right) = (1-a)\sqrt{(1-x^2)(1-y^2)} + a + xy - axy, \tag{8.23}$$

where we have defined $x = \sqrt{1-\gamma_0}$ and $y = \sqrt{1-\gamma_1}$.

It is clear that the state ρ_{gen} achieving a minimal discrimination error corresponds to that also minimising the above fidelity. Performing this minimisation over a gives the minimum fidelity:

$$F_{\min}\left(\rho'_{\text{gen}}\right) = \begin{cases} 1 & x = y \\ x & x < y = 1 \\ y & y < x = 1 \\ xy + \sqrt{(x^2-1)(y^2-1)} & \text{otherwise.} \end{cases} \tag{8.24}$$

These minima are achieved for $a = 0$ corresponding to the single qubit/photon Fock state $|1\rangle$. The trivial solution of $F_{\min}(\rho'_{\text{gen}}) = 1$ for all values of $x = y$ is achieved for both $a = 0, 1/2$.

The upper panel of Fig. 8.2 plots the quantum fidelity given in Eq. (8.23) as a function of a for varying values of γ_0 and γ_1, confirming that the minimisation occurs at $a = 0$, corresponding to a Fock state. Thus, for use in a signal-idler set-up CPF protocol, Bell states are sup-optimal sources compared to Fock states. Another tool for quantifying the distinguishability of quantum states is the trace distance, where the minimum error may be achieved through its maximisation. This function is similarly plotted in the lower panel of Fig. 8.2.

8.3.5 Biphoton states via integrate quantum photonics

A leading approach to generating bright and pure single-photon states on-chip is through the use of microring resonators (MRRs) [117–119]. They comprise a waveguide ring coupled to a bus waveguide that produces well-defined resonances when the ring's circumference is an integer number of wavelengths [120]. Further, when the waveguide itself is made of a $\chi^{(3)}$ material, such as silicon [121] or silicon nitride [122], photons can be generated via the

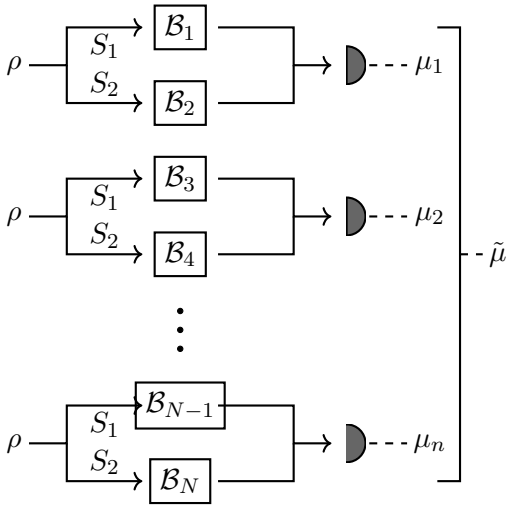

FIG. 8.3: Schematic diagram of idler-free channel position finding (CPF) for biphoton states exhibiting bipartite entanglement for channel arrays consisting of even N boxes.

spontaneous four-wave mixing process. Specifically, pumping the ring with a bright laser at frequency ω_p can cause two photons to be absorbed from the pump, generating a pair of photons at neighbouring frequencies ω_s and ω_i such that energy and momentum are conserved. The frequencies of these generated photons are thus $\omega_s = \omega_p + i \times \mathrm{FSR}$ and $\omega_i = \omega_p - i \times \mathrm{FSR}$ where FSR is the free spectral range of the rings and i indexes a particular resonance. This state is typically referred to as a 'biphoton' state and, assuming the weak pumping regime, can be written as

$$|\psi\rangle = \frac{1}{\sqrt{n}} \sum_{i=1}^{n} |\omega_{-i}\rangle \, |\omega_{+i}\rangle \, . \tag{8.25}$$

Here $|\omega_i\rangle$ represents a single photon in the ith frequency mode and n typically depends on phase-matching conditions for the MRR, which can reach up to $n = 40$ modes [123].

Use in a signal-idler protocol

When $n = 2$ the output is a Bell state in the frequency basis given by

$$|\psi_2\rangle = \frac{1}{\sqrt{2}}(|\omega_{-1}\rangle \, |\omega_{+1}\rangle + |\omega_{-2}\rangle \, |\omega_{+2}\rangle). \tag{8.26}$$

We have seen in Sec. 8.3.4 that such states, used in a signal-idler type set-up for each box, are sub-optimal compared to pure single-photon states. They are, however, relatively straightforward to generate on-chip at both visible and NIR frequencies, and can have a frequency resolution of ~ 1 pm (100's MHz) [124].

Consider the biphoton Bell state (Eq. (8.26)) in a signal-idler set-up for the task of quantum channel position finding, subject to the quantum channel given by Eq. (8.20). In such a protocol we send the first, $-i$, signal mode S_i into the box while retaining the second, $+i$, idler mode I_i for later joint measurement. Computing the fidelity between the two two-mode output states under ADCs with rates γ_0 and γ_1 we obtain

$$F(|\psi_2\rangle\langle\psi_2|_0, |\psi_2\rangle\langle\psi_2|_1) = \frac{1}{2}\left(\sqrt{1-\gamma_0}\sqrt{1-\gamma_1} + 1 + \sqrt{\gamma_0\gamma_1}\right), \tag{8.27}$$

yielding the lower and upper bounds

$$p_{\text{err}}^{N,M}(|\psi_2\rangle\langle\psi_2|) \geq \frac{N-1}{2N} F(|\psi_2\rangle\langle\psi_2|_0, |\psi_2\rangle\langle\psi_2|_1)^{4M}, \tag{8.28}$$

and

$$p_{\text{err}}^{N,M}(|\psi_2\rangle\langle\psi_2|) \leq (N-1) F(|\psi_2\rangle\langle\psi_2|_0, |\psi_2\rangle\langle\psi_2|_1)^{2M}. \tag{8.29}$$

Use in an idler-free protocol

A CPF protocol may be devised in which the full entanglement exhibited in a Bell state may be exploited across the multi-channel array in order to realise a quantum advantage. Such an advantage may be readily demonstrated due to the experimental availability of biphoton states.

Consider the CPF protocol for an even number of boxes N. Using as a source the two-mode biphoton state of Eq. (8.26), label each mode as a signal, S_1 and S_2, to be used as a probe between two adjacent boxes, as shown in Fig. 8.3. Then for any CPF problem comprising $N \geq 4$ individual channels, the global quantum channel acting on the state is

$$\mathcal{E}_i^{N/2} := \otimes_{j\neq i}(\mathcal{R}_{S_{1,j}} \otimes \mathcal{R}_{S_{2,j}}) \otimes (\mathcal{E}_{S_{1,i}} \otimes \mathcal{R}_{S_{2,i}}). \tag{8.30}$$

Computing the fidelity between the two two-mode output states under ADC pairs with rates (γ_0, γ_0) and (γ_1, γ_0) we obtain

$$F(|\psi_2\rangle\langle\psi_2|_{0,0}, |\psi_2\rangle\langle\psi_2|_{1,0}) = \frac{1}{2\sqrt{2}}\sqrt{\frac{\alpha}{\beta}}, \tag{8.31}$$

where

$$\alpha = 2 + 4\Delta + 2\Gamma + 4\Delta\Gamma + 4\Delta\gamma_0 - \gamma_1 + \gamma_0(1 + 2\Gamma + \gamma_0 + 5\gamma_1), \tag{8.32}$$

$$\beta = (1+\Delta)(1+\gamma_0), \tag{8.33}$$

and we have defined

$$\begin{aligned}\Gamma &= \sqrt{1-\gamma_0}\sqrt{1-\gamma_1},\\ \Delta &= \sqrt{\gamma_0\gamma_1}.\end{aligned} \tag{8.34}$$

Then, the even N idler-free CPF protocol has the following lower and upper bounds on the error probability in identifying the correct pair of channels of which one is the target:

$$\tilde{p}_{\text{err}}^{N,M}(|\psi_2\rangle\langle\psi_2|) \geq \frac{N-2}{2N} F(|\psi_2\rangle\langle\psi_2|_{0,0}, |\psi_2\rangle\langle\psi_2|_{1,0})^{4M}, \tag{8.35}$$

and

$$\tilde{p}_{\text{err}}^{N,M}(|\psi_2\rangle\langle\psi_2|) \leq \frac{N-2}{2} F(|\psi_2\rangle\langle\psi_2|_{0,0}, |\psi_2\rangle\langle\psi_2|_{1,0})^{2M}. \tag{8.36}$$

The task of CPF is to determine the location of the target channel, not just the pair in which it is contained. For the specific idler-free CPF protocol under consideration, there are two ways in which an overall error may be made. You may choose a pair of channels which does not contain the target then, within that pair, you always fail to identify the target. This happens with probability given by Eqs. (8.35) and (8.36). Otherwise, you successful choose the correct pair and then the task is to determine which of those two channels is, in fact, the target. To do this, since one knows the specification of the channels under study, one could engineer a secondary CPF protocol through the addition of two further reference channels on either side of the successfully located pair. Practically speaking one would simply reconsider now-known reference channels within the pattern. This would effectively realise a four-box CPF problem, in which after successfully determining the correct pair, one is certain which specific box contains the target channel. To maintain our energy constraint we choose to split our total number of probes in two, yielding $M/2$ probings for each stage of the overall idler-free CPF procedure.

Taking this two-stage approach into consideration, the N-box idler-free CPF protocol's error probability takes the following form, where we can employ the relevant lower and upper bounds as required:

$$p_{\text{err}}^{N,M/2}(|\psi_2\rangle\langle\psi_2|) = \tilde{p}_{\text{err}}^{N,M/2}(|\psi_2\rangle\langle\psi_2|) + \left[1 - \tilde{p}_{\text{err}}^{N,M/2}(|\psi_2\rangle\langle\psi_2|)\right] \tilde{p}_{\text{err}}^{4,M/2}(|\psi_2\rangle\langle\psi_2|). \tag{8.37}$$

The performance of such a biphoton state in both signal-idler and idler-free protocols is plotted in Figs. 8.4 and Fig. 8.5 along with the coherent state lower bound (Eq. (8.11)), single-photon lower (Eq. (8.14)) and upper bound (Eq. (8.15)), and the GHZ state's upper bound (Eq. (8.19)). It can be seen that the biphoton Bell state's upper bound in a signal-idler

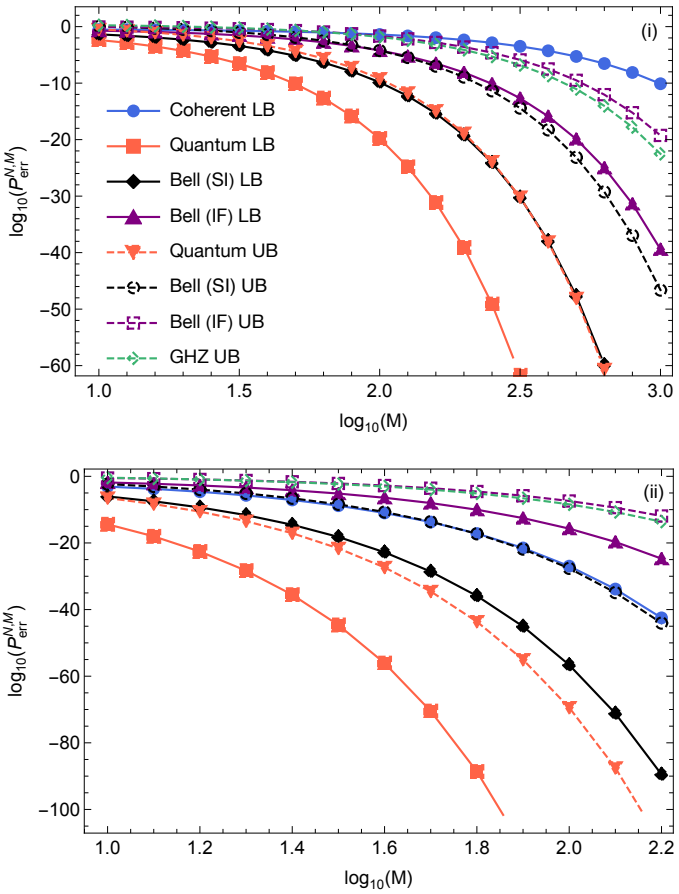

FIG. 8.4: Quantum channel position finding error probability $p_{\text{err}}^{N,M}$ with $N = 4$ as a function of number of uses M for four types of source: 1) Coherent state (blue), 2) Quantum single-photon state (red), 3) Bell biphoton state in both a signal-idler (SI) (black) and idler-free (IF) (purple) set-up, and 4) GHZ state (green). These plots show performance in locating the target channel with damping rate $\gamma_1 = 0$ (the identity channel), amongst reference channels with (i) $\gamma_0 = 0.2$, low damping, and (ii) $\gamma_0 = 0.8$, high damping. Lower and upper bounds are indicated by solid and dashed lines, respectively.

protocol follows very similarly the behaviour of the GHZ state's upper bound.In general, and particularly for low damping/high transmissivity, entanglement-based protocols can yield a quantum advantage in CPF. This is especially true for idler-free protocols, as also described in Ref. [108] under the continuous variable formalism. While a signal-idler protocol is most advantageous, one may instead use an idler-free protocol, forgoing the need for a quantum memory, while still retaining a quantum advantage provided channel losses are not too high. Note, however, that such a scheme as described here may only be applied to CPF problems comprising an even total number of channels. While this may appear constraining, this can

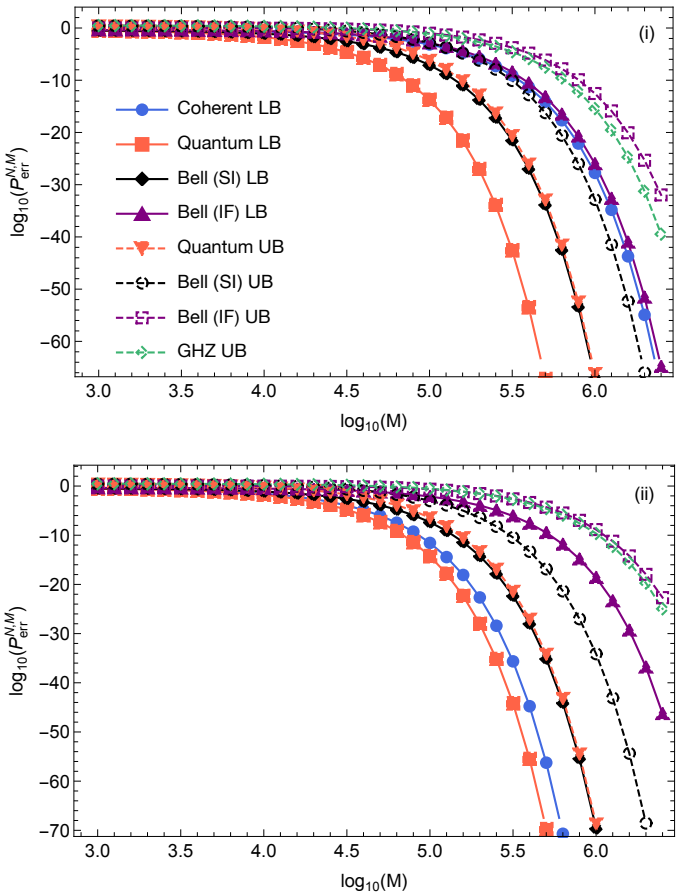

FIG. 8.5: Quantum channel position finding error probability $p_{\text{err}}^{N,M}$ with $N = 4$ as a function of number of uses M for four types of source: 1) Coherent state (blue), 2) Quantum single-photon state (red), 3) Bell biphoton state in both a signal-idler (SI) (black) and idler-free (IF) (purple) set-up, and 4) GHZ state (green). These plots show performance in locating a single target channel with damping rate γ_1 amongst reference channels with non-zero damping rates such that $\gamma_0 = \gamma_1 + 0.01$ where (i) $\gamma_1 = 0.2$, low damping, and (ii) $\gamma_1 = 0.8$, high damping. Lower and upper bounds are indicated by solid and dashed lines, respectively.

easily be achieved in an experiment by simply adding an extra channel when required.

Note that in all entanglement-based CPF approaches considered, namely, using the GHZ and biphoton (in both signal-idler and idler-free setups) states as sources, the average number of photons per channel use is equal to 1/2. One can adjust the protocol across these sources to consider equal energetic distributions; letting $M \to 2M$ means that the average number of photons per channel use is equal to 1, matching that for the single photon Fock state and the coherent state classical benchmark. For completeness, Fig. 8.6 plots the associated error

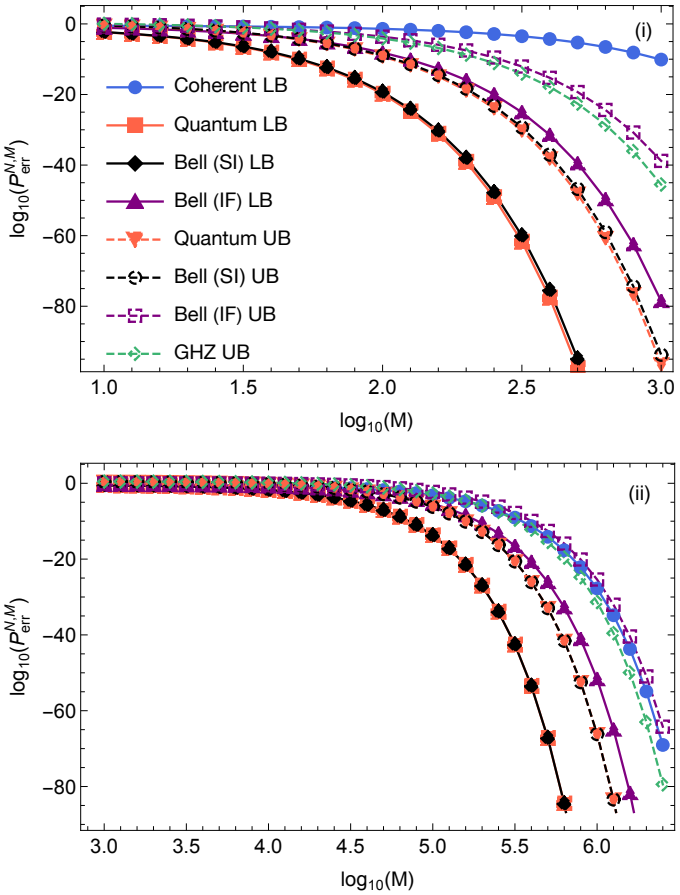

FIG. 8.6: Quantum channel position finding error probability $p_{\text{err}}^{N,M}$ with $N = 4$ as a function of number of uses M for four types of source: 1) Coherent state (blue), 2) Quantum single photon state (red), 3) Bell biphoton state in both a signal-idler (SI) (black) and idler-free (IF) (purple) set-up, and 4) GHZ state (green). In the latter three cases, we let $M \to 2M$ to model the performances when the average number of photons used each use is equal to 1. These plots show performance in locating the target channel in the low damping regime with (i) $\gamma_0 = 0.2$ and $\gamma_1 = 0$, and (ii) $\gamma_0 = 0.21$ and $\gamma_1 = 0.2$. Lower and upper bounds are indicated by solid and dashed lines, respectively.

probabilities for CPF arising from these changes in the low damping regime where quantum advantages are greatest, equivalent to modified versions of Fig. 8.4(i) and Fig. 8.5(i). Both the upper and lower bounds on the error probability in the signal-idler protocol almost coincide with those of the single photon state, with those for the idler-free protocol closely following them.

8.3.6 Practical receiver for quantum channel position finding based on photon counting

Attainment of bounds shown in Figs. 8.4 and 8.5 typically requires optimal detection at the output, the specifics of which is generally unknown. Even then they only provide bounds for the absolute performance which is given by the Helstrom limit [37, 125]. As a result, it is important to consider practical receiver designs to harness the input state's potential at performing the task. When the input and output states form a tensor product state across the N boxes, as for the cases studied in Sections 8.3.1 and 8.3.2, we can employ a strategy based on photon counting at the receiver end of each box and use post-processing to determine which hypothesis is true.

Consider using photon counting at the receiver. Then for some generic state ρ with field operator $\hat{a}$, the measurement result is a classical random variable n with distribution $p(n) = \langle n| \rho |n\rangle$, where $|n\rangle$ is the eigenstate of the number operator $\hat{n} = \hat{a}^\dagger \hat{a}$ with eigenvalue n.

The output of the ith box after M probes is the classical string of length M, $\mu_i^{\otimes M}$, consisting of zeros and ones corresponding to the absence or presence of photon counts. Modelling our receiver as a threshold detector, we know that the probability of detecting $m \equiv \mathrm{Tr}\, \mu^{\otimes M}$ photons in M trials, each with probability of success p, follows the binomial distribution

$$p_{\mathrm{det}}(p, M, m) = \binom{M}{m} p^m (1-p)^{M-m}. \tag{8.38}$$

In the case of coherent state inputs, whose initial photon distribution is Poissonian, we may compute the probability of detecting n photons at the output using their Fock bases such that

$$p_{\mathrm{C}}(n) = |\langle n|\tau\alpha\rangle|^2 = e^{-\tau}\frac{\tau^n}{n!} = e^{\gamma-1}\frac{(1-\gamma)^n}{n!}, \tag{8.39}$$

where we have applied the constraint $|\alpha| = 1$. Then the probability of getting a single 'click' in the photon detector is

$$p_{\mathrm{C}}(n=1) = e^{\gamma-1}(1-\gamma). \tag{8.40}$$

When our source consists of single qubit/photon states, then with photon counting at the output we have that

$$p_{\mathrm{Q}}(n=1) = 1-\gamma, \tag{8.41}$$

and it is clear that

$$p_{\mathrm{Q}}(n=1) > p_{\mathrm{C}}(n=1) \;\forall\; \gamma \in [0,1]\,. \tag{8.42}$$

Consider a relatively straightforward approach where the total number of output photons at each individual receiver is counted. Then the target channel is declared by choosing the one with the highest or lowest total photon count, dependent on the relative magnitudes of damping rates between the target and reference channels. Let the probability of measuring a photon at the output of our target(reference) channel be given by $p_T(p_R)$. Then the decision rule becomes

$$\begin{cases} \arg\max_i m_i & \text{if } p_T > p_R, \\ \arg\min_i m_i & \text{if } p_T < p_R. \end{cases} \tag{8.43}$$

First consider the case where $p_T > p_R$. In such a scenario the min/max receiver would determine that the target channel is the one whose output has the highest photon count, and would do so perfectly when all reference channel boxes output fewer photons than the target channel box. To account for the scenarios where any number of reference channels output an equal number of photons to the target channel, the decision is reduced to choosing at random between those boxes. Such a receiver design yields a total error probability

$$p_{\mathrm{err}}^{\mathrm{min/max}} = 1 - p_{\mathrm{succ}}^{\mathrm{min/max}}, \tag{8.44}$$

where the probability of success, $p_{\mathrm{succ}}^{\mathrm{min/max}}$, is given by

$$\begin{aligned} p_{\mathrm{succ}}^{\mathrm{min/max}} = \sum_{r=1}^{N} \sum_{m_T=0}^{M} & p_{\mathrm{det}}(p_R, M, m_R < m_T)^{N-r} \\ & \frac{1}{r}\binom{N-1}{r-1} p_{\mathrm{det}}(p_T, M, m_T) p_{\mathrm{det}}(p_R, M, m_T)^{r-1}. \end{aligned} \tag{8.45}$$

The index r is the number of boxes whose output total photon counts are the same, thus requiring a random decision between them. The probability that any given reference box yields an output lower than the target channel is given by

$$p_{\mathrm{det}}(p_R, M, m_R < m_T) = \sum_{m_R=0}^{m_T-1} p_{\mathrm{det}}(p_R, M, m_R), \tag{8.46}$$

which, to allow for a random choice between all N channels in the event that all outputs are 0, is defined such that

$$p_{\mathrm{det}}(p_R, M, m_R < 0)^0 = 1. \tag{8.47}$$

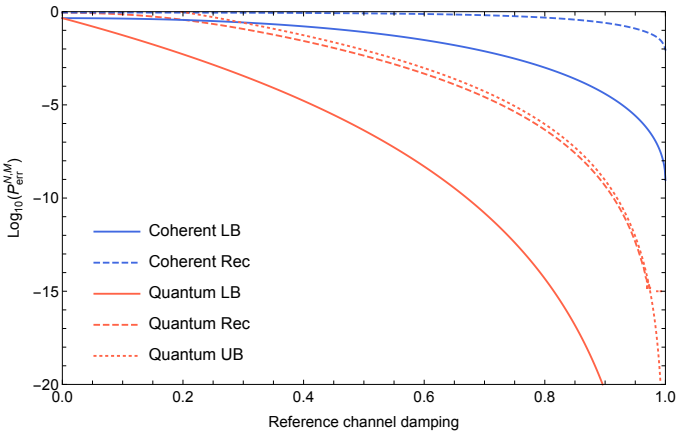

FIG. 8.7: Quantum channel position finding error probability $p_{\text{err}}^{N,M}$ with $N = 10$ and $M = 10$ as a function of reference channel damping γ_0 with target channel damping $\gamma_1 = 0$. Shown is the performance of a photon counting receiver "Rec" (dashed) on coherent states (blue) and single-photon states (red). Lower "LB" and upper "UB" bounds are indicated by solid and dotted lines, respectively.

The performance of such a photon counting receiver on CPF outputs using single-photon (Fock state) sources and classical coherent state sources are shown in Figs. 8.7 and 8.8. Fig. 8.7 shows how the error probability changes as a function of reference channel damping when the target channel is equal to the identity. Quantum-enhanced CPF using single-photon states may be achieved across almost the entire range of damping values, with the simple receiver based on direct photon counting capable of realising this for most of this range. Fig. 8.8 shows how the performance of each type of source, with the use of the photon counting receiver, changes with the size of the CPF array. This behaviour is shown for the addition of background channels of differing damping strength relative to the target channel of interest. It can be seen that, in general, coherent state CPF capabilities are more robust to increasing pattern size in that the performance remains fairly constant compared to Fock states with added reference channels. As one would expect, both classical and quantum sources' performances are affected more detrimentally when the background channels added are relatively similar in specification to the target channel, although this effect is greater for single-photon states employed in conjunction with our proposed photon counting receiver.

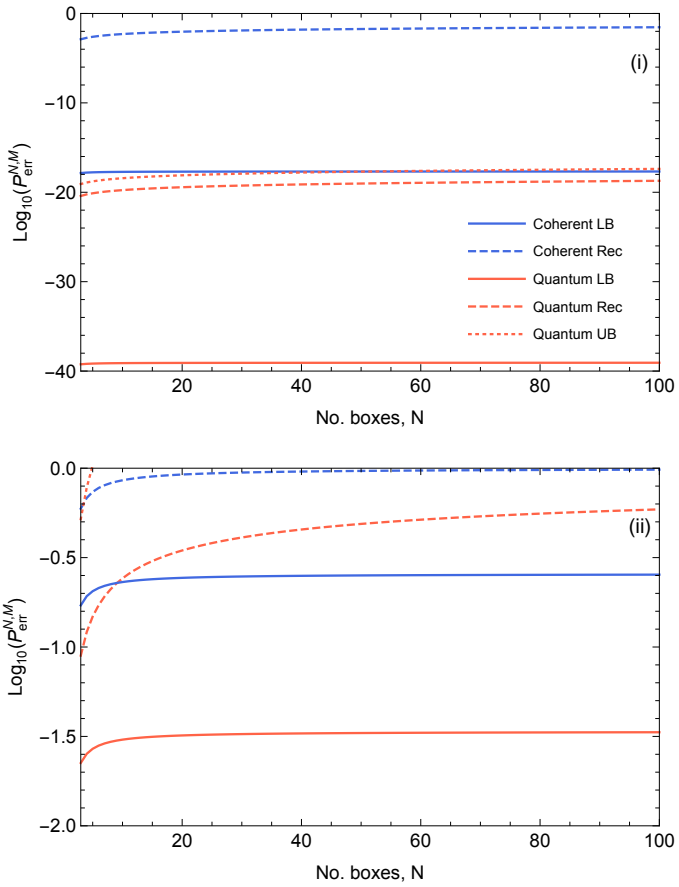

FIG. 8.8: Quantum channel position finding error probability $p_{\text{err}}^{N,M}$ with $M = 100$ as a function of the total number of boxes N. Target channel damping $\gamma_1 = 0.2$ with reference channel damping set to (i) $\gamma_0 = 0.8$, and (ii) $\gamma_0 = 0.3$. Shown is the performance of a photon counting receiver "Rec" (dashed) on coherent states (blue) and single-photon states (red). Lower "LB" and upper "UB" bounds are indicated by solid and dotted lines, respectively.

8.4 Conclusion

The research contained within this chapter provides performance comparisons of various types of source with respect to the problem of CPF where the channels are of differing transmissivity. The work is carried out in the discrete variable setting under the energetic constraint that each channel use (probing of the entire channel array) is limited to use, at most, one photon on average.

Considered in this work are the performances of various types of discrete variable quantum sources, namely, the single-photon (Fock) state, the GHZ state where entanglement is evenly

distributed across the CPF channel array and the biphoton (Bell) state. In the latter case, two protocols are considered: one considering signal-idler (QI) role across the two modes and another where both modes are used as a signal. In all cases, fidelity-based bounds on error probability are derived.

While the signal-idler approach for biphoton states tends to be sub-optimal compared to the use of Fock states, it is the most optimal amongst the entanglement-based approaches considered. Nonetheless, such a method may be experimentally demanding since it requires access to a quantum memory. Our idler-free protocol forgoes this need and still retains much of the desired quantum advantage in cases where channel damping is low. The biphoton state is one that may be readily generated and employed using MRRs which could form the basis of a proof-of-principle experiment for quantum-enhanced CPF using single-photon states.

9 Multiple quantum hypothesis testing for target metrology

Abstract

While quantum illumination (QI) can offer a quantum enhancement in target detection, its potential for performing target ranging remains unclear. With its capabilities hinging on a joint measurement between a returning signal and its retained idler, an unknown return time makes a QI-based protocol difficult to realise. This chapter outlines a potential QI-based approach to quantum target ranging based on recent developments in multiple quantum hypothesis testing and quantum-enhanced channel position finding (CPF). Applying CPF to time bins, one finds an upper bound on the error probability for quantum target ranging. However, using energetic considerations, we show that for such a scheme a quantum advantage may not be proven with current mathematical tools.

Relevant Publications

Content from the following publications is used in this chapter:

[3] A. Karsa and S. Pirandola, *Energetic Considerations in Quantum Target Ranging*, IEEE Rad. Conf. (RadarConf21), 1–4 doi: 10.1109/RadarConf2147009.2021.9455341.

9.1 Introduction

Since QI's inception several prototype experiments have been demonstrated [59, 69] however there are still many aspects inhibiting quantum radar's readiness for real-world implementation [11, 102]; one of which, also the subject of this chapter, is that of quantum target ranging. The issue with target ranging is the fact that signal-idler recombination becomes problematic. These two modes' return at the receiver must be synchronised to ensure that the joint measurement procedure is a success.

Quantum-enhanced channel position finding (CPF) [93] could form a crucial component to extending the QI protocol from simple detection to actual measurement. Fundamentally a pattern recognition problem, CPF is based on multiple quantum hypothesis testing [37,90,91] and quantum channel discrimination [126] where the goal is to locate the 'target' channel amongst an ensemble of 'background', or reference, channels [146]. The problem may be reformulated for target metrology by parameterising the quantum channels under study by some measurable target property, such as its position, range and velocity.

This chapter investigates a quantum-enhanced target ranging protocol based on CPF and QI and studies it as a potential solution to the QI ranging problem. In section 9.2 we outline the CPF problem and provide the relevant bounds on error probability in the cases where classical and entangled light sources are employed. Further, we briefly review the benefits afforded by the use of a conditional-nulling (CN) receiver [93] for the entangled case. In section 9.3 we apply the CPF model to target ranging and determine whether or not, under any physical parameter constraints, a quantum enhancement in ranging can be realised using such a multi-array QI-based approach.

9.2 Quantum channel position finding

Consider the task of quantum CPF comprising $m \geq 2$ input-output black boxes as shown in Fig. 9.1. For $i = 1, 2, \ldots m$, the ith box $\mathcal{B}_i$ contains either a background channel $\mathcal{E}^{(B)}$ or some target channel $\mathcal{E}^{(T)} \neq \mathcal{E}^{(B)}$ and the task is to locate its position. The assumption is made that the target channel occupies one box only, i.e., joint probabilities of the form $\mathrm{P}(\mathcal{B}_i = \mathcal{E}^{(T)}, \mathcal{B}_j = \mathcal{E}^{(T)})$ are all zero, and the target channel is in one of the boxes with certainty: $\mathrm{P}(\mathcal{B}_i = \mathcal{E}^{(B)}\ \forall i) = 0$. Identification of the target channel is a problem of symmetric quantum hypothesis testing (in which both error types are given equal weight and minimised

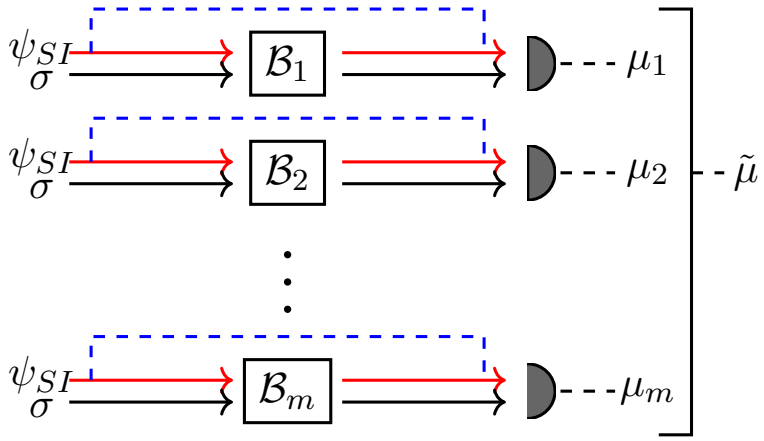

FIG. 9.1: Schematic diagram of channel position finding (CPF). For $i = 1, \ldots, m$ we have an ensemble of boxes B_i and the task is to locate the single target channel amongst background channels. In the classical strategy, our source σ is sent through the channel (black) with the output going straight to the receiver for post-processing. In the quantum strategy, we consider a maximally-entangled two-mode source ψ_{SI} comprising a signal (red), sent through the channel, and an idler (blue) which recombines with the output at the receiver. For each strategy, outputs from each box are combined to yield a final result, $\tilde{\mu}$, giving the target's location with some error probability.

simultaneously) where the task is to discriminate between N hypotheses given by

$$H_i : \mathcal{B}_i = \mathcal{E}^{(T)} \quad \text{and} \quad \mathcal{B}_{j\neq i} = \mathcal{E}^{(B)}. \tag{9.1}$$

For a fixed input the problem of CPF reduces to a multi-ary quantum state discrimination [37, 90].

9.2.1 CPF using classical light

In a classical strategy, the source is described as a state with positive P-representation with a tensor product structure over the system, $\otimes_{i=1}^{m}\sigma$. This represents a statistical mixture of coherent states where each of the m boxes is irradiated by M modes and MN_S photons in total. For such a source, the minimum error probability is lower-bounded by the Helstrom limit, which is the performance of the minimum error probability quantum receiver, given by

$$\mathrm{P}_{H,\mathrm{LB}} = \frac{m-1}{2m} F^4\left(\sigma^{(T)}, \sigma^{(B)}\right), \tag{9.2}$$

where $F\left(\sigma^{(T)},\sigma^{(B)}\right)$ is the fidelity between the states $\sigma^{(B/T)}=\mathcal{E}^{(B/T)}(\sigma)$, defined by [10,111]

$$\begin{aligned} F\left(\sigma^{(T)},\sigma^{(B)}\right) &:= \left\|\sqrt{\sigma^{(T)}}\sqrt{\sigma^{(B)}}\right\|_1 \\ &= \mathrm{Tr}\sqrt{\sqrt{\sigma^{(T)}}\sigma^{(B)}\sqrt{\sigma^{(T)}}}. \end{aligned} \tag{9.3}$$

Suppose the target and background channels have transmissivity/gain μ_T, μ_B and noise E_T, E_B, respectively. Then the general lower bound to the error probability for the classical benchmark, assuming a total of mM modes and mMN_S mean photons are irradiated over the entire system, is given by [93]

$$\mathrm{P}_{H,\mathrm{LB}}=\frac{m-1}{2m}c_{E_B,E_T}^{2M}\exp\left[-\frac{2MN_S(\sqrt{\mu_B}-\sqrt{\mu_T})^2}{1+E_B+E_T}\right], \tag{9.4}$$

with

$$c_{E_B,E_T}\equiv\left[1+(\sqrt{E_B(1+(E_T))}-\sqrt{E_T(1+E_B)})^2\right]^{-1}. \tag{9.5}$$

9.2.2 CPF using entangled light

For a quantum strategy, consider entangling each input state with an ancillary idler to form a two-mode squeezed vacuum state, $\psi_{SI}:=\sum_{k=0}^{\infty}\sqrt{N_S^k/(N_S+1)^{k+1}}\,|k,k\rangle$, for each of the m boxes. The idler systems are sent directly to the measurement with only the signals, each comprising N_S photons per mode, probing the individual boxes. Thus, with M modes per box, our entangled source takes the tensor product form $\psi_{SI}^{\otimes mM}$ which is acted on by the global quantum channel

$$\mathcal{E}_i\otimes\mathcal{I}=\left[\otimes_{k\neq i}(\mathcal{E}_k^{(B)}\otimes\mathcal{I}_k)\otimes(\mathcal{E}_i^{(T)}\otimes\mathcal{I}_i)\right], \tag{9.6}$$

where $\mathcal{I}$ is the identity channel. This leads to an upper bound (UB) to the Helstrom limit given by [93]

$$\mathrm{P}_{H,\mathrm{UB}}=(m-1)F^2\left(\Xi^{(T)},\Xi^{(B)}\right), \tag{9.7}$$

where $\Xi^{(T/B)}=(\mathcal{E}^{(T/B)}\otimes\mathcal{I})\psi_{SI}^{\otimes M}$.

Employing the generalised conditional-nulling (CN) receiver (see Ref. [93] for full details) allows far better detection results to be achieved. Suppose there exist two partially unambiguous positive operator-valued measures (POVMs), one corresponding to the target channel, $\{\Pi_T^t,\Pi_T^b\}$, and another for the background channel $\{\Pi_B^b,\Pi_B^t\}$, acting such that

$$\mathrm{Tr}\left[\Pi_T^t\Xi^{(T)}\right]=\mathrm{Tr}\left[\Pi_B^b\Xi^{(B)}\right]=1. \tag{9.8}$$

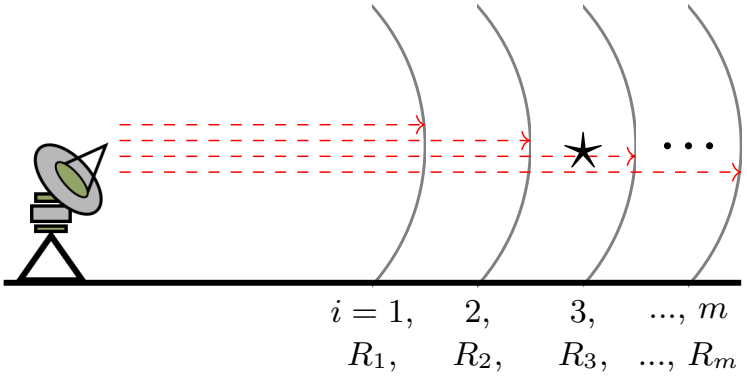

FIG. 9.2: Schematic diagram of quantum target ranging (QTR). A range of surveillance from $R_{\min}$ to $R_{\max}$ is split into m spherical shells with radius equal to the corresponding range R_i for $i = 1, \ldots, m$. A total of M signal-idler pulses with N_S mean photons per mode are generated at well-defined frequencies corresponding to each of the m range bins, chosen such that only the radiation returned from that range bin is collected by its associated receiver. Each range bin has an associated signal-return time such that, upon its potential return, it may be recombined with the corresponding, retained idlers for joint measurement.

Employing feed-forward across the entire channel arrangement and conditional-nulling of subsequent hypotheses, the CN receiver yields an overall error probability given by

$$\mathrm{P}^{\mathrm{CN}}_{\mathrm{err},m}(\zeta_1, \zeta_2) = \frac{1}{m}\frac{\zeta_2}{\zeta_1}\left(m\zeta_1 + (1-\zeta_1)^m - 1\right). \tag{9.9}$$

Here $\zeta_1 = \mathrm{Tr}\left[\Pi^t_T \Xi^{(B)}\right] = p(H_1|H_0)$ and $\zeta_2 = \mathrm{Tr}\left[\Pi^b_B \Xi^{(T)}\right] = p(H_0|H_1)$ are the Type-I and Type-II error probabilities associated with the two POVMs, respectively.

Note that the CN receiver applies to the QI case only in the limit of $N_S \ll 1$. In this limit one can construct some projector via the sum-frequency-generation (SFG) mechanism [62] to have $\mathrm{Tr}\left[\Xi^{(B)}\right] \simeq 1$ to leading order. Such a projector is possible because, in this limit, the idler is close to vacuum and, by allowing this approximation, Π^b_B may always be different from the identity.

9.3 Quantum target ranging

Quantum-enhanced CPF forms a crucial component towards enabling QI-based detection protocols to perform target-based metrology for measuring parameters such as location, range

and speed. CPF can be viewed as a proxy for these problems in which we reformulate the protocol such that the m hypotheses instead correspond to multiple space-time-frequency bins. Crucial to this is ensuring that the frequencies of each range bin's set of M signal-idler pulses are chosen to ensure that their respective receivers only collect radiation returned from their associated range bins. In such a setting, space bins would allow for the determination of target location, time bins would allow for range estimation, and frequency bins may be used for the measurement of speed via Doppler shift. The ranging problem is a major barrier towards real-world implementation of QI for target detection since the signal and idler modes must be synchronised at the receiver in order to perform an optimal joint measurement and obtain the best possible performances. For a target located at some unknown range to be determined, the return time is unknown and is thus problematic.

A potential solution would involve a modification to the direction finding protocol (see Ref. [93]), based on CPF, whereby we consider a fixed number m of non-overlapping range bins across some range interval of interest, as shown in Fig. 9.2. Then, by generating a sequence of M signal-idler pulses, at a well-defined frequency, for each of the m bins, the signals can be recombined (if returned at the corresponding range) with their respective idlers. All of the m sectors are simultaneously probed with the total energy irradiated equal to mMN_S, where N_S is the average number of photons per signal/idler mode and M is the total number of modes (experiment repeats). In such a scenario, the total energy the target is exposed to is at most mMN_S, with this upper limit applying when the target is located in the final, mth, sector.

Consider the thermal-loss channel $\mathcal{L}_\mu^N$ with loss parameter μ and mean number of thermal photons N so its output noise is given by $E = (1-\mu)N$. If the target is present in some sector, a proportion η of the N_S signal photons in each mode will be returned, which includes contributions from target reflectivity and transmission losses due to beam spreading. These will be mixed with thermal noise comprising N_B photons per mode at the receiver and the M signal modes are acted on by the target channel $\mathcal{E}^{(T)} = \left(\mathcal{L}_\eta^{N_B/(1-\eta)}\right)^{\otimes M}$ In contrast, if the target is absent, all of the M signal modes are lost and the return consists only of background noise, with N_B photons per mode. The corresponding background channel is given by $\mathcal{E}^{(B)} = \left(\mathcal{L}_0^{N_B}\right)^{\otimes M}$.

Using a quantum source comprising a tensor product of two-mode squeezed vacuum states $\psi_{SI}^{\otimes mM}$, each M-mode probing of each of the m sectors yields an ensemble of outputs corre-

sponding to the background and target channels, given by

$$\Xi^{(T)} = \left[(\mathcal{L}_{\eta}^{N_B/(1-\eta)} \otimes \mathcal{I})\psi_{SI}\right]^{\otimes M}, \tag{9.10}$$

$$\Xi^{(B)} = \left[(\mathcal{L}_{0}^{N_B} \otimes \mathcal{I})\psi_{SI}\right]^{\otimes M}. \tag{9.11}$$

Computing the error probability, i.e., Eq. (9.7), for the discrimination of these states yields the following asymptotic bound for QTR,

$$\mathrm{P}_{H,\mathrm{UB}}^{\mathrm{QTR}} \simeq (m-1)\exp\left(-\frac{M\eta N_S}{N_B+1}\right), \tag{9.12}$$

in the limits of $N_S \ll 1$ and $M \gg 1$, keeping total energy MN_S fixed.

By adapting the SFG receiver for QI [62] to the CN approach, the upper bound for QTR [Eq. (9.12)] may be significantly improved upon [93]. After multiple SFG cycles and the application of differing two-mode squeezing operations, the photon counting statistics of $\Xi^{(T/B)}$ allow for the realisation of two partially unambiguous POVMs for the CN receiver with corresponding mean error probability

$$\mathrm{P}_{\mathrm{CN}}^{\mathrm{QTR}} \simeq \frac{1}{2}(m-1)\exp\left(-\frac{2M\eta N_S}{N_B}\right). \tag{9.13}$$

Consider now probing this set of m possible range bins using a classical source. Described in Section 9.2.1, it comprises M modes, each with N_S photons, for each of the m sectors, employing a total of mMN_S photons across the entire protocol. For generic channel finding, the lower bound achievable using such a source is, using Eqs. (9.4) and (9.5) with $E_T = E_B = N_B$ and $\mu_T = \eta$, $\mu_B = 0$, given by

$$\mathrm{P}_{H,\mathrm{LB}} = \frac{m-1}{2m}\exp\left[-\frac{2M\eta N_S}{2N_B+1}\right]. \tag{9.14}$$

However, the separation of each of the m returning signals, while crucial for the QI-based protocol, is unnecessary for the classical source (its need arises from the fact that in any QI-based protocol, synchronised recombination is necessary for the joint measurement upon which it is based). This has particular implications for target-ranging since regardless of the target's true location, any signal sent out will certainly return. It is only when using an entangled source that all but one (corresponding to the target) of the returns are essentially discarded. As a result, there is, physically, no reason why the classical measurement process at the receiver should not incorporate the entire signal sent, that is, all of the mMN_S coherent photons. In other words, the coherent pulse can be sent out in just one go to explore all the

possible bins and the receiver just needs to be open and check for the return of the energetic pulse in each one of the bins. Thus, for classical target ranging (CTR), the lower bound of Eq. (9.14) becomes

$$\mathrm{P}_{H,\mathrm{LB}}^{\mathrm{CTR}} = \frac{m-1}{2m} \exp\left[-\frac{2mM\eta N_S}{2N_B+1}\right]. \tag{9.15}$$

To establish a quantum advantage in target-ranging, all that is needed is to find a suitable parameter regime whereby the following relation (sufficient condition) is satisfied:

$$\mathrm{P}_{\mathrm{CN}}^{\mathrm{QTR}} \leq \mathrm{P}_{H,\mathrm{LB}}^{\mathrm{CTR}}. \tag{9.16}$$

Using Eqs. (9.13) and (9.15), this is satisfied when

$$\ln m \leq 2M\gamma \frac{N_B(2-m)+1}{2N_B+1}, \tag{9.17}$$

where $\gamma = \eta N_S/N_B$ is the single-use signal-to-noise ratio (SNR). For any value of $N_B > 1$, the condition [Eq. (9.17)] cannot physically be satisfied for any $m > 2$. Thus, it is not possible to prove that the QI-based ranging protocol can achieve a quantum advantage over its equivalent classical counterpart (at least with the current mathematical tools). This result is a mathematical limitation of the approach since, while it provides a sufficient condition for there to exist a quantum advantage, it does not provide a necessary one.

While Eq. 9.17 provides a sufficient condition for a quantum advantage in target ranging using the scheme proposed here, the following will outline a necessary condition and its associated violations. Consider an adaptation of the CTR protocol (yielding the lower bound Eq. (9.15)) to a scheme where one sends a coherent state pulse of average photon number mMN_S to interrogate the m-bin range uncertainty interval. Performing homodyne detection alongside match filtering to maximise the SNR on each of the range bins' return signals yields corresponding outputs r_n where $1 \leq n \leq m$. The receiver then chooses for the target to be present in the bin $m^\star = \mathrm{argmax}(r_n)$ since all hypotheses are equally likely. In the case of two bins, the minimum error probability for such a receiver is equivalent to the binary discrimination error given by

$$\mathrm{P}_2^{\mathrm{CTR}\star} = Q\left(\sqrt{\frac{mM\eta N_S}{2N_B+1}}\right), \tag{9.18}$$

where $Q(x)$ is defined as

$$Q(x) = \sqrt{\frac{2}{\pi}} \int_x^\infty dy \exp\left(-\frac{y^2}{2}\right) \leq \frac{1}{2} \exp\left(-\frac{x^2}{2}\right), \tag{9.19}$$

providing an exponentially tight upper bound. Extending to an m-array problem comprising $m-1$ background bins, the upper bound to the error probability for such a receiver, using Eqs. (9.18) and (9.19), is given by

$$\mathrm{P}_{\mathrm{UB}}^{\mathrm{CTR}\star} \leq \frac{m-1}{2} \exp\left[-\frac{mM\eta N_S}{2(2N_B+1)}\right]. \tag{9.20}$$

Comparing this to Eq. (9.13) for QTR with a CN receiver, our condition for a quantum advantage becomes

$$m \leq 8 + \frac{4}{N_B}, \tag{9.21}$$

which is violated for $m > 8$ when $N_B > 4$. Using a CN receiver, currently the best known tool for testing multiple quantum hypotheses, a quantum advantage may only potentially be realised for $m \leq 8$.

9.4 Conclusion

In this chapter we have outlined and studied a potential QI-based quantum ranging protocol based on multiple quantum hypothesis testing and channel discrimination, using recent results of quantum-enhanced CPF. By modelling a discrete set of ranges as multiple quantum channels, a quantum ranging protocol may be established by the distribution of signals and recombination with idlers across fixed time intervals. The very nature of the QI protocol demands that such an approach must be taken, since it is crucially dependent on the ability to recombine bosonic modes at the correct time in order to perform a joint measurement to harness any potential advantage. In the optimal classical scenario using a coherent state source, this energetic distribution across range bins (or, equivalently, time bins) is unnecessary and, for all practical purposes, would not be done. As such, the results of this chapter show that, under fair energetic considerations and the currently available mathematical tools, it is not possible to show a quantum advantage in target ranging using a QI-based approach to CPF.

10 Conclusions and future work

The non-classical phenomena arising from quantum mechanics have revolutionised the development of a wide range of modern technologies, from computation [95–97] and communication [98–100] to sensing [11] and metrology [78]. Quantum target detection is a particular subset of quantum sensing problems of which quantum illumination (QI) forms its most fundamental formulation whereby the existence of quantum correlations in the system enhances the performance establishing them as a resource for a quantum advantage.

In this thesis, we have progressively explored some of the well-known open questions and limitations of QI. Beginning with source generation, with aims of loosening QI's transmitter requirements, Chap. 4 reformulated Tan *et al.*'s Gaussian QI in terms of arbitrary quantum correlations under both symmetric and asymmetric quantum hypothesis testing (QHT), showing that maximal entanglement is not strictly necessary for a quantum advantage to be achieved. In the same work, parallels were also drawn between quantum and classical radar theory to convey physical meaning to parameters. This showed that the performance entanglement-based quantum target detection, as in QI, is fundamentally limited by target range, particularly when considering experimental practicalities associated with the generation of a large number of entangled states within a reasonable time-frame.

Keeping to the theme of experimental practicalities, Chap. 5 considered the effect of a common methodology in microwave QI whereby the idler mode is immediately heterodyned rather than stored. Then, only the classical measurement outcomes need to be stored for later post-processing with that of the returned idler through, for example, a simulation of a phase-conjugating (PC) receiver. Our results prove, as expected, that such a method's performance is upper-bounded by that of coherent states with homodyne detection. Interestingly, however, if one could process the idler measurement outcomes to effectively clean it from the added noise, while retaining noise on the signal, one could digitally achieve a performance coinciding with a real PC receiver, without heterodyne.

The use of amplifiers is able to effectively recover weak signals, however, the resultant

signal-to-noise ratio (SNR) is bounded by that of the original. Noiseless linear amplifiers (NLAs) [147] can probabilistically amplify a coherent state while retaining its initial noise. Specifically, an NLA with gain g transforms a damped coherent state $|\sqrt{\kappa}\alpha\rangle \rightarrow |g\sqrt{\kappa}\alpha\rangle$ with probability of success $1/g^2$. When the NLA is unsuccessful, it returns a vacuum state. Thus, when considering its successful runs, the NLA can compensate for the effect of losses and therefore be of great value for QI and quantum target detection. For continuous variable quantum key distribution, such protocols have been shown to effectively increase the maximum transmission distance [148]. In the case of quantum target detection, one could mitigate all losses associated with the channel by setting $g = 1/\sqrt{\kappa}$.

Of course, there is a trade-off between the improved SNR achieved during a successful run and the resultant expected number of successful runs which would ultimately yield the error probability for a large number of uses. Chap. 6 showed preliminary results for the analysis of the effect of employing an NLA at the receiver for QI showing that they afforded a significant performance advantage compared to the equivalent non-NLA protocol. Further, to mitigate the technologically challenging implementation of a real NLA, one could consider a measurement-based approach based on heterodyne measurement outcomes with appropriate post-processing, based on rescaling and filtering. This would essentially implement a virtual NLA, as discussed in Sec. 6.3.

Microwave-based implementation issues are not solely limited to the TMSV state; the standard classical benchmark of coherent states with homodyne detection only really applies in the optical domain. For the purposes of QI benchmarking, where we require a low-energy signal, room temperature sources of this type do not exist and, further, homodyne of the returning signals, whose energy is even lower, is not possible. Chap. 7 studied this outlining a typical microwave coherent illumination approach and a potential alternative based on the output of a room temperature maser, comparing this to the optical coherent state. Our results show that the classical sources used in experiments are certainly not the theoretically optimal ones - however, they are the only ones that exist. Our alternative scheme is shown to have a performance coinciding with the optical coherent state benchmark, under certain conditions which may readily be met with current experimental capabilities.

Finally, an important next step for any quantum radar is its extension from a tool solely for detection to one that can perform measurements. A key example of this is the problem of quantum target ranging which, for a QI-based approach, is especially difficult due to the necessary simultaneous recombination of the signal and idler in a joint measurement in order to harness the full potential quantum advantage. Chap. 8 studied a potential solution to

this problem in the form of quantum channel position finding (CPF) which tasks one with locating a particular target channel amongst an ensemble of background channels. In the formalism of discrete variables, we studied this problem providing fidelity-based bounds on error probability for a wide class of quantum states constrained to having, at most, one photon per mode. Included in this analysis were means of source generation for a Bell-type state capable of achieving a quantum advantage in an idler-free CPF protocol. Further, for Fock states, a practical receiver design based on simple photon counting was shown to retain a quantum advantage over coherent state protocols. Chap. 9 extended CPF to QI-based target ranging showing that, under fair energetic considerations, a quantum advantage could not absolutely be proven based on current mathematical tools.

While the physical realisation of QI, particularly in the microwave, has proved to be littered with technical barriers, our understanding of these intricacies have developed tremendously since QI's inception [18]. As such, each of them is the subject of ongoing research across fields spanning beyond simple target detection, including the detection of gravitational waves, data readout [106] and biological probing [150], giving reason to be optimistic regarding future technological and theoretical breakthroughs.

Future work: Quantum target ranging

Results from Chap. 9 show that under fair energetic considerations from the perspective of the amount of energy by which the target is illuminated it is not possible to certainly ascertain a quantum advantage for any number of range bins. This complication arises from the fact that, for QI, the receiver must incorporate a joint measurement in which the signal and idler beams are recombined at a known instant in time, corresponding to the expected time of arrival of the returning signal from a particular range bin. Despite that not all probing pulses are used in the ranging protocol, the target is still susceptible to all radiation used. In the case of coherent states, such a separation of signals is not required since receiver reception is not time-sensitive with respect to the arrival of the returning signal. As such, the energy used to probe each range bin may be used in its entirety to probe all bins simultaneously.

One may alternatively consider a protocol where, for the two-mode squeezed vacuum (TMSV) source, the idler beam is beam splitted into equal components corresponding to each of the range bins under consideration to provide each associated arrival time's receiver for the necessary QI entanglement. Meanwhile, as in the case of coherent states, the entire signal may be used to probe the full range interval.

Future work: Alternative quantum sources

Gaussian states and their associated treatment offers a convenient way to mathematically model physical processes that are readily accessible within quantum optics experiments. As such, much of the research regarding QI and quantum target detection more broadly has been confined to the realms of Gaussianity. Consideration of more exotic, non-Gaussian, quantum sources, such as photon-subtracted TMSV have been shown to theoretically improve the potential quantum advantage over coherent states to the point where the advantage persists even at low background noise [151]. Recently, Ref. [152] has studied the effects of both photon-addition and photon-subtraction on TMSV states as QI sources showing potential quantum advantages.

Literature on photon-addition/subtraction for QI only considers such an operation on the TMSV comparing the resultant non-Gaussian state's performance to a coherent state of equivalent signal strength. However, it has been shown that the use of photon-added coherent states can significantly reduce the error probability in quantum state discrimination compared to coherent states [153]. In fact, the process of photon-addition on coherent states yields a non-Gaussian state whose Wigner function has increased negativity with each additional photon; this negativity is a strong indicator for non-classicality [154]. Thus, a comparison between photon-addition/subtraction on TMSV states versus coherent states could be valuable.

Future work: Noiseless linear amplifiers (NLAs)

As outlined in Sec. 6.4, future work here would entail the determination of the number of accepted data points left after post-selection, M_{acc}. Ideally, this would involve an optimisation over both NLA gain, g, and the number of events, M_{acc}, alongside digital receiver designs such as that studied in Chap. 5.

Finally, the use of an NLA could be considered alongside a source which is not maximally-entangled (as was considered in Chap. 4) to allow for an experimentally cheaper way to implement QI.

Future work: Unambiguous state discrimination

The underlying theory of QI is based on quantum state discrimination. Its task is to indicate precisely which state the returning quantum system is in; it may be the returning signal, indicating the presence of a target, or simply the background. Naturally, these two possible states are non-orthogonal so with any quantum measurement it is impossible to yield a conclusive result. There is always a non-zero error probability. This fact has formed the basis of much of the research surrounding QI resulting in the development of measurement strategies optimised to carry out the discrimination with respect to minimising the inevitable error probability. These strategies, such as those considered in this thesis, are all ambiguous.

There does however exist an alternative approach: unambiguous state discrimination [155–158]. Given an unknown quantum state of interest and a projective measurement in some basis, it is possible to rule out any possible state which is orthogonal to the basis state corresponding to the measurement outcome. This exclusion of possible states is a natural attribute of quantum measurements. While minimum-error measurements minimise the probability of the result being wrong, unambiguous measurements never give an incorrect result. They allow one to unambiguously (with zero error probability) distinguish between non-orthogonal states with the caveat that sometimes the protocol will fail. Recently the ultimate limits of unambiguous discrimination of quantum channels have been studied [159].

Unambiguous state discrimination for the purposes of target detection is largely unstudied, particularly within the realms of continuous variables. Very recently, practical receivers for the unambiguous discrimination of coherent states have been studied [160]. There are promising opportunities for research here across continuous variable protocols such as QI.

References

[1] A. Karsa, G. Spedalieri, Q. Zhuang and S. Pirandola, *Quantum illumination with a generic Gaussian source*, Phys. Rev. Res. 2(**2**), 023414 (2020). doi: 10.1103/PhysRevResearch.2.023414.

[2] A. Karsa and S. Pirandola, *Noisy receivers for quantum illumination*, IEEE Trans. Aerosp. Electron. Syst. Magazine 35(**11**), 22–29 (2020). doi: 10.1109/MAES.2020.3004019.

[3] A. Karsa and S. Pirandola, *Energetic Considerations in Quantum Target Ranging*, IEEE Rad. Conf. (RadarConf21), 1–4 (2021). doi: 10.1109/RadarConf2147009.2021.9455341.

[4] A. Karsa and S. Pirandola, *Classical benchmarking for microwave quantum illumination*, IET Quant. Comm. 2(**4**), 246–257 (2021). doi: 10.1049/qtc2.12025.

[5] A. Karsa, J. Carolan and S. Pirandola, *Quantum channel position finding using single photons*, Phys. Rev. A (**105**), 023705 (2022). doi: 10.1103/PhysRevA.105.023705.

[6] A. Karsa, M. Ghalaii and S. Pirandola, *Noiseless linear amplification in quantum target detection using Gaussian states*, under review, (2022). arXiv: 2201.02474.

[7] M. A. Nielsen and I. Chuang, *Quantum computation and quantum information*, Cambridge University Press (2011). isbn: 1107002176.

[8] S. L. Braunstein and P. Van Loock, *Quantum information with continuous variables*, Revs. Mod. Phys 77(**2**), 513 (2005). doi: 10.1103/RevModPhys.77.513.

[9] X. Wang, T. Hiroshima, A. Tomita, Akihisa and M. Hayashi, *Quantum information with Gaussian states*, Phys. Rep. 448(**1–4**), 1–111 (2007). doi: 10.1016/j.physrep.2007.04.005.

[10] C. Weedbrook, S. Pirandola, R. García-Patrón, N. J. Cerf, T. C. Ralph, J. H. Shapiro and S. Lloyd, *Gaussian quantum information*, Rev. Mod. Phys. **84**(**2**), 621 (2012). doi: 10.1103/RevModPhys.84.621.

[11] S. Pirandola, B. R. Bardhan, T. Gehring, C. Weedbrook and S. Lloyd, *Advances in photonic quantum sensing*, Nat. Photon. **12**, 724–733 (2018). doi: 10.1038/s41566-018-0301-6.

[12] M. A. Richards, *Fundamentals of radar signal processing*, McGraw-Hill, (2005). isbn: 9780071444743.

[13] M. Lanzagorta, *Quantum radar*, Synth. Lect. on Quant. Comp., Morgan & Claypool Publishers (2011). doi: 10.2200/S00384ED1V01Y201110QMC005.

[14] M. I. Skolnik, *Introduction to radar*, Radar Handbook, McGraw-Hill, (2008). isbn: 9780071485470.

[15] D. Jenn, *Radar and Laser Cross Section Engineering*, American Institute of Aeronautics and Astronautics, Inc. (2005). doi: 10.2514/4.105630.

[16] E. L. Lehmann and J. P. Romano, *Testing statistical hypotheses*, Springer (2005). doi: 10.1007/0-387-27605-X.

[17] T. M. Cover and J. A. Thomas, *Elements of Information Theory*, Wiley, (2006). isbn: 978-0-471-24195-9.

[18] S. Lloyd, *Enhanced sensitivity of photodetection via quantum illumination*, Science 321(**5895**), 1463-1465 (2008). doi: 10.1126/science.1160627.

[19] S. H. Tan, B. I. Erkmen, V. Giovannetti, S. Guha, S. Lloyd, L. Maccone, S. Pirandola and J. H. Shapiro, *Quantum illumination with Gaussian states*, Phys. Rev. Lett. 101(**25**), 253601 (2008). doi: 10.1103/PhysRevLett.101.253601.

[20] S. Barzanjeh, S. Guha, C. Weedbrook, D. Vitali, J. H. Shapiro and S. Pirandola, *Microwave quantum illumination*, Phys. Rev. Lett. 114(**8**), 080503 (2015). doi: 10.1103/PhysRevLett.114.080503.

[21] C. Weedbrook, Christian, S. Pirandola, J. Thompson, V. Vedral and M. Gu, *How discord underlies the noise resilience of quantum illumination*, New Journ. of Phys. 18(**4**), 043027 (2016). doi: 10.1088/1367-2630/18/4/043027.

[22] A. Ferraro, Alessandro, S. Olivares and M. G. A. Paris, *Gaussian states in continuous variable quantum information*, arXiv preprint quant-ph/0503237 (2005). arXiv: quant-ph/0503237.

[23] S. Olivares, *Quantum optics in the phase space*, Eur. Phys. Journ. Spec. Top., **203**, 3-24 (2012). doi: 10.1140/epjst/e2012-01532-4.

[24] A. Serafini, *Quantum Continuous Variables: A Primer of Theoretical Methods*, (2017). doi: 10.1201/9781315118727.

[25] D. F. Walls and G. J. Milburn, *Quantum optics*, Springer (2008). doi: 10.1007/978-3-540-28574-8.

[26] R. L. Hudson, *When is the Wigner quasi-probability density non-negative?*, Rep. Math. Phys. (**6**), 249 (1974). doi: 10.1016/0034-4877(74)90007-X.

[27] F. Soto and P. Claverie, *When is the Wigner function of multidimensional systems nonnegative?*, J. Math. Phys. (**24**), 97 (1983). doi: 10.1063/1.525607.

[28] S. Pirandola, A. Serafini and S. Lloyd, *Correlation matrices of two-mode bosonic systems*, Phys. Rev. A 79(**5**), 052327 (2009). doi: 10.1103/PhysRevA.79.052327.

[29] R. J. Glauber, *Coherent and incoherent states of the radiation field*, Phys. Rev. 131(**6**), 2766 (1963). doi: 10.1103/PhysRev.131.2766.

[30] P. Marek, M. S. Kim and J. Lee, *Nonclassicality in phase space and nonclassical correlation*, Phys. Rev. A 79(**5**), 052315 (2009). doi: 10.1103/PhysRevA.79.052315.

[31] J. Williamson, *On the algebraic problem concerning the normal forms of linear dynamical systems*, Am. Journ. Math. 58(**1**), 141–163 (1936). doi: 10.2307/2371062 .

[32] A. Serafini, F. Illuminati and S. De Siena, *Symplectic invariants, entropic measures and correlations of Gaussian states*, Journ. of Phys. B 37(**2**), L21–L28 (2003). doi: 10.1088/0953-4075/37/2/L02.

[33] A. Serafini, *Multimode uncertainty relations and separability of continuous variable states*, Phys. Rev. Lett. 96(**11**), 110402 (2006). doi: 10.1103/PhysRevLett.96.110402.

[34] R. Simon, *Peres-Horodecki separability criterion for continuous variable systems*, Phys. Rev. Lett. 84(**12**), 2726 (2000). doi: 10.1103/PhysRevLett.84.2726.

[35] L. Duan, G. Giedke, J. I. Cirac and P. Zoller, *Inseparability criterion for continuous variable systems*, Phys. Rev. Lett. 84(**12**), 2722 (2000). doi: 10.1103/PhysRevLett.84.2722.

[36] J. L. Pereira, L. Banchi and S. Pirandola, *Symplectic decomposition from submatrix determinants*, Proc. R. Soc. A (**477**): 20210513 (2021). doi: 10.1098/rspa.2021.0513.

[37] C. W. Helstrom, *Quantum detection and estimation theory*, Journ. of Stat. Phys. 1, 231-252 (1969). doi: 10.1007/BF01007479.

[38] J. Watrous, *The theory of quantum information*, Cambridge University Press (2018). isbn: 9781107180567.

[39] B. Schumacher, Benjamin and M. A. Nielsen, *Quantum data processing and error correction*, Phys. Rev. A 54(**4**), 2629 (1996). doi: 10.1103/PhysRevA.54.2629.

[40] K. M. R. Audenaert, J. Calsamiglia, R. Muñoz-Tapia, E. Bagan, Ll. Masanes, A. Acin and F. Verstraete, *Discriminating States: The Quantum Chernoff Bound*, Phys. Rev. Lett. 98(**16**), 160501 (2007). doi: 10.1103/PhysRevLett.98.160501.

[41] S. Pirandola and S. Lloyd, *Computable bounds for the discrimination of Gaussian states*, Phys. Rev. A 78(**1**), 012331 (2008). doi: 10.1103/PhysRevA.78.012331.

[42] F. Hiai and D. Petz, *The proper formula for relative entropy and its asymptotics in quantum probability*, Commun. Math. Phys. **143**, 99-114 (1991). doi: 10.1007/BF02100287.

[43] T. Ogawa and H. Nagaoka, *Strong converse and Stein's lemma in quantum hypothesis testing*, Asymptotic Theory Of Quantum Statistical Inference: Selected Papers, 28-42, World Scientific, (2005). doi: 10.1142/9789812563071_0003.

[44] S. Pirandola, S. L. Braunstein, R. Laurenza, C. Ottaviani, T. P. W. Cope, G. Spedalieri and L. Banchi, *Theory of channel simulation and bounds for private communication*, Quant. Sci. and Tech. 3(**3**), 035009, (2018). doi: 10.1088/2058-9565/aac394.

[45] L. Banchi, S. L. Braunstein and S. Pirandola, *Quantum fidelity for arbitrary Gaussian states*, Phys. Rev. Lett. 115(**26**), 260501 (2015). doi: 10.1103/PhysRevLett.115.260501.

[46] K. Li, *Second-order asymptotics for quantum hypothesis testing*, Annals of Statistics 42(**1**), 171-189 (2014). doi: 10.1214/13-AOS1185.

[47] M. Tomamichel and M. Hayashi, *A hierarchy of information quantities for finite block length analysis of quantum tasks*, IEEE Trans. Inf. Theory 59(**11**), 7693–7710 (2013). doi: 10.1109/TIT.2013.2276628.

[48] K. M. R. Audenaert, M. Nussbaum, A. Szkola and F. Verstraete, *Asymptotic Error Rates in Quantum Hypothesis Testing*, Commun. Math. Phys. 279, 251-283 (2008). doi: 10.1007/s00220-008-0417-5.

[49] G. Spedalieri and S. L. Braunstein, *Asymmetric quantum hypothesis testing with Gaussian states*, Phys. Rev. A 90(**5**), 052307 (2014). doi: 10.1103/PhysRevA.90.052307.

[50] M. F. Sacchi, *Entanglement can enhance the distinguishability of entanglement-breaking channels*, Phys. Rev. A 72(**1**), 014305 (2005). doi: 10.1103/PhysRevA.72.014305.

[51] Harris Corporation, *Quantum sensors program*, AFRL-RI-RS-TR-2009-208 Final Technical Report, August (2009). Available Online.

[52] J. H. Shapiro and S. Lloyd, *Quantum illumination versus coherent-state target detection*, New Journ. of Phys. 11(**6**), 063045 (2009). doi: 10.1088/1367-2630/11/6/063045.

[53] R. Di Candia, H. Yiğitler, G. Paraoanu R. Jäntti, *Two-way covert quantum communication in the microwave regime*, PRX Quantum 2(**2**), 020316 (2021). doi: 10.1103/PRXQuantum.2.020316.

[54] G. De Palma and J. Borregaard, *Minimum error probability of quantum illumination*, Phys. Rev. A 98(**1**), 012101 (2018). doi: 10.1103/PhysRevA.98.012101.

[55] G. Spedalieri and S. Pirandola, *Optimal squeezing for quantum target detection*, Phys. Rev. Research (**3**), L042039 (2021). doi: PhysRevResearch.3.L042039.

[56] C. W. S. Chang, M. Simoen, J. Aumentado, C. Sabín, P. Forn-Díaz, A. M. Vadiraj, F. Quijandría, G. Johansson, I. Fuentes and C. M. Wilson, *Generating multimode entangled microwaves with a superconducting parametric cavity*, Phys. Rev. App. 10(**4**), 044019 (2018). doi: 10.1103/PhysRevApplied.10.044019.

[57] B. Yurke, L. R. Corruccini, P. G. Kaminsky, L. W. Rupp, A. D. Smith, A. H. Silver, R. W. Simon and E. A. Whittaker, *Observation of parametric amplification and deamplification in a Josephson parametric amplifier*, Phys. Rev. A, 39(**5**), 2519 (1989). doi: 10.1103/PhysRevA.39.2519.

[58] K. Heshami, D. G. England, P. C. Humphreys, P. J. Bustard, V. M. Acosta, J. Nunn and B. J. Sussman, *Quantum memories: emerging applications and recent advances*, Journ. Mod. Opt. 63(**20**), 2005-2028 (2016). doi: 10.1080/09500340.2016.1148212.

[59] S. Barzanjeh, S. Pirandola, D. Vitali and J. M. Fink *Microwave quantum illumination using a digital receiver*, Science Advances 6(**19**), (2020). doi: 10.1126/sciadv.abb0451.

[60] S. Guha and B. I. Erkmen, *Gaussian-state quantum-illumination receivers for target detection*, Phys. Rev. A 80(**5**), 052310 (2009). doi: 10.1103/PhysRevA.80.052310.

[61] J. Calsamiglia, J. I. de Vicente, R. Muñoz-Tapia and E. Bagan, *Local discrimination of mixed states*, Phys. Rev. Lett. 105(**8**), 080504 (2010). doi: 10.1103/PhysRevLett.105.080504.

[62] Q. Zhuang, Z. Zhang and J. H. Shapiro, *Optimum mixed-state discrimination for noisy entanglement-enhanced sensing*, Phys. Rev. Lett. 118(**4**), 040801 (2017). doi:

10.1103/PhysRevLett.118.040801.

[63] Q. Zhuang, Z. Zhang and J. H. Shapiro, *Entanglement-enhanced Neyman–Pearson target detection using quantum illumination*, Journ. Opt. Soc. Am. B 34(**8**), 1567-1572 (2017). doi: 10.1364/JOSAB.34.001567.

[64] E. D. Lopaeva, I. Ruo Berchera, I. P. Degiovanni, S. Olivares, G. Brida and M. Genovese, *Experimental realization of quantum illumination*, Phys. Rev. Lett. 110(**15**), 153603 (2013). doi: 10.1103/PhysRevLett.110.153603.

[65] D. G. England, B. Balaji, B. J. Sussman, *Quantum-enhanced standoff detection using correlated photon pairs*, Phys. Rev. A 99(**2**), 023828 (2019). doi: 10.1103/PhysRevA.99.023828.

[66] Z. Zhang, M. Tengner, T. Zhong, F. N. C. Wong and J. H. Shapiro, *Entanglement's benefit survives an entanglement-breaking channel*, Phys. Rev. Lett. 111(**01**), 010501 (2013). doi: 10.1103/PhysRevLett.111.010501.

[67] Z. Zhang, S. Mouradian, F. N. C. Wong and J. H. Shapiro, *Entanglement-enhanced sensing in a lossy and noisy environment*, Phys. Rev. Lett. 114(**11**), 110506 (2015). doi: 10.1103/PhysRevLett.114.110506.

[68] C. W. S. Chang, A. M. Vadiraj, J. Bourassa, B. Balaji and C. M. Wilson, *Quantum-enhanced noise radar*, Appl. Phys. Lett. 114 (**11**), 112601, (2019). doi: 10.1063/1.5085002.

[69] D. Luong, C. W. Sandbo Chang, A. M. Vadiraj, A. Damini, C. M. Wilson and B. Balaji, *Receiver operating characteristics for a prototype quantum two-mode squeezing radar*, IEEE Trans. Aerosp. Electron. Syst. 56(**3**), 2041–2060 (2020). doi: 10.1109/TAES.2019.2951213.

[70] J. H. Shapiro, *The quantum illumination story*, IEEE Trans. Aerosp. Electron. Syst., Magazine 35(**4**), 8-20 (2020). doi: 10.1109/MAES.2019.2957870.

[71] F. Daum, *Quantum radar cost and practical issues*, IEEE Trans. Aerosp. Electron. Syst. Magazine 35(**11**), 8–20 (2020). doi: 10.1109/MAES.2020.2982755.

[72] J. Bourassa and C. M. Wilson, *Progress Toward an All-Microwave Quantum Illumination Radar*, IEEE Trans. Aerosp. Electron. Syst. Magazine 35(**11**), 58–69 (2020). doi: 10.1109/MAES.2020.3024422.

[73] L. Maccone, Lorenzo and C. Ren, *Quantum radar*, Phys. Rev. Lett. 124(**20**), 200503

(2020). doi: 10.1103/PhysRevLett.124.200503.

[74] R. G. Torromé, N. B. Bekhti-Winkel and P. Knott, *Introduction to quantum radar*, arXiv preprint arXiv:2006.14238 (2020). arXiv: 2006.14238.

[75] E. Agudelo, J. Sperling and W. Vogel, *Quasiprobabilities for multipartite quantum correlations of light*, Phys. Rev. A 87(**3**), 033811 (2013). doi: 10.1103/PhysRevA.87.033811.

[76] J. Sperling, M. Bohmann, W. Vogel, G. Harder, B. Brecht, V. Ansari and C. Silberhorn, *Uncovering quantum correlations with time-multiplexed click detection*, Phys. Rev. Lett. 115(**2**), 023601 (2015). doi: 10.1103/PhysRevLett.115.023601.

[77] F. Shahandeh, A. P. Lund and T. C. Ralph, *Quantum correlations in nonlocal boson sampling*, Phys. Rev. Lett. 119(**12**), 120502 (2017). doi: 10.1103/PhysRevLett.119.120502.

[78] G. Spedalieri, C. Lupo, S. L. Braunstein and S. Pirandola, *Thermal quantum metrology in memoryless and correlated environments*, Quant. Sci. and Tech. **4**, 015008 (2018). doi: 10.1088/2058-9565/aae284.

[79] S. Pirandola, *Entanglement Reactivation in Separable Environments*, New Journ. of Phys. 15(**11**), 113046 (2013). doi: 10.1088/1367-2630/15/11/113046.

[80] K. Modi, A. Brodutch, H. Cable, T. Paterek and V. Vedral, *The classical-quantum boundary for correlations: Discord and related measures*, Rev. Mod. Phys. 84(**4**), 1655-1707 (2012). doi: 10.1103/RevModPhys.84.1655.

[81] S. Pirandola, G. Spedalieri, S. L. Braunstein, N. J. Cerf, and S. Lloyd, *Optimality of Gaussian discord*, Phys. Rev. Lett. 113(**4**), 140405 (2014). doi: 10.1103/PhysRevLett.113.140405.

[82] P. Giorda and M. G. A. Paris, *Gaussian Quantum Discord*, Phys. Rev. Lett. 105(**2**), 020503 (2010). doi: 10.1103/PhysRevLett.105.020503.

[83] G. Adesso and A. Datta, *Quantum versus Classical Correlations in Gaussian States*, Phys. Rev. Lett. 105(**3**), 030501 (2010). doi: 10.1103/PhysRevLett.105.030501.

[84] S. Pirandola, R. Laurenza, C. Ottaviani and L. Banchi, *Fundamental Limits of Repeaterless Quantum Communications*, Nat. Commun. 8, 15043 (2017). doi: 10.1038/ncomms15043.

[85] J. I. Marcum, *A Statistical Theory of Target Detection by Pulsed Radar: Mathematical Appendix*, IRE Trans. Inf. Theory 6(**2**), 59–267 (1960). doi: 10.1109/TIT.1960.1057560.

[86] W. Albersheim, *A closed-form approximation to Robertson's detection characteristics*, Proc. of the IEEE 69(**7**), 839-839 (1981). doi: 10.1109/PROC.1981.12082.

[87] S. Bandyopadhyay, *More nonlocality with less purity*, Phys. Rev. Lett. 106(**21**), 210402 (2011). doi: 10.1103/PhysRevLett.106.210402.

[88] Q. Zhuang, Z. Zheshen and J. H. Shapiro, *Quantum illumination for enhanced detection of Rayleigh-fading targets*, Phys. Rev. A 96(**2**), 020302 (2017). doi: 10.1103/PhysRevA.96.020302.

[89] C. Eichler, D. Bozyigit and A. Wallraff, *Characterizing quantum microwave radiation and its entanglement with superconducting qubits using linear detectors*, Phys. Rev. A, 86(**3**), 032106 (2012). doi: 10.1103/PhysRevA.86.032106.

[90] A. Chefles, *Quantum state discrimination*, Contemp. Phys. 41(**6**), 401-424 (2000). doi: 10.1080/00107510010002599.

[91] S. M. Barnett and S. Croke, *Quantum state discrimination*, Adv. Opt. Photon. 1(**2**), 238-278 (2009). doi: 10.1364/AOP.1.000238.

[92] A. Chefles and S. M. Barnett, *Strategies for discriminating between non-orthogonal quantum states*, Journ. Mod. Opt. 45(**6**), 1295-1302 (1998). doi: 10.1080/09500349808230919.

[93] Q. Zhuang and S. Pirandola, *Entanglement-enhanced testing of multiple quantum hypotheses*, Commun. Phys. **3**, 103 (2020). doi: 10.1038/s42005-020-0369-4.

[94] U. Herzog and J. A. Bergou, *Optimum unambiguous discrimination of two mixed quantum states*, Phys. Rev. A 71(**5**), 050301 (2005). doi: 10.1103/PhysRevA.71.050301.

[95] D. P. DiVincenzo, *Quantum computation*, Science 270(**5234**), 255-261 (1995). doi: 10.1126/science.270.5234.255.

[96] R. Raussendorf and H. J. Briegel, *A one-way quantum computer*, Phys. Rev. Lett. 86(**22**), 5188 (2001). doi: 10.1103/PhysRevLett.86.5188.

[97] H. J. Briegel, D. E. Browne, W. Dür, R. Raussendorf and M. Van den Nest, *Measurement-based quantum computation*, Nat. Phys. 5(**1**), 19-26 (2009). doi: 10.1038/nphys1157.

[98] N. Gisin and R. Thew, *Quantum communication*, Nat. Phot. 1(**3**), 165-171 (2007). doi: 10.1038/nphoton.2007.22.

[99] M. Hillery, V. Bužek and A. Berthiaume, *Quantum secret sharing*, Phys. Rev. A 59(**3**), 1829 (1999). doi: 10.1103/PhysRevA.59.1829.

[100] S. Pirandola, U. L. Andersen, L. Banchi, M. Berta, D. Bunandar, R. Colbeck, D. Englund, T. Gehring, C. Lupo, C. Ottaviani, J. L. Pereira, M. Razavi, J. Shamsul Shaari, M. Tomamichel, V. C. Usenko, G. Vallone, P. Villoresi and P. Wallden, *Advances in Quantum Cryptography*, Adv. Opt. Photon. 12(**4**) 1012-1236, (2020). doi: 10.1364/AOP.361502.

[101] J. Fiurasek and N. J. Cerf, *Gaussian postselection and virtual noiseless amplification in continuous-variable quantum key distribution*, Phys. Rev. A (**86**), 060302(R) (2012). doi: 10.1103/PhysRevA.86.060302.

[102] M. Brandsema, *Current readiness for quantum radar implementation*, IEEE Conf. on Ant. Meas. & App. (CAMA), 1–4 (2018). doi: 10.1109/CAMA.2018.8530617.

[103] J. D. Breeze, E. Salvadori, J. Sathian, N. McN. Alford and C. W. M. Kay, *Continuous-wave room-temperature diamond maser*, Nature **555** (7697), 493-496 (2018). doi: 10.1038/nature25970.

[104] H. Wu, X. Xie, W. Ng, S. Mehanna, Y. Li, M. Attwood and M. Oxborrow, *Room-temperature quasi-continuous-wave pentacene maser pumped by an invasive Ce: YAG luminescent concentrator*, Phys. Rev. App. 14(**6**), 064017 (2020). doi: 10.1103/PhysRevApplied.14.064017.

[105] M. M. Wilde, M. Tomamichel, S. Lloyd and M. Berta, *Gaussian hypothesis testing and quantum illumination*, Phys. Rev. Lett. 119(**12**), 120501 (2017). doi: 10.1103/PhysRevLett.119.120501.

[106] S. Pirandola, *Quantum reading of a classical digital memory*, Phys. Rev. Lett. 106(**9**), 090504 (2011). doi: 10.1103/PhysRevLett.106.090504.

[107] S. Mukamel, M. Freyberger, W. Schleich, M. Bellini, A. Zavatta, G. Leuchs, C. Silberhorn, R. W. Boyd, L. L. Sánchez-Soto, A. Stefanov, M. Barbieri, A. Paterova, L. Krivitsky, S. Shwartz, K. Tamasaku, K. Dorfman, F. Schlawin, V. Sandoghdar, M. Raymer, A. Marcus, O. Varnavski, T. Goodson III, Z. Zhou, B. Shi, S. Asban, M. Scully, G. Agarwal, T. Peng, A. V. Sokolov, Z. Zhang, M. S. Zubairy, I. A. Vartanyants, E. del Valle and F. Laussy, *Roadmap on quantum light spectroscopy*, Journ. Phys. B: At., Mol. Opt. Phys., 53(**7**), 072002 (2020). doi: 10.1088/1361-6455/ab69a8.

[108] J. L. Pereira, L. Banchi, Q. Zhuang, Quntao and S. Pirandola, *Idler-free channel posi-*

tion finding, Phys. Rev. A, 104(**4**), 042614 (2021). doi: 10.1103/PhysRevA.103.042614.

[109] E. Bagan, J. A. Bergou, S. S. Cottrell and M. Hillery, *Relations between coherence and path information*, Phys. Rev. Lett. 116(**16**), 160406 (2016). doi: 10.1103/PhysRevLett.116.160406.

[110] T. Ogawa and H.Nagaoka, *Strong converse to the quantum channel coding theorem*, IEEE Trans. Inf. Theory 45(**7**), 2486–2489 (1999). doi: 10.1109/18.796386.

[111] H. Barnum, Howard and E. Knill, *Reversing quantum dynamics with near-optimal quantum and classical fidelity*, Journ. Math. Phys. **43**, 2097-2106 (2002). doi: 10.1063/1.1459754.

[112] S. Zhang, Y. Feng, X. Sun and M. Ying, *Upper bound for the success probability of unambiguous discrimination among quantum states*, Phys. Rev. A 64(**6**), 062103 (2001). doi: 10.1103/PhysRevA.64.062103.

[113] A. Montanaro, *A lower bound on the probability of error in quantum state discrimination*, 2008 IEEE Inf. Theory Workshop, pp. 378-380 (2008). doi: 10.1109/ITW.2008.4578690.

[114] D. Qiu and L. Li, *Minimum-error discrimination of quantum states: Bounds and comparisons*, Phys. Rev. A 81(**4**), 042329 (2010). doi: 10.1103/PhysRevA.81.042329.

[115] R. Jozsa, *Fidelity for mixed quantum states*, Journ. Mod. Opt. 41(**12**), 2315-2323 (1994). doi: 10.1080/09500349414552171.

[116] A. Uhlmann, *The "transition probability" in the state space of $a^{\star}$-algebra*, Rep. Math. Phys. 9(**2**), 273-279 (1976). doi: 10.1016/0034-4877(76)90060-4.

[117] S. Clemmen, K. Phan Huy, W. Bogaerts, R. G. Baets, Ph. Emplit and S. Massar, *Continuous wave photon pair generation in silicon-on-insulator waveguides and ring resonators*, Opt. Express 17(**19**), 16558-16570 (2009). doi: 10.1364/OE.17.016558.

[118] J. Silverstone *et al.*, *Qubit entanglement between ring-resonator photon-pair sources on a silicon chip*, Nat. Commun. **6**, 7948 (2015). doi: 10.1038/ncomms8948.

[119] L. Caspani, C. Xiong, B. J. Eggleton, D. Bajoni, M. Liscidini, M. Galli, R. Morandotti and D. J. Moss , *Integrated sources of photon quantum states based on nonlinear optics*, Light Sci. Appl. **6**, e17100 (2017). doi: 10.1038/lsa.2017.100.

[120] W. Bogaerts, P. De Heyn, T. Van Vaerenbergh, K. De Vos, S. Kumar Selvaraja, T. Claes, P. Dumon, P. Bienstman, D. Van Thourhout and R. Baets, *Silicon microring*

resonators, Laser Photon. Rev., 6(**1**), pp.47-73 (2012). doi: 10.1002/lpor.201100017.

[121] J. Silverstone, D. Bonneau, K. Ohira, N. Suzuki, H. Yoshida, N. Iizuka, M. Ezaki, C. M. Natarajan, M. G. Tanner, R. H. Hadfield, V. Zwiller, G. D. Marshall, J. G. Rarity, J. L. O'Brien and M. G. Thompson , *On-chip quantum interference between silicon photon-pair sources*, Nat. Photon. **8**, 104–108 (2014). doi: 10.1038/nphoton.2013.339.

[122] A. Dutt, K. Luke, S. Manipatruni, A. L. Gaeta, P. Nussenzveig and M. Lipson, *On-Chip Optical Squeezing*, Phys. Rev. Applied, 3(**4**), 044005 (2015). doi: 10.1103/PhysRevApplied.3.044005.

[123] P. Imany, J. A. Jaramillo-Villegas, O. D. Odele, K. Han, D. E. Leaird, J. M. Lukens, P. Lougovski, M. Qi and A. M. Weiner, *50-GHz-spaced comb of high-dimensional frequency-bin entangled photons from an on-chip silicon nitride microresonator*, Opt. Express 26(**2**), 1825-1840 (2018). doi: 10.1364/OE.26.001825.

[124] S. Ramelow, A. Farsi, S. Clemmen, D. Orquiza, K. Luke, M. Lipson and A. L. Gaeta, *Silicon-Nitride Platform for Narrowband Entangled Photon Generation*, (2015). arXiv: 1508.04358.

[125] A. D. Holevo, *Statistical decision theory for quantum systems*, Journ. of Multivariate Analysis 3(**4**), 337-394 (1973). doi: 10.1016/0047-259X(73)90028-6.

[126] M. Hayashi, *Quantum Information Theory: Mathematical Foundation*, Springer (2017). doi: 10.1007/978-3-662-49725-8.

[127] C. M. Caves, *Quantum limits on noise in linear amplifiers*, Phys. Rev. D (**26**), 1817 (1982). doi: 10.1103/PhysRevD.26.1817.

[128] C. M. Caves, J. Combes, Z. Jiang, and S. Pandey, *Quantum limits on phase-preserving linear amplifiers*, Phys. Rev. A (**86**), 063802 (2012). doi: 10.1103/PhysRevA.86.063802.

[129] T. C. Ralph and A. P. Lund, *Nondeterministic noiseless linear amplification of quantum systems*, AIP Conference Proceedings (**1110**), 155-160 (2009). doi: 10.1063/1.3131295.

[130] S. Pandey, Z. Jiang, J. Combes, and C. M. Caves, *Quantum limits on probabilistic amplifiers*, Phys. Rev. A (**88**), 033852 (2013). doi: 10.1103/PhysRevA.88.033852.

[131] M. Barbieri, F. Ferreyrol, R. Blandino, R. Tualle-Brouri, and P. Grangier, *Nondeterministic noiseless amplification of optical signals: a review of recent experiments*, Laser Phys. Lett. (**8**), 411 (2011). doi: 10.1002/lapl.201010143.

[132] F. Ferreyrol, M. Barbieri, R. Blandino, S. Fossier, R. Tualle-Brouri, and P. Grangier,

Implementation of anondeterministic optical noiseless amplifier, Phys. Rev.Lett. (**104**), 123603 (2010). doi: 10.1103/PhysRevLett.104.123603.

[133] H. M. Chrzanowski, N. Walk, S. M. Assad, J. Janousek, S. Hosseini, T. C. Ralph, T. Symul, and P. K. Lam, *Measurement-based noiseless linear amplification for quantum communication*, Nat. Photon. (**8**), 333-338 (2014). doi: 10.1038/nphoton.2014.49.

[134] R. J. Donaldson, R. J. Collins, E. Eleftheriadou, S. M.Barnett, J. Jeffers, and G. S. Buller, *Experimental implementation of a quantum optical state comparison amplifier*, Phys. Rev. Lett. (**114**), 120505 (2015). doi: 10.1103/PhysRevLett.114.120505.

[135] R. Blandino, A. Leverrier, M. Barbieri, J. Etesse, P. Grangier, and R. Tualle-Brouri, *Improving the maximum transmission distance of continuous-variable quantum key distribution using a noiseless amplifier*, Phys. Rev. A (**86**), 012327 (2012). doi: 10.1103/PhysRevA.86.012327.

[136] M. Ghalaii, C. Ottaviani, R. Kumar, S. Pirandola and M. Razavi, *Long-Distance Continuous-Variable Quantum Key Distribution With Quantum Scissors*, IEEE Journal of Selected Topics in Quantum Electronics (**26**), 1-12, (2020). doi: 10.1109/JSTQE.2020.2964395.

[137] M. Ghalaii, C. Ottaviani, R. Kumar, S. Pirandola and M. Razavi, *Discrete-Modulation Continuous-Variable Quantum Key Distribution Enhanced by Quantum Scissors*, IEEE Journal on Selected Areas in Communications (**38**), 506-516 (2020). doi: 10.1109/JSAC.2020.2969058.

[138] B. Xu, C. Tang, H. Chen, W. Zhang, and F. Zhu, *Improving the maximum transmission distance of four-state continuous-variable quantum key distribution by using a noiseless linear amplifier*, Phys. Rev. A (**87**), 062311 (2013). doi: 10.1103/PhysRevA.87.062311.

[139] J. Dias and T. C. Ralph, *Quantum repeaters using continuous-variable teleportation*, Phys. Rev. A (**95**), 022312 (2017). doi: 10.1103/PhysRevA.95.022312.

[140] K. P. Seshadreesan, H. Krovi, and S. Guha, *Continuous-variable quantum repeater based on quantum scissors and mode multiplexing*, Phys. Rev. Research (**2**), 013310 (2020). doi: 10.1103/PhysRevResearch.2.013310.

[141] M. Ghalaii and S. Pirandola, *Capacity-approaching quantum repeaters for quantum communications*, Phys. Rev. A (**102**), 062412 (2020). doi: 10.1103/PhysRevA.102.062412.

[142] G. Y. Xiang, T. C. Ralph, A. P. Lund, N. Walk, and G. J. Pryde, *Heralded noiseless linear amplification and distillation of entanglement*, Nat. Photon. (**4**), 316-319 (2010). doi: 10.1038/nphoton.2010.35.

[143] Kaushik P. Seshadreesan, Hari Krovi, and Saikat Guha, *Continuous-variable entanglement distillation over a pure loss channel with multiple quantum scissors*, Phys. Rev. A (**100**), 022315 (2019). doi: 10.1103/PhysRevA.100.022315.

[144] J. Zhao, J. Dias, J. Y. Haw, T. Symul, M. Bradshaw, R. Blandino, T. Ralph, S. M. Assad, and P. K. Lam, *Quantum enhancement of signal-to-noise ratio with a heralded linear amplifier*, Optica 4(**11**), 1421-1428 (2017). doi: 10.1364/OPTICA.4.001421.

[145] S. M. Assad, M. Bradshaw, and P. K. Lam, *Phase estimation of coherent states with a noiseless linear amplifier*, Int. J. Quantum Inf. 15(**1**), 1750009 (2017). doi: 10.1142/S0219749917500095.

[146] Q. Zhuang and S. Pirandola, *Ultimate limits for multiple quantum channel discrimination*, Phys. Rev. Lett. 125(**8**), 080505 (2020). doi: 10.1103/PhysRevLett.125.080505.

[147] T. C. Ralph and A. P. Lund, *Nondeterministic noiseless linear amplification of quantum systems*, AIP Conference Proceedings 1110(**1**), 155-160 (2009). doi: 10.1063/1.3131295.

[148] R. Blandino, A. Leverrier, M. Barbieri, J. Etesse, P. Grangier and R. Tualle-Brouri, *Improving the maximum transmission distance of continuous-variable quantum key distribution using a noiseless amplifier*, Phys. Rev. A 86(**1**), 012327 (2012). doi: 10.1103/PhysRevA.86.012327.

[149] H. M. Chrzanowski, N. Walk, S. M. Assad, J. Janousek, S. Hosseini, T. C. Ralph, T. Symul and P. K. Lam , *Measurement-based noiseless linear amplification for quantum communication*, Nat. Photon. 8(**4**), 333–338 (2014). doi: 10.1038/nphoton.2014.49.

[150] G. Spedalieri, S. Pirandola and S. L. Braunstein, *Symmetric and asymmetric discrimination of bosonic loss: Toy applications to biological samples and photodegradable materials*, Phys. Rev. A 98(**5**), 053836 (2018). doi: 10.1103/PhysRevA.98.053836.

[151] S. Zhang, J. Guo, W. Bao, J. Shi, C. Jin, X. Zou and G. Guo, *Quantum illumination with photon-subtracted continuous-variable entanglement*, Phys. Rev. A 89(**6**), 062309 (2014). doi: 10.1103/PhysRevA.89.062309.

[152] R. Gupta, S. Roy, T. Das and A. S. De, *Quantum illumination with noisy probes: Conditional advantages of non-Gaussianity*, arXiv preprint arXiv:2107.02774 (2021).

arXiv: 2107.02774.

[153] S. Guerrini, M. Z. Win, M. Chiani and A. Conti, *Quantum discrimination of noisy photon-added coherent states*, IEEE J. Sel. Areas Inf. Theory 1(**2**), 469-479 (2020). doi: 10.1109/JSAIT.2020.3012944.

[154] A. Kenfack and K. Życzkowski, *Negativity of the Wigner function as an indicator of non-classicality*, J. Opt. B: Quantum Semiclass. Opt. 6(**10**), 396 (2004). doi: 10.1088/1464-4266/6/10/003.

[155] I. D. Ivanovic, *How to differentiate between non-orthogonal states*, Phys. Lett. A 123(**6**), 257-259 (1987). doi: 10.1016/0375-9601(87)90222-2.

[156] D. Dieks, *Overlap and distinguishability of quantum states*, Phys. Lett. A 126(**5-6**), 303-306 (1988). doi: 10.1016/0375-9601(88)90840-7.

[157] A. Peres, *How to differentiate between non-orthogonal states*, Phys. Lett. A 128(**1-2**), 19 (1988). doi: 10.1016/0375-9601(88)91034-1.

[158] U. Herzog and J. A. Bergou, *Optimum unambiguous discrimination of two mixed quantum states*, Phys. Rev. A 71(**5**), 050301 (2005). doi: 10.1103/PhysRevA.71.050301.

[159] Q. Zhuang, *Ultimate limits of approximate unambiguous discrimination*, Phys. Rev. Res. 2(**4**), 043276 (2020). doi: 10.1103/PhysRevResearch.2.043276.

[160] J. S. Sidhu, M. S. Bullock, S. Guha and C. Lupo, *Unambiguous discrimination of coherent states*, arXiv preprint arXiv:2109.00008 (2021). arXiv: 2109.00008.